

ICRR
ANNUAL
REPORT

APRIL 2005 – MARCH 2006

Institute for Cosmic Ray Research
University of Tokyo

INSTITUTE
FOR
COSMIC RAY RESEARCH
UNIVERSITY OF TOKYO

ANNUAL REPORT
(APRIL 2005 – MARCH 2006)

Editorial Board

TAKEUCHI, Yasuo

MIYOKI, Shinji

©**Institute for Cosmic Ray Research, University of Tokyo**

5-1-5, Kashiwanoha, Kashiwa, Chiba 277-8582 Japan

Telephone: (81)4-7136-3102

Facsimile: (81)4-7136-3115

WWW URL: <http://www.icrr.u-tokyo.ac.jp>

TABLE OF CONTENTS

Preface	
Research Divisions	1
Neutrino and Astroparticle Division	
High Energy Cosmic Ray Division	
Astrophysics and Gravity Division	
Observatories and a Research Center	48
Norikura Observatory	
Akeno Observatory	
Kamioka Observatory	
Research Center for Cosmic Neutrinos	
Appendix A. ICRR International Workshops	57
Appendix B. ICRR Seminars	58
Appendix C. List of Publications — 2005 fiscal year	58
(a) Papers Published in Journals	
(b) Conference Papers	
(c) ICRR Report	
Appendix D. Doctoral Theses	64
Appendix E. Public Relations	64
(a) ICRR News	
(b) Public Lectures	
(c) Visitors	
Appendix F. Inter-University Researches	67
Appendix G. List of Committee Members	71
(a) Board of Councillors	
(b) Advisory Committee	
(c) User's Committee	
Appendix H. List of Personnel	72

PREFACE

Starting from April 2004, Japanese national universities have become independent corporations and were set up outside of the government organizations. We therefore are supposed to have much more autonomy. However the new mechanism of the budget allocation from the government to the universities is inadequate to initiate big and long term scientific projects to be conducted in the universities. It is also known to be difficult to increase the number of scientific staffs for the long term programs. A new contrivance for the budget allocation from the government is urgently needed in order to keep activities in basic science in Japanese universities and institutions.

The Institute for Cosmic Ray Research, the inter-university institute, is closely associated with Japanese universities and foreign institutes. The experimental facilities located at the institute are jointly established and used by about 350 physicists in our community. We hope that we will continue to keep good collaborations and to keep providing important results on cosmic rays physics and related subjects although the university system has been drastically changed.

The institute has been re-organized into three research divisions; Neutrino and Astroparticle Division, High Energy Cosmic Ray Division, and Astrophysics and Gravity Division. In each division, a few different types of experiments are conducted.

The next big project of the institute is the gravitational wave detector (LIGO), by which the direct detection of the gravitational wave (GW) is aimed. The detection of the GW will prove the Einstein's theory of general relativity and can provide the details of the dynamic feature of the universe.

The study of the cosmic ray had often played a leading role when the particle physics had made a significant development. The pions and muons were discovered in the cosmic rays and those discoveries had brought a fruitful study of the elementary particles using particle accelerators. The discovery of the neutrino mass has again brought a triumph to the cosmic ray research and it has opened up a new field.

At Kamioka underground observatory, the Super-Kamiokande experiment is continuously producing interesting results. There are some other projects in Kamioka, for example, dark matter experiments and geo-physics experiments, which make use of advantages of the underground environments. The construction of the prototype gravitational wave antenna is also in progress.

In 2003, the Telescope Array project has been approved and its construction has begun. The existence of the highest energy cosmic rays beyond the ZGK cut-off indicated by the AGASA group is a big puzzle. If it is confirmed, it may suggest a new physics. There is a steady flow of data from the experiment at Yangbajing (Tibet), and from the cosmic gamma-ray telescope (CANGAROO) deployed over the desert of Woomera (Australia).

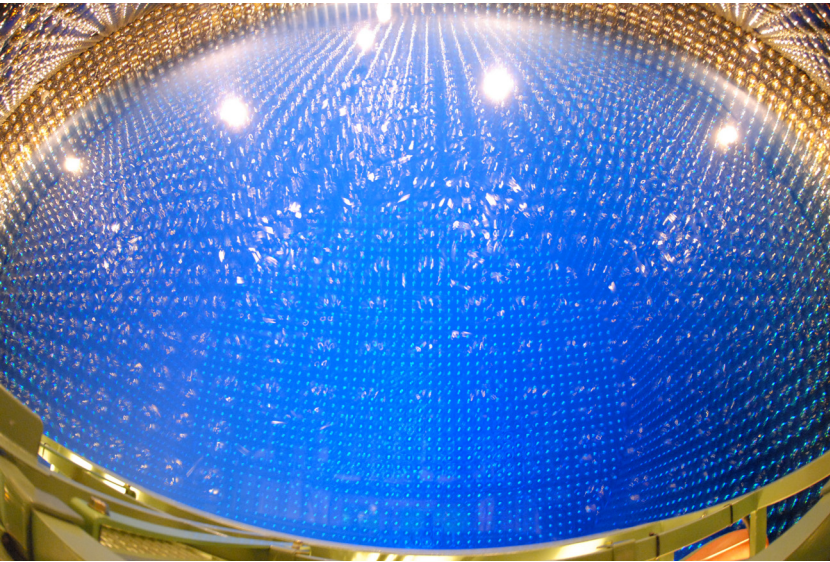
The underground physics and the ground based cosmic ray measurements overseas are the back-bone of the institute.



Yoichiro Suzuki,
Director of ICRR



The ICRR building at Kashiwa, Chiba, Japan.



The inner detector of Super-Kamiokande-III during the full reconstruction. The purified water is under filling.



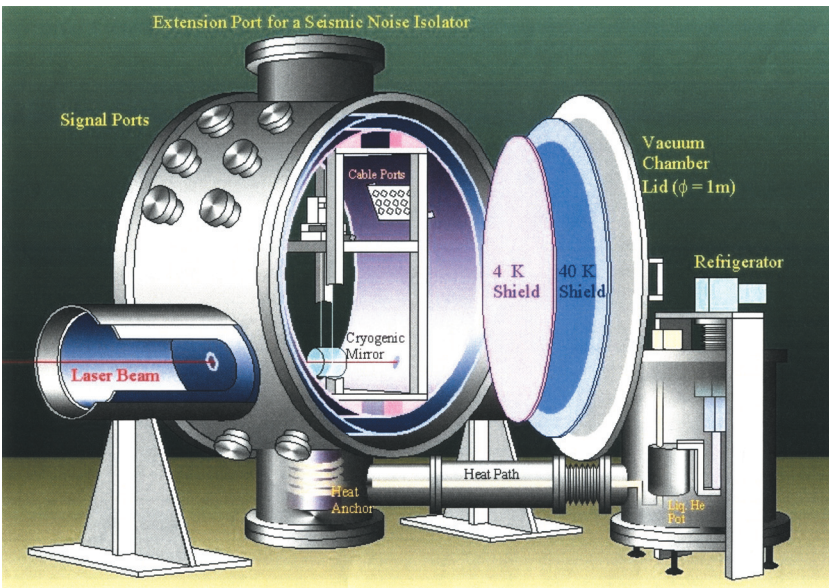
The system of four imaging atmospheric Cherenkov telescopes of 10m diameter of CANGAROO project for detection of very high energy gamma-rays. The whole system is in operation since March 2004 in Woomera, South Australia.



Tibet-III air shower array (37000 m²) at Yangbajing, Tibet (4300 m in altitude).



Air fluorescence telescopes (left) and a scintillator surface detector (right) of the Telescope Array experiment under construction in Utah, USA for the study of extremely high energy cosmic rays.



Cryogenic mirror suspension system for Large Scale Cryogenic Gravitational Wave Telescope.

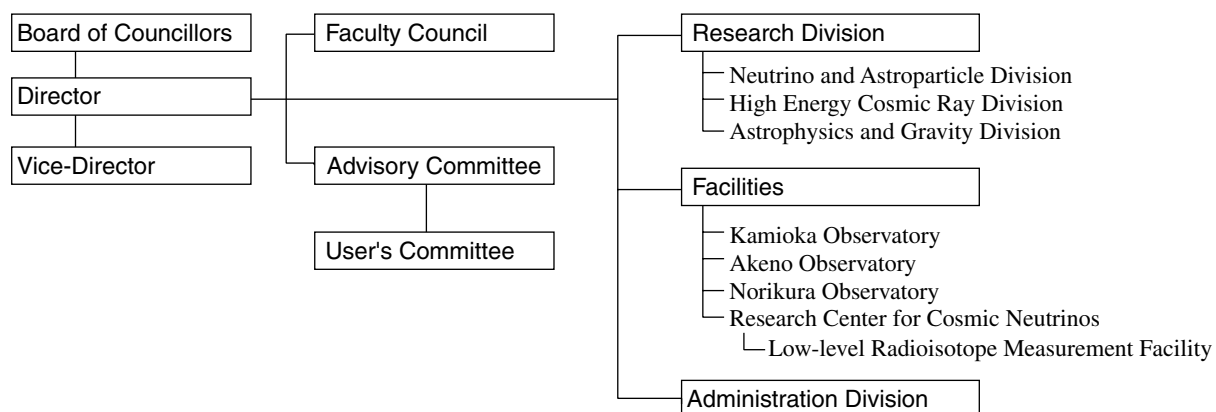


Wide-view telescope of 2.5 m diameter (left telescope) in Arizona, USA for the Sloan Digital Sky Survey project.



A public lecture held by Research Center for Cosmic Neutrinos.

Organization



Number of Staff Members in 2004

	Scientific Staff	Technical Staff	Research Fellows	Administrators and Secretaries	
Neutrino and Astroparticle Div.	16	5	5	6	32
High Energy Cosmic Ray Div.	14	11	20	4	49
Astrophysics and Gravity Div.	8	0	6	1	15
Administration	0	0	0	13	13
Total	37	15	31	24	109

FY 2000–2005 Budget

	2000	2001	2002	2003	2004	2005
Personnel expenses	589 879	418 475	460 332	434 874	444 498	557 392
Non-personnel expenses	1 423 789	1 518 584	1 518 065	1 785 449	2 054 950	1 816 943
Total	2 013 668	1 937 059	1 978 397	2 220 323	2 499 448	2 374 335

(in 1 000 yen)

RESEARCH DIVISIONS

Neutrino and Astroparticle Division

Overview

Super-Kamiokande Experiment

K2K Experiment

XMASS Experiment

High Energy Cosmic Ray Division

Overview

CANGAROO-III Project

TA: Telescope Array Experiment

Tibet AS γ Project

Ashra Project

Astrophysics and Gravity Division

Overview

TAMA Project

LCGT Project

Construction of CLIO at Kamioka

Sloan Digital Sky Survey

Theory Group

Investigation of Possible Dark Matter Direct Detection in Electron Accelerators

Heavy wino-like neutralino dark matter annihilation into antiparticles

The relic abundance of the LKP dark matter in Universal Extra Dimension model

Abundance of cosmological relics in low-temperature scenarios

Constraint on Right-Handed Squark Mixings from $B_s - \bar{B}_s$ Mass Difference

Moduli Dynamics in Heavy Gravitino Scenario

Gravitino Overproduction in Inflaton Decay

Q-ball Instability due to U(1) Breaking

The oscillation effects on thermalization of the neutrinos in the universe with low reheating temperature

Unification of Dark Energy and Dark Matter

511 keV Gamma Ray from Moduli Decay in the Galactic Bulge

Evolution of Dark Energy and its implications to the Determination of Neutrino Masses and the Curvature of the Universe

NEUTRINO AND ASTROPARTICLE DIVISION

Overview

The Neutrino and Astroparticle division has been studying neutrino physics and astroparticle physics using Super-Kamiokande(SK) and related experiments.

The SK detector is located in the underground experimental site at Kamioka observatory. The detector was built from 1991 to 1995 and data taking was started in 1996. In 1998, the SK collaboration announced the discovery of neutrino oscillations using atmospheric neutrinos. Another evidence for neutrino oscillations was found in 2001 using solar neutrinos by comparing solar neutrino data from SK and SNO. The SK detector has been used as the far detector of the artificial neutrino beam experiment (K2K) performed from 1999 and neutrino oscillation was confirmed in 2002. After the discovery of neutrino oscillations, detailed studies of neutrino oscillations have been performed at SK. In the analysis of atmospheric neutrinos, oscillation parameters, oscillation mode (whether ν_μ oscillates to ν_τ or $\nu_{sterile}$) and L/E dependence of oscillation have been studied. In the solar neutrino analysis, oscillation parameters has been determined in 2002 and now searching for energy spectrum distortion and day/night time variation expected from the obtained solution. SK has been monitoring neutrinos from supernova burst. If a supernova burst occurs at the distance to the center of our galaxy, SK is able to detect about 8,000 neutrino events. SK is also searching for nucleon decay as the direct evidence of Grand Unified Theories. A high intensity neutrino beam experiment using J-PARC (T2K) is expected to start in 2009 and SK detector will be the far detector of the experiment. High precision measurement of oscillation parameters and the third oscillation pattern (from the third neutrino mass eigenstate to the first eigenstate) will be investigated by T2K. After the accident in 2001, SK detector had been running using about 5,200 50cm-diameter PMTs until October 2005. Mounting about 6000 PMTs in order to fully reconstruct the detector was started in October 2005 and it will be finished by April 2006. Data taking with full water will resume in July 2006.

Another activity of the Neutrino and Astroparticle division is a multi-purpose experiment using liquid xenon aiming at the detection of cold dark matter, neutrino absolute mass using neutrinoless double beta decay, and low energy solar neutrinos. An R&D study for the liquid xenon detector is being performed at Kamioka observatory.

Recent progress of research activities in the Neutrino and Astroparticle division is presented here.

Super-Kamiokande Experiment

[Spokesperson : Yoichiro Suzuki]

Kamioka Observatory, ICRR, Univ. of Tokyo, Gifu, 506-1205

In collaboration with the members of:

Kamioka Observatory, ICRR, Univ. of Tokyo, Japan; RCCN, ICRR, Univ. of Tokyo, Japan; Boston Univ., USA; BNL, USA; Univ. of California, Irvine, USA; California State Univ., Dominguez Hills, USA; Chonnam National Univ., Korea; Duke Univ., USA; George Mason Univ., USA; Gifu Univ., Japan; Univ. of Hawaii, USA; Indiana Univ., USA; KEK, Japan; Kobe Univ., Japan; Kyoto Univ., Japan; LANL, USA; Louisiana State Univ., USA; Univ. of Maryland, USA; Univ. of Minnesota, USA; Miyagi Univ. of Education, Japan; SUNY, Stony Brook, Japan; Nagoya Univ., Japan; Niigata Univ., Japan; Okayama Univ., Japan; Osaka Univ., Japan; Seoul National Univ., Japan; Shizuoka Seika College, Japan; Shizuoka Univ., Japan; Sungkyunkwan Univ., Korea; Tohoku Univ., Japan; Univ. of Tokyo, Japan; Tokai Univ., Japan; Tokyo Inst. of Tech., Japan; Inst. of Experimental Physics, Poland; Univ. of Washington, USA.

Introduction

Super-Kamiokande(SK) is a large water Cherenkov detector, located 1000 m underground in Kamioka mine, Japan. 50 kton of pure water is contained in a stainless steel tank of 39.3 meters in diameter and 41.4 m in height. SK took data from April 1996 to July 2001 (SK-I phase) using 11,146 20-inch photomultipliers(PMTs) for inner detector and 1,885 8-inch PMTs for outer detector. After the accident in November 2001, the detector was reconstructed in 2002 using about 5200 20-inch PMTs. The detector has been running as the second phase of the experiment(SK-II) since December 2002.

In this report, those results are described.

SK Full Reconstruction

The full reconstruction of the Super-Kamiokande detector was performed in 2005. In the accident in 2001, about 60% of PMTs are lost and the detector was reconstructed using survived PMTs in 2002. About 6000 new PMTs are produced from 2003 through 2005 and mounting those PMTs was performed from July 2005 through April 2006.

The PMTs are assembled with acrylic and FRP cases in order to prevent shock wave production even if a PMT is broken. (It was also done for all PMTs re-mounted in 2002). The assembly work started in July 2005 and finished by March 2006. Mounting assembled PMTs was performed from October 2005 through April 2006. Connecting the cable of each PMT to the cable running from the electronics huts to inside the tank was also done parallel to the mounting work.

Atmospheric neutrinos

Cosmic ray interactions in the atmosphere produce neutrinos. The prediction of the absolute flux has an uncertainty of at least $\pm 20\%$. However, the flavor ratio of the atmospheric neutrino flux, $(\nu_\mu + \bar{\nu}_\mu)/(\nu_e + \bar{\nu}_e)$, has been calcu-



Fig. 1. PMTs are assembled with acrylic and FRP cases to prevent shock wave production.

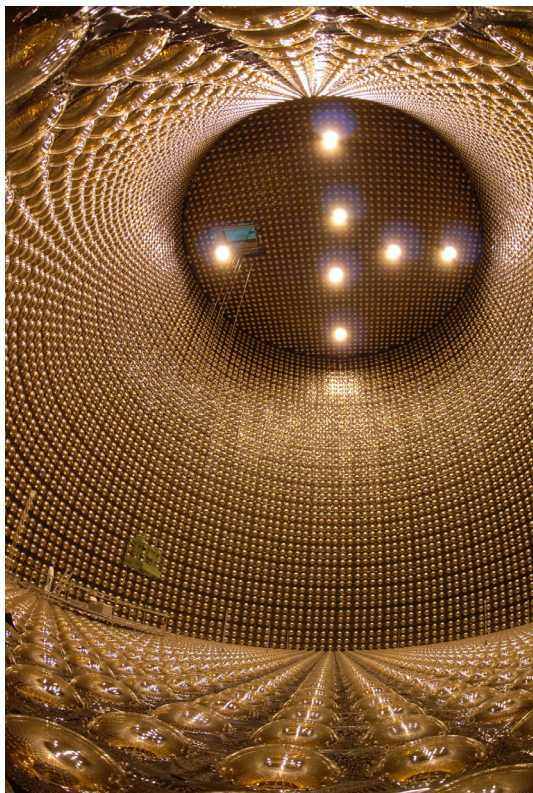


Fig. 2. About 6000 new PMTs are mounted from October 2005 through April 2006. The photograph was taken during mounting bottom PMTs in March 2006.

Table 1. Summary of the atmospheric $(\mu/e)_{data}/(\mu/e)_{MC} (\equiv R)$ ratio measurement.

	SK-I		SK-II	
	Data	MC	Data	MC
Sub-GeV				
e -like	3353	2879.8	1842	1554.5
μ -like	3227	4212.8	1723	2215.4
R	$0.658 \pm 0.016 \pm 0.035$		$0.656 \pm 0.022 \pm 0.033$	
Multi-GeV				
e -like	746	680.5	417	426.2
μ -like(FC+PC)	1562	2029.5	806	1103.8
R	$0.702^{+0.032}_{-0.030} \pm 0.101$		$0.746^{+0.047}_{-0.044} \pm 0.056$	

lated to an accuracy of better than 5%. Another important feature of atmospheric neutrinos is that the fluxes of upward and downward going neutrinos are expected to be nearly equal for $E_\nu > (\text{a few GeV})$ where the geomagnetic effect on primary cosmic ray is negligible.

SK-I observed 12,180 fully-contained (FC) events and 911 partially-contained (PC) events during 1489 days of data taking and SK-II observed 6605 FC events and 427 PC events during 804 days. FC events deposit all of their Cherenkov light in the inner detector, while PC events have exiting tracks which deposit some Cherenkov light in the outer detector. The neutrino interaction vertex was required to have been reconstructed within the 22.5 kiloton fiducial volume, defined to be > 2 m from the PMT wall.

The FC events were classified into “sub-GeV” ($E_{vis} < 1330$ MeV) and “multi-GeV” ($E_{vis} > 1330$ MeV) samples. The numbers of observed and predicted events for sub- and multi-GeV energy regions in SK are summarized in Table 1. The prediction is based on the recent precise measurements of primary cosmic rays by BESS and AMS and a three dimensional calculation of the neutrino flux by Honda et al. The hadronic interaction model of cosmic rays is also improved in the calculation.

Among FC events, single-ring events are identified as e -like or μ -like based on a Cherenkov ring pattern. All the PC events were assigned to be multi-GeV μ -like. Using the number of e -like and μ -like events, the ratio of (μ/e) was obtained and it is significantly smaller than the expectation as shown in the table. Momentum resolution for SK-II is slightly worse than SK-I. This is because the number of ID PMTs in SK-II is about a half of SK-I. However, the performance of the vertex reconstruction, the ring counting, and the particle identification in SK-II are almost the same as in SK-I.

The zenith angle distributions for the sub- and multi-GeV samples are shown in Fig. 3. The μ -like data from SK exhibited a strong up-down asymmetry in zenith angle (Θ) while no significant asymmetry was observed in the e -like data. The data were compared with the Monte Carlo expectation without neutrino oscillations and the best-fit expectation for $\nu_\mu \leftrightarrow \nu_\tau$ oscillations. The oscillated Monte Carlo reproduced well the zenith angle distributions of the data. Some fraction of the

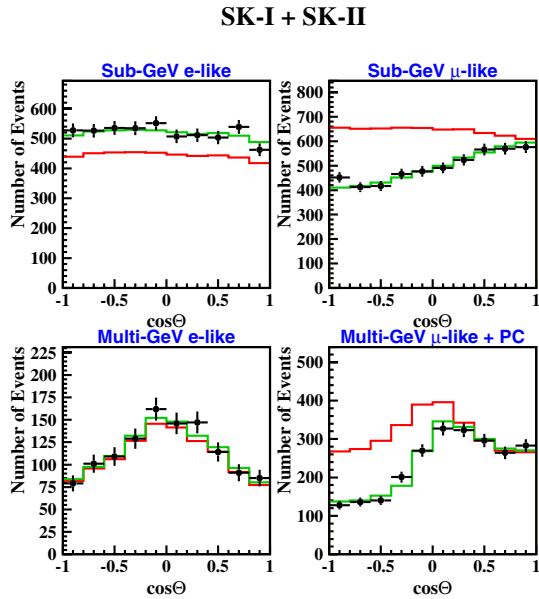


Fig. 3. The zenith angle distributions for sub-GeV e -like, sub-GeV μ -like, multi-GeV e -like and multi-GeV (FC+PC) μ -like events. $\cos\Theta = 1$ means down-going particles. The red histograms show the MC prediction for the no neutrino oscillation case. The green histograms show the Monte Carlo prediction for $\nu_\mu \leftrightarrow \nu_\tau$ oscillations with $\sin^2 2\theta = 1.0$ and $\Delta m^2 = 2.5 \times 10^{-3} \text{eV}^2$.

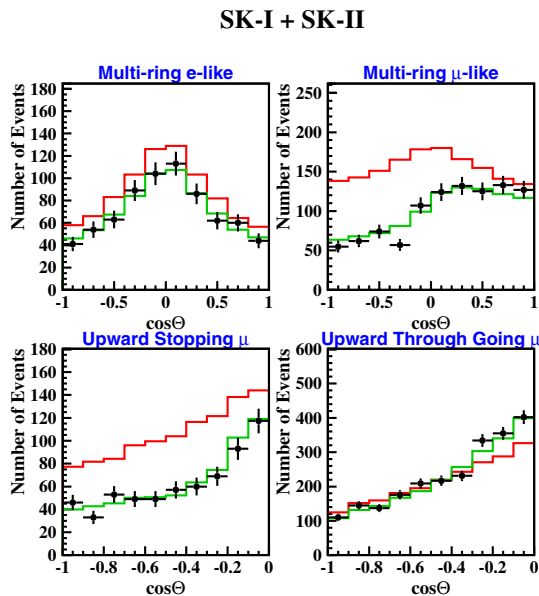


Fig. 4. The zenith angle distributions for multi-ring sub-GeV μ -like (upper left) and multi-ring multi-GeV μ -like (lower left) samples. The zenith angle distributions of upward stopping muons (upper right) and upward through-going muons (lower right). The red histograms show expectations without neutrino oscillations. The green histograms show the expected flux for the $\nu_\mu \leftrightarrow \nu_\tau$ oscillation with $\sin^2 2\theta = 1.0$ and $\Delta m^2 = 2.5 \times 10^{-3} \text{eV}^2$.

multi-ring events is also subdivided into e -like and μ -like events using the event pattern of the most energetic Cherenkov ring in each event. Fig. 4 shows the zenith angle distribution of multi-ring events and they also agree well with the expectations from neutrino oscillations.

Energetic atmospheric ν_μ 's passing through the Earth interact with rock surrounding the detector and produce muons via charged current interactions. These neutrino events are observed as upward going muons. Upward going muons are classified into two types. One is “upward through-going muons” which have passed through the detector, and the other is “upward stopping muons” which come into and stop inside the detector. The mean neutrino energies of upward through-going muons and upward stopping muons are ~ 100 GeV and ~ 10 GeV, respectively. SK-I observed 1856 upward through-going muons and 458 upward stopping muons during 1646 days' live time and SK-II observed 889 and 228 events during 828 days, respectively. Fig. 4 shows the zenith-angle distributions of those upward muons. They agree with the expectations assuming neutrino oscillations.

We carried out a neutrino oscillation analysis using the entire SK-I [1] and II atmospheric neutrino data. Fig. 5 shows the allowed neutrino oscillation parameter regions for $\nu_\mu \leftrightarrow \nu_\tau$ oscillations. The best fit oscillation parameters are $\sin^2 2\theta = 1.0$ and $\Delta m^2 = 2.5 \times 10^{-3} \text{eV}^2$. The allowed oscillation parameter range is obtained to be $\sin^2 2\theta > 0.93$ and $\Delta m^2 = (1.9 - 3.1) \times 10^{-3} \text{eV}^2$ at 90% C.L.

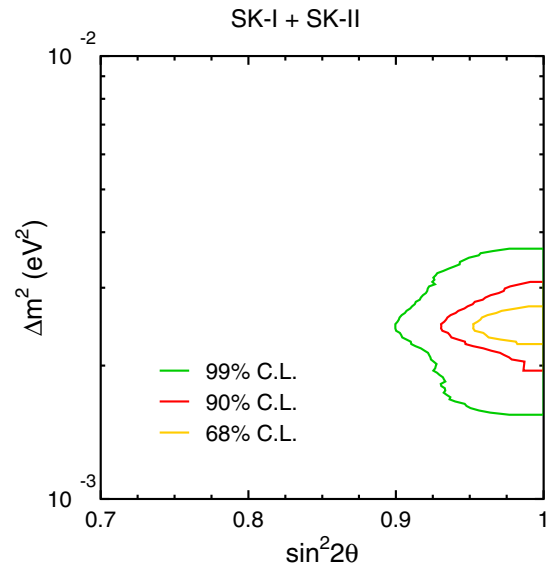


Fig. 5. Allowed region of $\nu_\mu \rightarrow \nu_\tau$ neutrino oscillation parameters obtained by SK by using contained atmospheric neutrino events and the upward-going muon events.

The atmospheric neutrino data is well described by the neutrino oscillations shown above. In this case, the survival probability of ν_μ is given by a sinusoidal function of L/E , where L is the travel distance, E is the neutrino energy. However, the sinusoidal L/E dependence of the survival probability of ν_μ has not yet been directly observed. We used a selected sample of these atmospheric neutrino events, those with good resolution in L/E , to search for an oscillation max-

imum in the L/E distribution.

The neutrino energy, E , was estimated from the total energy of charged particles observed in the inner detector. The flight length of neutrinos, L , which ranges from approximately 15 km to 13,000 km depending on the zenith angle, was estimated from the reconstructed neutrino direction. The neutrino direction was taken to be along the total momentum vector from all observed particles. Since the correlation between neutrino directions and the directions of observed particles are taken into account in Monte Carlo simulations, we applied same analysis both for real events and Monte Carlo events. We applied a cut to reject low energy or horizontal-going events since they have either large scattering angles or large $dL/d\Theta_{\text{zenith}}$.

Fig. 6 shows the observed L/E distribution after taking ratio to the Monte Carlo events without neutrino oscillations. In the figure, a dip, which should corresponds to the first oscillation maximum, is observed around $L/E = 500 \text{ km/GeV}$. The distribution was fit assuming $\nu_\mu \leftrightarrow \nu_\tau$ oscillations. The best-fit expectation shown in the figure corresponds to $(\sin^2 2\theta, \Delta m^2) = (1.00, 2.3 \times 10^{-3} \text{ eV}^2)$. Fig. 7 shows the contour plot of the allowed oscillation parameter regions. The result is consistent with that of the oscillation analysis using zenith angle distributions. The observed L/E distribution gives the first direct evidence that the neutrino survival probability obeys the sinusoidal functions as predicted by neutrino flavor oscillations.

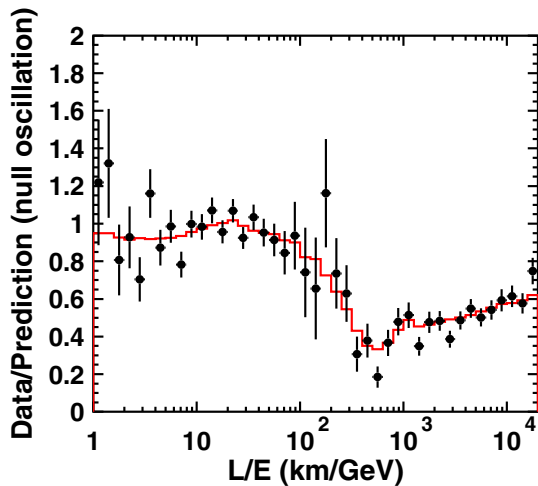


Fig. 6. Ratio of the data to the MC events without neutrino oscillation (points) as a function of the reconstructed L/E together with the best-fit expectation for 2-flavor $\nu_\mu \leftrightarrow \nu_\tau$ oscillation (red line). The error bars are statistical only.

Another interest is an observation of ν_τ in the atmospheric neutrinos since there has not been apparent evidence for the appearance of ν_τ charged current interactions due to $\nu_\mu \leftrightarrow \nu_\tau$ oscillations. We have performed a search for the ν_τ appearance by using the SK-I atmospheric neutrino data [2]. The analysis is based on two statistical methods: a likelihood analysis and a neural network. Since τ 's produced in the Super-K detector would immediately decay into many hadrons, the event pattern would be similar to that of high-energy multi-ring ν_e events. Using the statistical difference in τ -like and

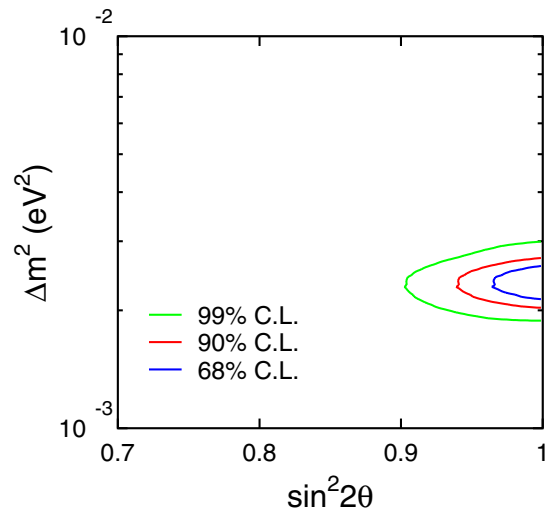


Fig. 7. 68, 90 and 99% C.L. allowed oscillation parameter regions for 2-flavor $\nu_\mu \leftrightarrow \nu_\tau$ oscillations obtained in the L/E analysis.

background events, we have derived the variables to select an enriched sample of ν_τ charged current events in the atmospheric neutrino data. The differences appear in the energy spectrum, the number of charged pions in the final state, the fraction of lepton energy with respect to neutrino energy and so on. We optimized a combination of the variables and defined a likelihood function so that the signal to noise ratio becomes the maximum. We also use the neural network for the analysis. Before these analyses, we applied a pre-selection: (1) fiducial events, (2) multi-GeV, and (3) the most energetic ring is e -like.

After the pre-selection and cuts based on the likelihood and neural network, we fit the zenith angle distribution of a ν_τ enriched sample to a combination of the expected ν_τ and the atmospheric neutrinos (ν_μ and ν_e) including oscillations with the oscillation parameter, $\sin^2 2\theta = 1.0$ and $\Delta m^2 = 2.1 \times 10^{-3} \text{ eV}^2$. Fig. 8 shows the fitted zenith angle distribution. Using τ selection efficiencies estimated by Monte Carlo study, we concluded the number of tau events with SK-I exposure is $138 \pm 48^{+14.8}_{-31.6}$ for the likelihood analysis and $134 \pm 48^{+16.0}_{-27.2}$ for the neural network while 78.4 ± 26 and 8.4 ± 27 are expected for each analysis. Thus the fitted results are found to be consistent with pure $\nu_\mu \leftrightarrow \nu_\tau$ oscillations and ν_τ appearance.

The two flavor neutrino oscillations successfully described the SK atmospheric neutrino data. However, any contributions by electron neutrinos have not been observed yet. We extended our neutrino oscillation analysis in order to treat three neutrino flavors. For the analysis, $\Delta m_{23}^2 \sim \Delta m_{13}^2 \equiv \Delta m^2 \gg \Delta m_{12}^2$ was assumed. If the parameter θ_{13} in the mixing matrix of lepton sector (MNS matrix) is finite, neutrino oscillations among $\nu_\mu \leftrightarrow \nu_e$ may be observed. Moreover, the mixing parameter is affected by potentials caused by matter and oscillations are expected to have a resonance around 5 GeV. Therefore, we can expect an increase at upward-going Multi-GeV e -like samples. Fig. 9 shows the result of the three-flavor neutrino oscillation analysis. Though there was no significant excess of electrons, we set an upper limit on θ_{13} . More statis-

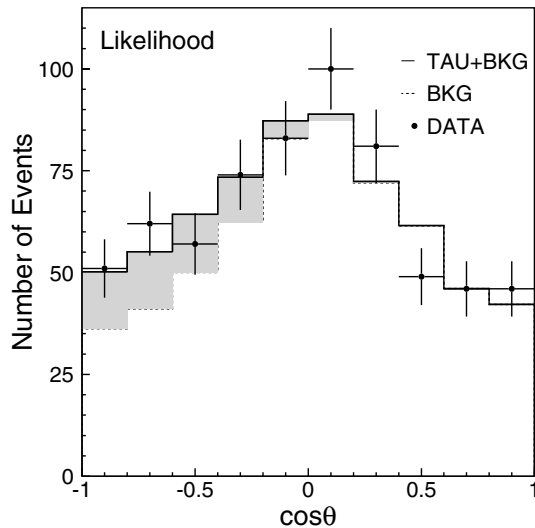


Fig. 8. The zenith angle distribution for tau candidate events in the likelihood analysis. The dashed histogram (background neutrinos) and the solid line (excess by ν_τ) show the best fit for the data.

tics is needed to have better sensitivity [3].

Solar neutrinos

SK detects solar neutrinos through neutrino-electron scattering, $\nu + e \rightarrow \nu + e$, with which the energy, direction and time of the recoil electron are measured. Due to its large fiducial mass of 22.5 kilotons, SK gives the most precise measurement of the solar neutrinos' flux with accurate information of the energy spectrum and time variations. For this precision experiment precise calibrations are performed for the energy scale, energy resolution, angular resolution and the vertex position resolution using a LINAC and ^{16}N radioisotope generated by a DT neutron generator.

The SK-I measurement from May 1996 until July 2001 yielded 22,400 solar neutrino events with the 5 MeV energy threshold. This corresponds to the ^8B solar ν flux of 2.35 ± 0.02 (stat.) ± 0.08 (sys.) $\times 10^6 \text{ cm}^{-2} \text{ s}^{-1}$ assuming the events purely due to $\nu_e e$ elastic scattering and the undistorted ^8B beta decay spectrum. We have submitted the full paper[5] in this year.

In this year, we also reported preliminary results from SK-II solar neutrino analysis, obtained from 791 day live-time runs between 2002 Dec. 24 and 2006 Oct. 5 with the analysis energy threshold set at 7.0 MeV. The obtained solar neutrino flux is 2.38 ± 0.05 (stat.) $^{+0.16}_{-0.15}$ (syst.) $\times 10^6 \text{ cm}^{-2} \text{ s}^{-1}$. This is consistent with the SK-I result, but with a larger error. The day- and night-time fluxes in 7.5 MeV – 20MeV energy region are 2.31 ± 0.07 (stat.) $\times 10^6 \text{ cm}^{-2} \text{ s}^{-1}$ and 2.46 ± 0.07 (stat.) $\times 10^6 \text{ cm}^{-2} \text{ s}^{-1}$, respectively, means day-night asymmetry of -6.4 ± 4.3 (stat.)%. The systematic errors on the day/night asymmetry are under study.

The possible time variation of the solar neutrino signal was also studied. Figure 10 shows the time variation of SK-I and SK-II. There was no indication of the time variation.

The preliminary energy spectrum of the solar neutrino signals in SK-II was also obtained. The energy spectrum of the

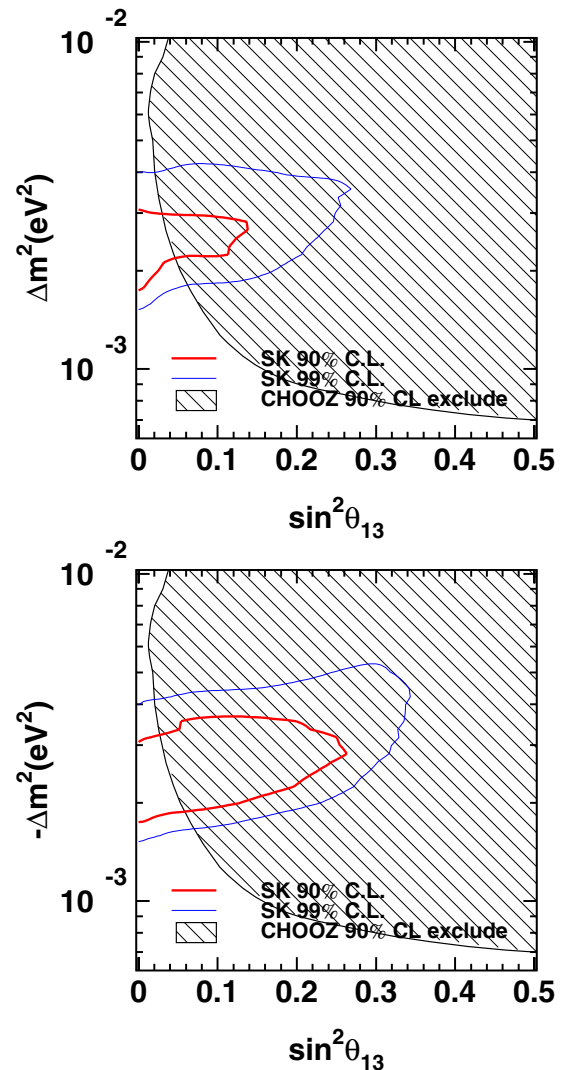


Fig. 9. The allowed region for $(\Delta m^2, \sin^2 \theta_{13})$ in case of normal (upper figure) and inverted (lower figure) hierarchy. We assumed positive Δm^2 . The red and blue contours correspond to allowed regions obtained by this analysis. The hatched region corresponds to 90% C.L. excluded area by CHOOZ experiment.

solar neutrinos is independent from SSM, and it is sensitive to the neutrino oscillation parameters. Therefore, a SSM-independent study of the solar neutrino oscillation is possible from the energy spectrum observation. Figure 11 shows the energy spectra from SK-I and SK-II. The energy spectrum of SK-II is consistent with that of SK-I. No indication was found for the energy spectrum distortion.

The preliminary neutrino oscillation analysis with SK-I and SK-II data samples was also obtained. Figure 12 shows a 2-flavor oscillation analysis result from SK-I and SK-II. This analysis uses only energy shape and day/night flux difference. Therefore, it is SSM-independent. A large area in the neutrino oscillation parameter region are excluded from SK. A global analysis with other experiments are on going.

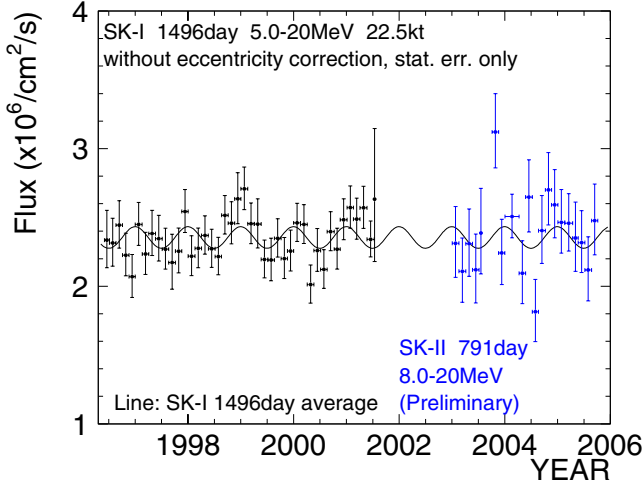


Fig. 10. Time variation of the solar neutrino signal of SK-I and SK-II. The vertical axis is the observed ^8B solar neutrino flux. The solid line shows the SK-I average without the Earth orbit's eccentricity correction.

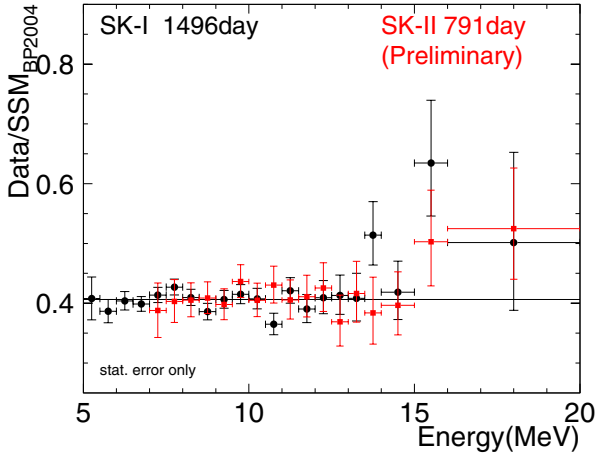


Fig. 11. Energy spectrum of the solar neutrino signal. The black and red points correspond to SK-I final result and SK-II 791 days data, respectively. The horizontal axis is the total energy of the recoil electrons. The vertical axis is the ratio of the event rates between the observation and the BP04 SSM prediction. The horizontal line shows the SK-I flux value.

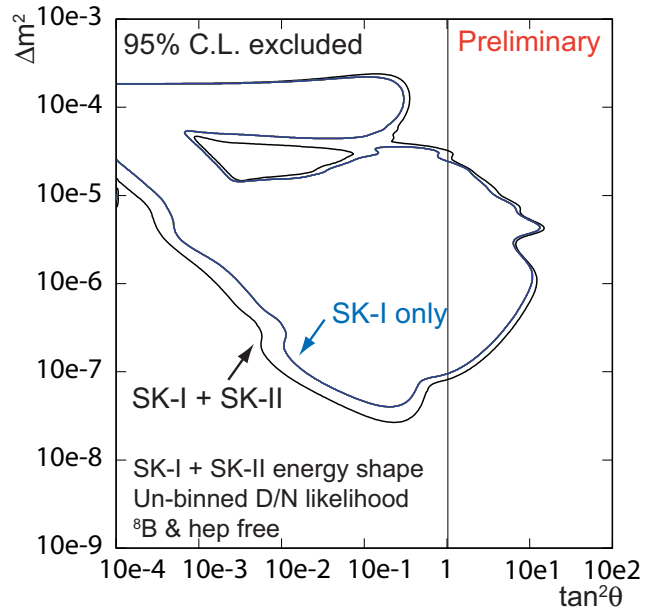


Fig. 12. A 2-flavor oscillation analysis result from SK-I and SK-II. The blue and black lines correspond to SK-I only and SK-I + SK-II combined, respectively. The input data are energy spectrum shape and un-binned day/night flux difference likelihood. The ^8B and hep solar neutrino fluxes are treated as free.

Search for nucleon decay

Proton decays and bound neutron decays (nucleon decays in general) is a most dramatic prediction of Grand Unified Theories in which three fundamental forces of elementary particles are unified into a single force. Super-Kamiokande (SK) is the world largest detector to search for nucleon decays and it has accumulated data of 91.6 kt-yrs (SK-I) and 25.9 kt-yrs (SK-II) resulting in 117.5 kt-yrs data in total. Various nucleon decay modes have been looked for in the SK but we found no significant signal excess so far.

A proton decay into one positron and one neutral pion ($p \rightarrow e^+\pi^0$) is one of most popular decay mode. This decay mode is mediated by super-heavy gauge bosons and discovery of the signal would give us the information of the mass of the gauge mesons. To discriminate the signal from atmospheric neutrino background, we reconstruct the number of particles (Cherenkov rings) and reconstruct the total visible energy corresponding to parent proton mass and total momentum corresponding to proton's Fermi momentum. Even the photo-coverage area is about half (19%) in SK-II, we achieved high detection efficiency of signals as 41% and low background levels as 0.1 events in 25.9 kt-yrs of SK-II. Because there are no candidate events in SK-I + SK-II data, we obtained lower limit on the partial lifetime of the proton, $\tau/B_{p \rightarrow e^+\pi^0} > 6.9 \times 10^{33}$ years at a 90% confidence level.

Moreover, we looked for SUSY favored decay modes which include K mesons in final state; $p \rightarrow \bar{\nu}K^+$, $n \rightarrow \bar{\nu}K^0$, $p \rightarrow \mu^+K^0$, and $p \rightarrow e^+K^0$. In $p \rightarrow \bar{\nu}K^+$ search, we looked for 236 MeV/c monochromatic muons from the decay of K^+ . Figure 13 shows the comparison between data and fitting results of muon momentum distribution for single-ring μ -like events. We observed no excess of signal. In any other modes,

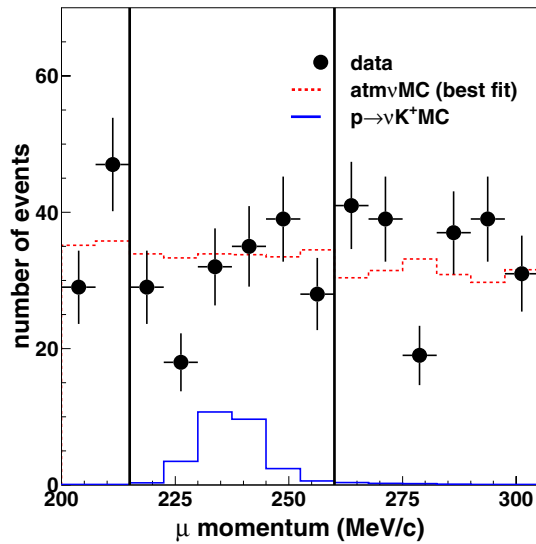


Fig. 13. The comparison between data and fitting results of muon momentum distribution for single-ring μ -like events. The filled circles show data with statistical errors. The solid line shows $p \rightarrow \bar{\nu}K^+$ MC. The dashed line shows the best fitted atmospheric neutrino MC with free normalization.

there are no significant signal excess. Therefore we conclude that there is no evidence of nucleon decays and we calculated partial lifetime limits taking into account systematic uncertainties. Obtained limits are 2.3×10^{33} , 1.3×10^{32} , 1.3×10^{33} , 1.0×10^{33} , years at 90% confidence level for $p \rightarrow \bar{\nu}K^+$, $n \rightarrow \bar{\nu}K^0$, $p \rightarrow \mu^+K^0$, and $p \rightarrow e^+K^0$ modes, respectively [3].

Supernova neutrinos

Kamiokande and IMB observed neutrino burst from supernova 1987a. Those observations confirmed that the energy release by neutrinos is about several $\times 10^{53}$ erg. Super-Kamiokande is able to detect several thousand neutrino events if it happens near the center of our galaxy.

During 1703.9 days of SK-I data taking period, there was no evidence of such supernova explosions, and the 90% C.L. upper limit on the rate of supernova explosions within 100 kpc is obtained to be 0.49 explosions per year.

After the reconstruction of SK-II, the realtime supernova monitor system was restarted again as in SK-I. If a supernova is detected, this monitor reports it to shift persons in 5–10 minutes later. This monitor also sends a signal to SNEWS (the SuperNova Early Warning System) which takes coincidence of signals from SK, SNO, and LVD. Until now, no coincidence events were observed.

Due to the half photocoverage of SK-II, the energy threshold for the real time monitor was raised from 6.5 MeV to 8.5 MeV. However, since dominant signals of supernova neutrinos have around 15 MeV energy, the decrease of the detection efficiency is small, and SK-II still has 100% efficiency for galactic supernovae.

Bibliography

- [1] Super-Kamiokande Collaboration, “A Measurement of Atmospheric Neutrino Oscillation Parameters by Super-

Kamiokande I”, Phys. Rev. D 71 (2005) 112005.

- [2] Super-Kamiokande Collaboration, “A measurement of atmospheric neutrino flux consistent with tau neutrino appearance”, Submitted to Phys. Rev. Lett., hep-ex/0607059.
- [3] Super-Kamiokande Collaboration, “Three flavor neutrino oscillation analysis of atmospheric neutrinos in Super-Kamiokande”, Phys. Rev. D 74 (2006) 032002.
- [4] K. Kobayashi *et al.* (Super-Kamiokande Collaboration), “Search for nucleon decay via modes favored by supersymmetric grand unification models in Super-Kamiokande-I”, Phys. Rev. D 72, (2005) 052007.
- [5] Super-Kamiokande Collaboration, “Solar Neutrino Measurements in Super-Kamiokande-I”, Accepted by Phys. Rev. D, hep-ex/0508053.
- [6] G. Guillian *et al.* (Super-Kamiokande Collaboration), “Observation of the Anisotropy of 10-TeV Primary Cosmic Ray Nuclei Flux with the Super-kamiokande-I detector”, Submitted to Phys. Rev.D.

K2K Experiment

[Spokesperson : K. Nishikawa]

High Energy Accelerator Research Organization, Japan, Tsukuba 305-0801

In collaboration with the members of:

ICRR, University of Tokyo, Japan; Kyoto University, Japan; KEK, High Energy Accelerator Research Organization, Japan; Kobe University, Japan; Osaka University, Japan; Hiroshima University, Japan; Okayama University, Japan; Niigata University, Japan; Tokyo University of Science, Japan; Tohoku University, Japan; Miyagi Edu. University, Japan; Nagoya University, Japan; Chonnam University, Korea; Seoul National University, Korea; Dongshin University, Korea; Korea University, Korea; University of California at Irvine, USA; State University of New York at Stony Brook, USA; Boston University, USA; University of Washington at Seattle, USA; Louisiana State University, USA; Massachusetts Institute of Technology, USA; University of Hawaii at Manoa, USA; Duke University, USA; TRIUMF, Canada; University of British Columbia, Canada; University of Barcelona, Spain; University of Valencia, Spain; INRM, Russia; CEA Saclay, France; University of Rome, Italy; University of Geneva, Swiss; University of Warsaw, Poland; A. Soltan Institute for Nuclear Studies, Poland; Institute for Nuclear Research, Russia;

The discovery of the neutrino oscillation by Super-Kamiokande in 1998 has led to the conclusion that neutrino has a finite mass. The discovery implies the existence of new physics beyond the standard model of the elementary particles at a huge energy scale. Since the observed neutrino mass difference of $\Delta m^2 \sim 3 \times 10^{-3} \text{eV}^2$ suggests the oscillation length is about a few hundred km for one GeV neutrinos, this phenomena can be experimentally tested by using the artificially

created neutrino beam with the detector placed at a few hundred km away from the neutrino production point.

The k2k experiment was planned to detect such oscillation effect and to determine the oscillation parameters precisely. The neutrino beam created at KEK has a mean energy of 1.3 GeV and was sent to the Super-Kamiokande detector, 250 km west of KEK, every 2.2 seconds with the duration of 1.1 μ second. In the site of KEK, at the distance of 300 m from the target, we have prepared near detectors which mainly consist of 1 kt water Cherenkov detector, fine grained scintillation fiber detector (FGD), a lead glass calorimeter, and the muon ranger. The supplemental detectors are also placed. The arrangement of the front detectors at the beginning of the experiment is shown in Fig. 1. We started the physics run in June 1999 and the experiment was completed in November 2004. Now we have analyzed all the data, which corresponds to 9.2×10^{19} protons on target (POT). The near detector data from this period include 2.3×10^{19} POT without the lead glass (K2K-IIa), and then 2.2×10^{19} POT with a fully-active scintillator detector (SciBar) in its place (K2K-IIb and K2K-IIc).

There are several beam monitors, proton profile monitors, the muon monitor and the pion monitor, placed along the neutrino beam line. The decay length is about 200 m, therefore the beam is not scaled exactly by $1/r^2$ law. The flux ratio of the near to the far detector was obtained by the beam Monte Carlo calculation by taking into account of the spread and emittance of the beam at the target, the production of the pions, the focusing effect by the HORN and the decay of pions to neutrinos. This time, we employ the results from the HARP experiment as an input for simulation of pion production. The beam calculation was validated by the pion monitor which measured the produced pion directions and momentum.

The beam flux and the spectrum were measured by the front detectors. ICRR group has a responsibility of providing the Super-Kamiokande data and the construction of the 1 kt front detector and the analysis of the data from those detector components. The coverage of PMT in the 1 kt front detector is same as the Super-Kamiokande detector with the 40% of the total inner detector surface. The 1kt detector provides information of the absolute neutrino flux and the spectrum of

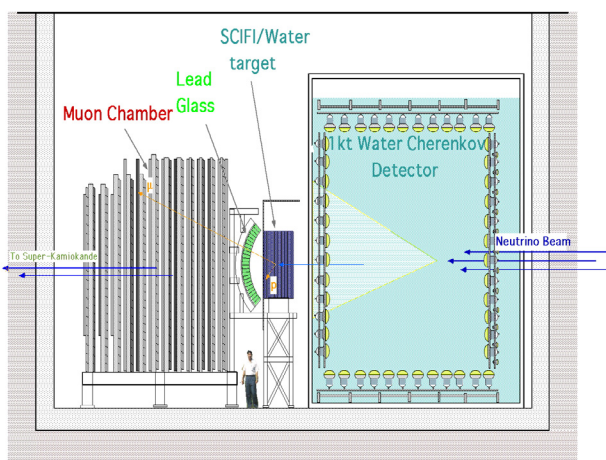


Fig. 1. The arrangement of the near detectors.

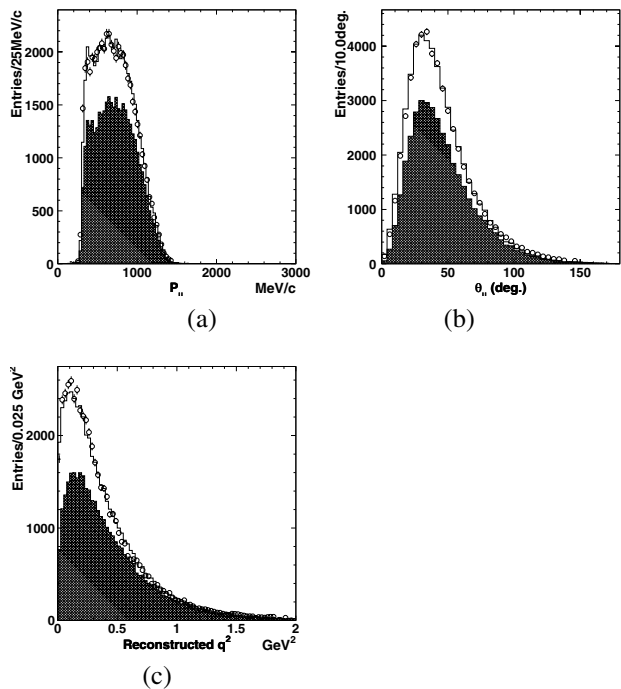


Fig. 2. Muon momentum (p_μ), direction (θ_μ) and reconstructed q^2 distributions: (a) the p_μ distribution of 1KT fully contained 1-ring μ -like sample, (b) 1KT θ_μ for the same sample, (c) 1KT reconstructed q^2 for the same sample. Open circles represent data, while histograms are MC predictions using the best fit systematic uncertainties.

the neutrino beam. Figure 2 shows (a) the muon momentum spectrum, (b) the muon direction and (c) the reconstructed q^2 by using the single ring fully contained events at 1 kt detector. The observed spectrum is well reproduced by the Monte Carlo simulation in which beam energy spectrum and neutrino interaction in water are taken into account. Combining the 1 kt data and the FGD data together with constraints of the results from the HARP experiment and the measurement of pion monitor, the expected neutrino energy spectrum was obtained for the far detector. All the systematic errors due to detector bias or uncertainty of neutrino interactions were carefully taken into account.

The synchronization of the timing between KEK 12 GeV Proton Synchrotron and Super-Kamiokande detector was performed using a GPS system. Figure 3 shows the timing distribution of the fully contained events observed at Super-Kamiokande with respect to the proton beam injection timing. The time of flight of neutrinos from KEK to Super-Kamiokande ($\sim 830 \mu$ sec) is corrected in the figure.

Neutrino events were clearly observed near $\Delta T=0$ and the spread in the timing was consistent with the duration of beam injection at KEK 12 GeV PS. In total, 112 events were identified as K2K beam induced events at Super-Kamiokande. Using the large number of observed neutrino events at front detectors, expected number of neutrino events at Super-Kamiokande was calculated to be $158.1_{-8.6}^{+9.2}(\text{syst})$ assuming no-oscillation.

58 μ -like single ring events were observed and the neutrino energy spectrum obtained from the energy and scattering angle of the observed muons is shown in Fig. 4. From the

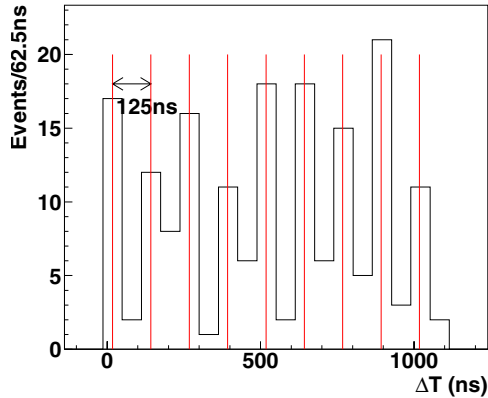


Fig. 3. The timing distribution of fully contained event observed at Super-Kamiokande with respect to the beam injection timing. Periodical structure coming from proton beam bunches is seen in the Super-Kamiokande, 250 km away from the accelerator.

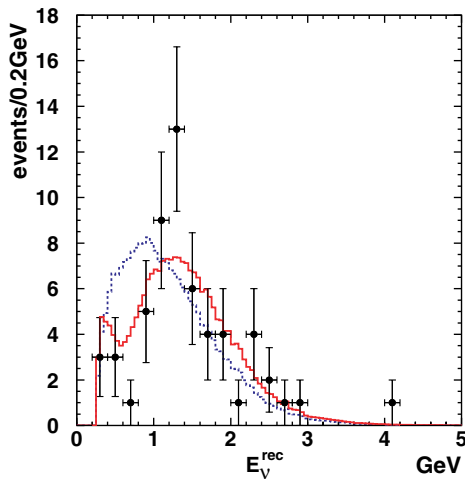


Fig. 4. The reconstructed E_ν distribution from single ring fully contained events at SK. Points with error bars are data. The solid line is the best fit spectrum. The dashed line shows the expected spectrum without oscillation. Both histograms are normalized by the number of events observed(58).

deficit of observed number of events together with the shape distortion of neutrino energy spectrum, we have concluded that probability of null oscillation is 0.0015% (4.3σ). The allowed region of Δm^2 and $\sin^2 2\theta$ is shown in Fig. 5. The obtained result for neutrino oscillation parameters are consistent with that from atmospheric neutrino oscillations.

We have also searched for the ν_e appearance in a beam of ν_μ , which is the signature of finite value of the unknown mixing parameter θ_{13} . As a result, no evidence for a ν_e appearance signal was found. Therefore, we set bounds on the oscillation parameters. Figure 6 shows the upper bound on the oscillation parameters for two flavor mixing, at the 90% and 99% confidence level (C.L.). At $\Delta m^2 = 2.8 \times 10^{-3} \text{eV}^2$, we set an upper limit of $\sin^2 2\theta_{13} = 0.26$ at 90% confidence level, assuming $\sin^2 2\theta_{\mu e} = \frac{1}{2} \sin^2 2\theta_{13}$ and $\Delta m_{\mu e}^2 \sim \Delta m_{13}^2$.

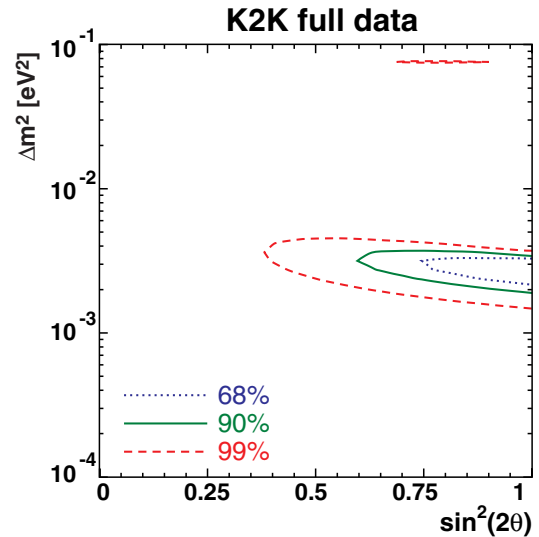


Fig. 5. Allowed regions of ν_μ - ν_τ oscillation parameters. Dashed, solid and dot lines are 68.4%, 90% and 99% C.L. contours, respectively.

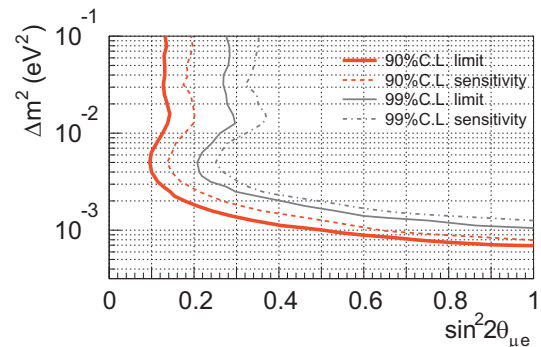


Fig. 6. The upper bound on ν_μ to ν_e oscillation parameters at 90% and 99% C.L. The sensitivities of the K2K experiment for each C.L. are also indicated with dashed lines.

Bibliography

- [1] K2K collaboration, Detection of accelerator produced neutrinos at a distance of 250 km, *Phys. Lett. B*, 511, 178–184, 2001.
- [2] K2K collaboration, Indication of neutrino oscillation in a 250 km long baseline experiment, *Phys. Rev. Lett.*, 90, 041801, 2003.
- [3] K2K collaboration, Search for Electron Neutrino Appearance in a 250 km Long-baseline Experiment, *Phys. Rev. Lett.*, 93, 051801, 2004.
- [4] K2K collaboration, Measurement of single π^0 production in neutral current neutrino interactions with water by a 1.3 GeV wide band muon neutrino beam, *Phys. Lett. B*, 619, 255, 2005.
- [5] K2K collaboration, Evidence for muon neutrino oscillation in an accelerator-based experiment *Phys. Rev. Lett.*, 94, 081802, 2005.
- [6] K2K Collaboration, Search for coherent charged pion production in neutrino carbon interactions, *Phys. Rev. Lett.*, 95, 252301 2005.

- [7] K2K Collaboration, An improved search for $\nu/\mu - \bar{\nu}_i$ ν/e oscillation in a long-baseline accelerator experiment, *Phys. Rev. Lett.*, 96, 181801, 2006.
- [8] K2K Collaboration, Measurement of the quasi-elastic axial vector mass in neutrino oxygen interactions, *Phys. Rev. D*, 74, 052002, 2006.
- [9] K2K Collaboration, Measurement of neutrino oscillation by the K2K experiment, *Accepted by Phys. Rev. D*, hep-ex/0606032.

XMASS Experiment

[Spokesperson : Yoichiro Suzuki]

Kamioka Observatory, ICRR, Univ. of Tokyo, Gifu, 506-1205

In collaboration with the members of:

Kamioka Observatory, ICRR, Univ. of Tokyo, Japan; RCCN, ICRR, Univ. of Tokyo, Japan; Waseda Univ., Japan; Yokohama National Univ., Japan; Miyagi Univ. of Education, Japan; Nagoya Univ., Japan; Saga Univ., Japan; Gifu Univ., Japan; Seoul National Univ., Korea; INR-Kiev, Russia; Univ. of California, Irvine, USA; Sejon Univ., Korea.

Overview

XMASS is a multi-purpose experiment using liquid xenon aiming at the detection of cold dark matter, neutrino absolute mass using neutrinoless double beta decay, and low energy solar neutrinos. An R&D study for the liquid xenon detector is being performed at Kamioka observatory.

Astronomical observations suggest that there is “dark matter” (non-luminous particles with mass) in the universe. One of the most likely candidates for dark matter is a weakly interacting massive particle (WIMP) like the lightest supersymmetry particle. A recoil of xenon by dark matter produces scintillation light in liquid xenon.

The Super-Kamiokande measurements show that neutrinos have masses. However, we do not know yet the absolute mass of neutrinos and the whether neutrino masses are Majorana type or Dirac type. Xenon nuclei with mass number 136 is one of the double beta nuclei which is best suited for this research.

The solar neutrino spectrum is measured only above 5 MeV by SK and SNO so far. The spectrum of low energy solar neutrinos (pp and ^7Be neutrinos and etc.) are not measured yet. If a 10-ton class liquid xenon detector is constructed, it will be able to detect those neutrinos by $\nu+e$ scattering with a rate of about 10 events/day.

Liquid xenon has the following advantages:

- A large light yield of 42,000 photons/MeV, which is as good as NaI(Tl) scintillator, enables detection of small energy signals like dark matter recoil.
- Because of the higher atomic number of xenon ($Z=54$) and higher density of liquid xenon ($\sim 3\text{g/cm}^3$), external gamma-ray background can be reduce in a short distance from the detector wall by self-shielding.

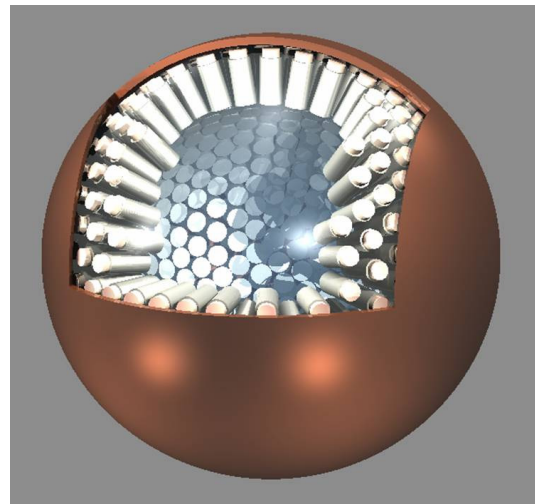


Fig. 1. Schematic view of the proposed 800 kg liquid xenon detector aiming at dark matter search. The detector has a sensitivity of $10^{-45} \sim 10^{-44}\text{cm}^2$ in cross section which is more than two orders of magnitude better than the current best limits in the world.

- 175 nm scintillation light of liquid xenon can be read out by typical PMTs of bi-alkaline photocathode with a quartz window.
- Purification is easier than other materials (e.g. distillation is possible).
- Isotope separation is possible. It is possible to enrich ^{136}Xe for double beta decay and deplete ^{136}Xe for solar neutrino measurements.

A 3 kg fiducial volume liquid xenon detector has been developed for the R&D study and test data was taken in 2003 and 2004.

We plan to make an 800 kg detector (Fig.1) aiming to search for dark matter down to $10^{-45} \sim 10^{-44}\text{cm}^2$ in cross section which is more than two orders of magnitude better than the current best limits in the world.

R&D study by a 3 kg fiducial volume detector

Fig. 2 shows the 30 liter (3 kg fiducial volume) liquid xenon detector developed for the R&D study. It is a 30 cm cubic detector viewed by 54 2-inch PMTs. The PMTs are Hamamatsu R8778 which were developed by collaborating with Hamamatsu and can be used for low background purposes and also can be used at liquid xenon temperature ($\sim 170\text{K}$). The detector is placed in a low background setup which consists of 5 cm-thick pure copper (OFHC), EVOH sheets, 15 cm-thick lead, 10 cm-thick boric acid, and 15 cm-thick polyethylene for reducing gamma rays, neutron and radon backgrounds.

Test data was taken in December 2003 and August 2004. Fig. 3 shows the background distributions for the latest measurement with an improved analysis. We reduced background at low energy in 10 cm cube at the center of the detector by one order of magnitude. This was achieved by identifying and reducing misreconstructed events which were expected to dominate in the low energy background. There is enough detection efficiency ($> 50\%$) for energy larger than 50 keV even after applying this reduction. The background,



Fig. 2. 3 kg fiducial volume liquid xenon detector constructed for R&D study

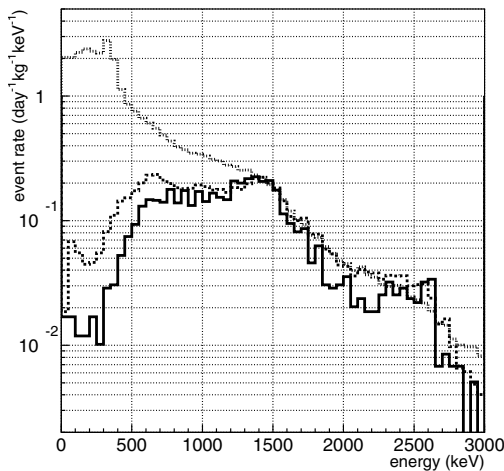


Fig. 3. Background spectrum measured by the 3 kg fiducial volume detector. The dashed, dotted and solid histograms show the rate of the events which were observed in all volume, 20 cm and 10 cm cube centered at the center of the detector, respectively.

10^{-2} events/keV/day/kg, is as expected by Monte Carlo simulations.

Development of hexagonal PMTs for 800 kg detector

For the 800 kg detector, we are developing hexagonal PMTs shown in Fig. 4. These PMTs are important because (1) the hexagonal shape maximizes photo electron yield which enables us to lower the energy threshold to around 5 keV, (2) they can be used in liquid xenon so that the effect of misreconstruction observed in the prototype detector will be negligible, (3) background will be further reduced by improving the material of the PMTs. Based on these improvements, we expect 10^{-4} events/kg/day/keV in the 800 kg detector at an energy region where signals of dark matter can be observed.

Bibliography

- [1] Y. Suzuki et al., “Low energy solar neutrino detection by using liquid xenon,” Aug. 2000, hep-ph/0008296.



Fig. 4. Hexagonal PMT for the 800 kg detector.

- [2] Y. D. Kim, “The status of XMASS experiment,” proceedings of the International Conference on Non-Accelerator New Physics, Dubna, Russia, 20–25 June 2005.
- [3] Y. Takeuchi, “Distillation purification of xenon for krypton of radon contamination in liquid xenon,” presentation in the Workshop on Applications of Rare Gas Xenon to Science and Technology, Tokyo, Japan, 8-10 Mar. 2005.
- [4] Y. Koshio, “The current status of XMASS using 100 kg detector,” presentation in the Workshop on Applications of Rare Gas Xenon to Science and Technology, Tokyo, Japan, 8-10 Mar. 2005.

HIGH ENERGY COSMIC RAY DIVISION

Overview

Three major research activities of the High Energy Cosmic Ray division are the study of very high energy gamma-rays by the CANGAROO group, extremely high energy cosmic rays by the Telescope Array (TA) group, and very high energy cosmic rays and gamma-rays by the Tibet AS γ Collaboration. Other activities, such as experiments utilizing the Akeno observatory, the Norikura observatory, the Mt. Chacaltaya observatory (jointly operated with Bolivia), and the emulsion-pouring facilities are closely related to inter-university joint research programs. Also an all-sky high resolution air-shower detector (Ashra) has been developed and is under installation on the Hawaii island.

The CANGAROO project (Collaboration of Australia and Nippon for a GAMMA-Ray Observatory in the Outback) is a set of large imaging Cherenkov telescopes to make a precise observation of high-energy air showers originated by TeV gamma-rays. It started as a single telescope with a relatively small mirror (3.8 m in diameter) in 1992. In 1999 a new telescope with a 7-m reflector has been built, and now it has a 10-m reflector with a fine pixel camera. The main purpose of this project is to explore the violent, non-thermal universe and to reveal the origin of cosmic-rays. An array of four 10-m telescopes has been completed in March 2004 so that more sensitive observation of gamma-rays is realized with its stereoscopic imaging capability of Cherenkov light. Several gamma-ray sources have been detected in the southern sky and detailed study of these sources are now ongoing.

At the Akeno observatory, a series of air shower arrays of increasing geometrical sizes were constructed and operated to observe extremely high energy cosmic rays (EHECRs). The Akeno Giant Air Shower Array (AGASA) was operated from 1991 to January 2004 and covered the ground area of 100 km² as the world largest air shower array. In 13 years of operation, AGASA observed a handful of cosmic rays exceeding the theoretical energy end point of the extra-galactic cosmic rays (GZK cutoff) at 10²⁰ eV. The Telescope Array (TA), a large plastic scintillator array with air fluorescence telescopes under construction in Utah, USA, will succeed AGASA and measure the EHECRs with an order of magnitude larger aperture than that of AGASA to unveil the origin of super-GZK cosmic rays discovered by AGASA. It will be completed by March 2007.

An air shower experiment aiming to search for celestial gamma-ray point sources started in 1990 with Chinese physicists at Yangbajing (Tibet, 4,300 m a.s.l.) and has been successful. This international collaboration is called the Tibet AS γ Collaboration. An extension of the air shower array was completed in 1995 and an emulsion chamber has been combined with this air shower array since 1996 to study the primary cosmic rays around the knee energy region. After successive extensions carried out in 1999, 2002 and 2003, the total area of the air shower array amounts to 37,000 m². The

sun's shadow in cosmic rays affected by the solar magnetic was observed for the first time in 1992, utilizing its good angular resolution at multi-TeV energy region. From this experiment with better statistics, we expect new information to be obtained on the large-scale structure of the solar and interplanetary magnetic field and its time variation due to the 11-year-period solar activities.

A new type of detector, called Ashra (all-sky survey high resolution air-shower detector), has been developed and the first-phase stations are under installation near the Mauna Loa summit in the Hawaii Island. It monitors optical and particle radiation from high-energy transient objects with a wide field-of-view. Real observation will start soon.

CANGAROO-III Project

[Spokespersons : R.W. Clay, M. Mori, and T. Tanimori]

In collaboration with the members of:

Institute for Cosmic Ray Research, University of Tokyo, Chiba, Japan; School of Chemistry and Physics, University of Adelaide, Australia; Mt Stromlo and Siding Spring Observatories, Australian National University, Australia; Dept. of Radiological Sciences, Ibaraki Prefectural University of Health Sciences, Ibaraki, Japan; Faculty of Science, Ibaraki University, Ibaraki, Japan; Institute of Space and Astronautical Science, Japan Aerospace Exploration Agency, Kanagawa, Japan; School of Allied Health Sciences, Kitasato University, Kanagawa, Japan; Department of Physics, Konan University, Hyogo, Japan; Department of Physics, Kyoto University, Kyoto, Japan; Solar-Terrestrial Environment Laboratory, Nagoya University, Aichi, Japan; National Astronomical Observatory of Japan, National Institutes of Natural Sciences, Tokyo, Japan; Faculty of Engineering, Shinshu University, Nagano, Japan; Department of Physics, Tokai University, Kanagawa, Japan; Department of Physics, Yamagata University, Yamagata, Japan; Faculty of Management Information, Yamanashi Gakuin University, Yamanashi, Japan.

Status of the Project

The CANGAROO-III stereoscopic Cherenkov telescope system has been in operation since March 2004 with four imaging Cherenkov telescopes of 10 m diameter. Three of the four telescopes are currently used in observations as the first telescope, completed in 2000 and having been used as CANGAROO-II, has degraded and is equipped a different electronics system from the others. A stereoscopic triggering system was installed at the beginning of 2005 and works smoothly now, rejecting most single muon events, which are the major background component at low energies.

Single muon ring events are, on the other hand, useful for calibrating the telescopes since their Cherenkov light yield is

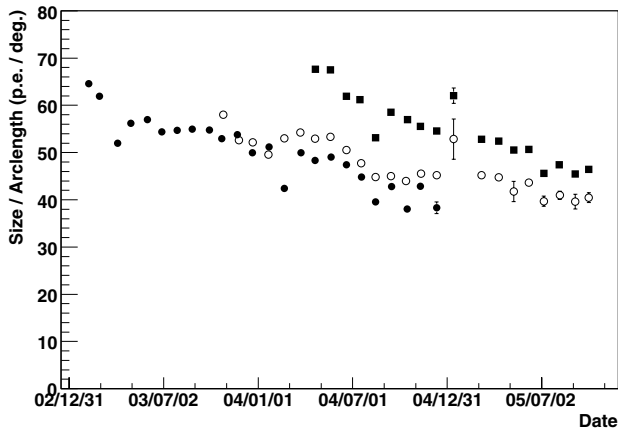


Fig. 1. Size / arclengths for single muon ring events plotted as a function of time (preliminary). This calibration parameter is almost proportional to the net total response of the telescope. The size / arclengths of T2, T3 and T4 are represented by filled circles, open circles and filled squares, respectively. The degradation rate is about 5 % / yr.

well known and atmospheric extinction for the light is negligible because of their proximity. Therefore, we have kept taking muon ring events, spending some time daily even after equipping the stereoscopic triggering system. A calibration procedure for muon data has been established [1] and the calibrated total responses of the telescopes are shown in Fig. 1 as a function of time. It is clearly seen that the responses of each telescope have gradually got worse with age, with that of T2 (second oldest telescope) reaching about 60 % of its initial value at the beginning of 2005.

Maintenance work to clean the surface of the mirror segments was carried out in September and October, 2005. Measurements of the net total reflectivity utilizing star light have been done before and after cleaning the mirrors with water. Reflectivities were successfully improved by a factor of 1.3 ~ 1.6 [2]. Detailed comparison of those measurements with the muon calibration is now underway.

During the maintenance period, mirror segment alignments have been readjusted with an accuracy of $0^\circ.06 \sim 0^\circ.08$. Flash ADC boards developed by the Kyoto group have also been tested.

CANGAROO-III Results

In the 29th International Cosmic Ray Conference held in Pune, India in August 2005, eight contributed papers were presented from CANGAROO [3, 4, 5, 6, 7, 8, 9, 10]. We reported CANGAROO-III upper limits to the fluxes from SN 1006 and PSR B1706-44 [5]. Observations with the CANGAROO-I 3.8 m telescope yielded fluxes for these sources, but these were in conflict with severe upper limits later set by H.E.S.S. ¹ [11, 12]. We have given the first priority to stereoscopic observations of these sources by CANGAROO-III and analyses of the data to resolve the

¹ High Energy Stereoscopic System, which is located in Namibia with four imaging Cherenkov telescopes of 12 m diameter. The collaboration is led by Max-Planck-Institut für Kernphysik, Heidelberg, Germany.

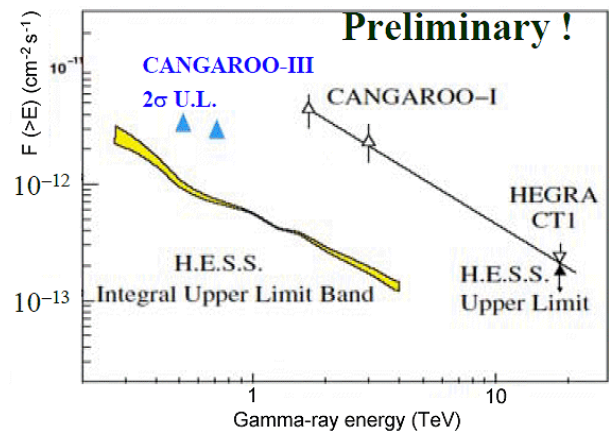


Fig. 2. TeV gamma-ray fluxes from SN 1006, from which TeV gamma-ray signals have been detected by CANGAROO-I (open triangles) and HEGRA CT1 (filled triangle), but the flux upper limits have later been set by H.E.S.S. [11] CANGAROO-III reported the 2σ flux upper limits in ICRC 2005 as shown by the gray triangles [5].

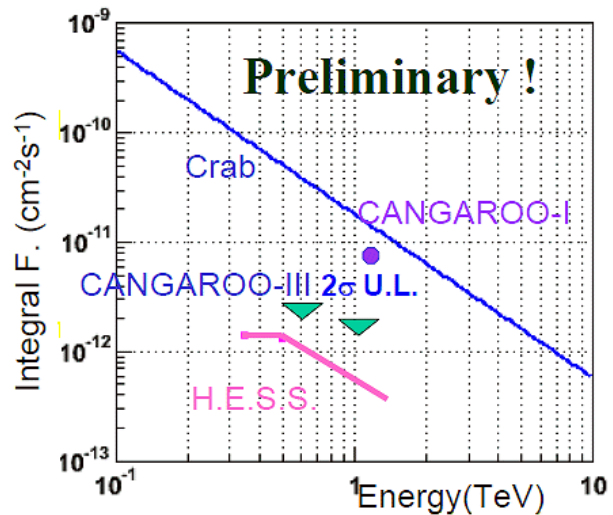


Fig. 3. TeV gamma-ray fluxes from PSR B1706-44. The filled triangles represent 2σ flux upper limits obtained by CANGAROO-III [5], which are significantly lower than the CANGAROO-I flux (filled circle).

above inconsistencies. The 2σ flux upper limits obtained by CANGAROO-III are about five times lower than the CANGAROO-I fluxes as shown in Fig. 2 and 3.

The Vela pulsar region is another source having been under the same situation as the above sources. However, H.E.S.S. recently reported a significant detection of TeV gamma rays from this region but the TeV emission apparently differs in position from the CANGAROO-I source and is extended over the ROSAT X-ray “jet” connecting the pulsar and the strong radio source Vela X [13]. CANGAROO-III also looked at this region in 2004 using the two telescopes (T2 and T3) and a marginal excess of TeV gamma rays has been found [1]. The CANGAROO-III gamma-ray spectrum is consistent with that of H.E.S.S. as shown in Fig. 4. No significant gamma-ray signal has been detected from the pulsar

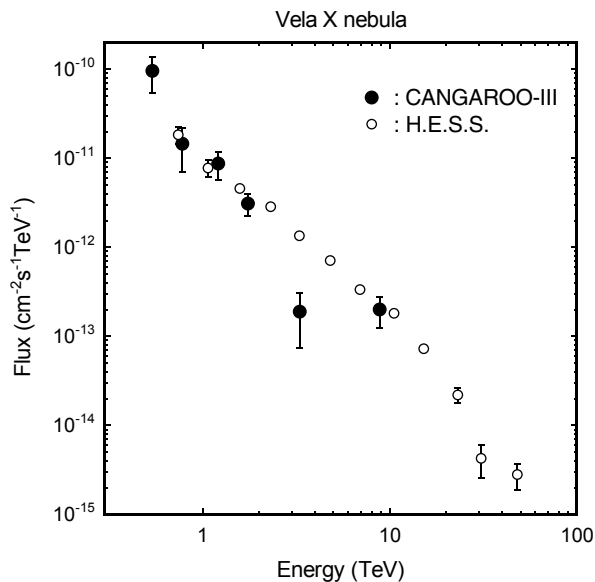


Fig. 4. Differential gamma-ray spectra from Vela X obtained by CANGAROO-III [1] and H.E.S.S. [13]

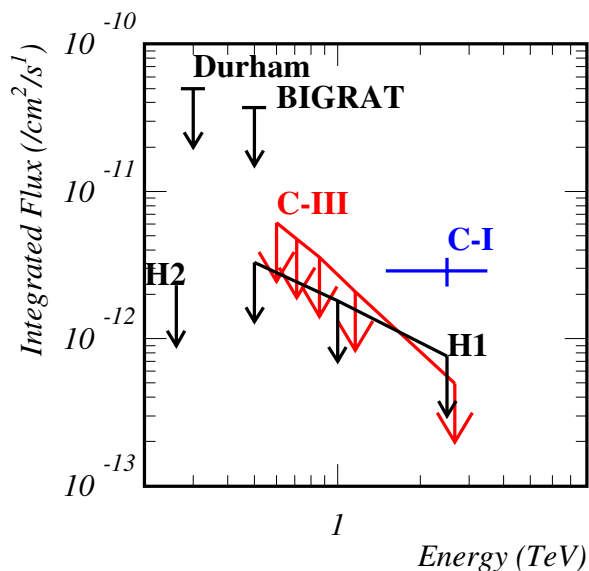


Fig. 5. Upper limits to the TeV gamma-ray flux from the Vela pulsar region. C-I and C-III indicate the CANGAROO-I flux and the CANGAROO-III 2σ upper limits, respectively [1]. Preliminary results from H.E.S.S. (99.9 % C.L. upper limits) are indicated by H1 [14] and H2 [15]. See [1] and references therein for the other points.

position or the CANGAROO-I position and the 2σ flux upper limits have been set as 5.8×10^{-12} photons $\text{cm}^{-2} \text{s}^{-1}$ above 600 GeV and 4.7×10^{-13} photons $\text{cm}^{-2} \text{s}^{-1}$ above 2.7 TeV. The latter is about six times lower than the CANGAROO-I flux as shown in Fig. 5. The analysis procedures have been tested using observed data of the Crab Nebula and Monte Carlo simulations, and for the final result, the Fisher discriminant is used. Fisher discriminant distributions obtained from observed Crab data and simulations are shown in Fig. 6. The distribution of gamma-ray-like events reasonably agrees with that of gamma-ray simulations.

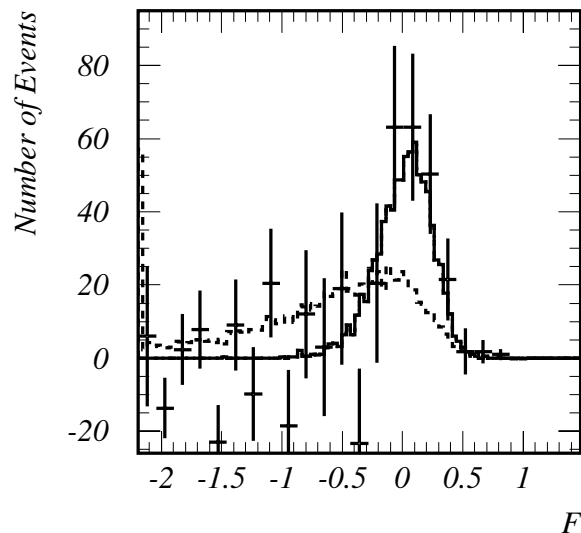


Fig. 6. Distributions of the Fisher discriminant, F . The histogram with error bars is excess counts over the background obtained from the Crab observations. The solid and dashed histograms are the distributions of gamma-ray Monte Carlo simulations and background events, respectively.

The gamma-ray signals from SN 1006, PSR B1706–44 and Vela have not been confirmed by CANGAROO-III. In fact, the flux upper limits obtained by CANGAROO-III are significantly lower than the CANGAROO-I fluxes. A possible reason for the old detections is that the number of degrees of freedom, in fine-tuning cuts in image parameters to maximize apparent significance of signals, were not properly taken into account in the quoted detection significance. This must be checked by re-analyzing the old data. However, supernova remnants RX J1713.7–3946, RX J0852.0–4622, and the Galactic Center have first been detected by CANGAROO at TeV energies and their signals have later been confirmed by H.E.S.S. These TeV sources have an important place in clarifying the origin of Galactic cosmic rays.

Methods to improve energy resolution of the CANGAROO-III stereoscopic system have been considered on the basis of Monte Carlo simulations [16]. Energy resolution of about 15 % can be achieved at 1.5 TeV by using a method developed, requiring all of the available three telescopes triggered.

Considerations and Developments for the Future Project

Future ground-based gamma-ray observatories after CANGAROO-III have been considered including the upgrade phase of the current system. From the aspect of the system design, there are three straightforward extensions from the current experiment [17]:

1. low energy extension using a telescope of a large aperture or at a high altitude to explore the unopened gamma-ray window (10 ~ 100 GeV),

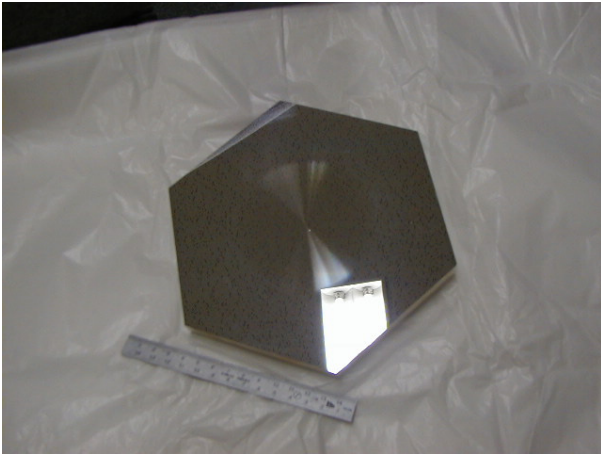


Fig. 7. Sample metal (aluminum alloy) mirror tested for the future experiment.

2. higher sensitivity or high energy extension using *a telescope of a large effective area* to get better statistics,
3. better time coverage using *a telescope of a wide field of view* to observe transient sources.

To realize a Cherenkov telescope of a very large diameter (30 m class) as a possibility, reduction of the cost is very essential. Design considerations utilizing Cassegrain-type optics have been done to reduce the telescope weight but not to sacrifice the current optical performance as an imaging Cherenkov telescope [18]. We found some possible solutions that fulfill our optical requirements, but further studies on the cost issue are necessary.

The mirror segments used in CANGAROO-III are made of the Fiber Reinforced Plastic (FRP), which is of light weight for the rigidity but has some difficulty adjusting the shape of its surface. A sample metal (aluminum alloy) mirror has been made and tested as a possible alternative (Fig. 7). A preliminary measurement shows that the focusing quality of the metal mirror is apparently better than that of the FRP mirror [2], but the sample is still under various tests.

Bibliography

- [1] “A Search for Sub-TeV Gamma Rays from the Vela Pulsar Region with CANGAROO-III”, R. Enomoto *et al.*, *Astrophys. J.*, **638**, 397 (2006).
- [2] Master’s thesis in Japanese, M. Yuasa, University of Tokyo (2006).
- [3] “Very high energy gamma-ray observations of the Galactic plane with the CANGAROO-III telescopes”, M. Ohishi *et al.*, *Proc. of 29th ICRC (Pune)*, **4**, 39 (2005).
- [4] “Stereoscopic observations with the CANGAROO-III telescopes at the large zenith angles”, T. Nakamori *et al.*, *Proc. of 29th ICRC (Pune)*, **4**, 203 (2005).
- [5] “Recent status of the analyses for stereoscopic observations with the CANGAROO-III telescopes”, T. Tanimori *et al.*, *Proc. of 29th ICRC (Pune)*, **4**, 215 (2005).
- [6] “Observation of TeV Gamma-ray from the Active Radio Galaxy Centaurus A with CANGAROO-III”, S. Kabuki *et al.*, *Proc. of 29th ICRC (Pune)*, **4**, 379 (2005).
- [7] “Search for Very High Energy Gamma-Rays from Active Galactic Nuclei with CANGAROO-III Telescope”, Y. Sakamoto *et al.*, *Proc. of 29th ICRC (Pune)*, **4**, 387 (2005).
- [8] “Optical measurements by cooled CCD cameras for CANGAROO-III”, R. Kiuchi *et al.*, *Proc. of 29th ICRC (Pune)*, **5**, 315 (2005).
- [9] “Status of the CANGAROO-III Project”, K. Nishijima *et al.*, *Proc. of 29th ICRC (Pune)*, **5**, 327 (2005).
- [10] “Performance of the Imaging Atmospheric Cherenkov Telescope System of CANGAROO-III”, T. Yoshikoshi *et al.*, *Proc. of 29th ICRC (Pune)*, **5**, 343 (2005).
- [11] “Upper limits to the SN1006 multi-TeV gamma-ray flux from H.E.S.S. observations”, F. Aharonian *et al.*, *Astron. Astrophys.*, **437**, 135 (2005).
- [12] “Search for TeV emission from the region around PSR B1706–44 with the H.E.S.S. experiment”, F. Aharonian *et al.*, *Astron. Astrophys.*, **432**, L9 (2005).
- [13] “First detection of a VHE gamma-ray spectral maximum from a Cosmic source: H.E.S.S. discovery of the Vela X nebula”, F. Aharonian *et al.*, *Astron. Astrophys.*, **448**, L43 (2006).
- [14] “Search for TeV Emission from the Direction of the Vela and PSR B1706–44 Pulsars with the H.E.S.S. Experiment”, B. Khélifi *et al.*, 2nd Int. Symp. on High Energy Gamma Ray Astronomy (Heidelberg), *APS Conf. Proc.* **745**, p. 335 (2004).
- [15] “VHE observations of pulsar wind nebulae with H.E.S.S.”, B. Khélifi *et al.*, *Proc. of 29th ICRC (Pune)*, **4**, 127 (2005).
- [16] Master’s thesis in Japanese, S. Kawasaki, University of Tokyo (2006).
- [17] “VHE Gamma-Ray Future Project: Beyond CANGAROO”, T. Yoshikoshi, *Proc. of Towards a Network of Atmospheric Cherenkov Detectors VII (Palaiseau)*, 359 (2005).
- [18] Master’s thesis in Japanese, Y. Yukawa, University of Tokyo (2006).

TA: Telescope Array Experiment

Spokespersons:

M. Fukushima / ICRR, University of Tokyo
P. Sokolsky / Dept. of Physics, University of Utah

Collaborating Institutions:

Chiba Univ., Chiba, Japan; ICRR, Univ. of Tokyo, Kashiwa, Japan; Kanagawa Univ., Yokohama, Japan; KEK/IPNS, Tsukuba, Japan; Kinki Univ., Higashi-Osaka, Japan; Musashi Inst. of Tech., Tokyo, Japan; Nat. Inst. of Rad. Sci., Chiba, Japan; Osaka City Univ., Osaka, Japan; Rutgers Univ., Piscataway, NJ 08854, USA; Saitama Univ., Saitama, Japan; Shibaura Inst. of Tech., Saitama, Japan; Tokyo Inst. of Tech., Tokyo, Japan; Univ. of Montana, MT 59812, USA; Univ. of Utah, Salt Lake City, UT 84112, USA; Yamanashi Univ., Kofu, Japan

Super-GZK Cosmic Rays

The AGASA air shower array observed 11 extremely-high energy cosmic rays (EHECRs) exceeding the energy of 10^{20} eV in 13 years of operation (see AGASA section for details). The rate of such events is consistent with a continued spectrum with a power law of $E^{-2.7}$ and the expected GZK-cutoff structure due to the interaction of EHE protons with the cosmic microwave background [1] was not observed. The Fly's Eye air fluorescence telescope also reported an event with 3×10^{20} eV in 1994 [2].

High energy astronomical objects such as the active galactic nuclei and radio galaxies were searched as a possible origin of such EHECRs, but none were found in the arrival direction of these events within 100 Mpc of our galaxy [3]. More distant origins may be considered, but only if a special mechanism to allow a longer propagation of EHECRs to take place, for example the violation of special relativity [4] or the EHE neutrinos as the carrier of such energy [5].

It was therefore conceived that super-GZK ($E > 10^{20}$ eV) cosmic rays may be generated by the decay of super-heavy particles in the nearby universe. Energies beyond 10^{20} eV are easily attained if the mass of the particle is at the Grand Unification scale. A concentration of the particles in the galactic halo makes the non-observation of GZK-cutoff viable. Such super-heavy particles may be surviving as a relic particle of the Big Bang or presently generated by the decay of topological defects [6]. An abundant generation of EHE gamma rays and neutrinos, in place of protons and nuclei, is expected in the decay of such particles.

Overview of TA

The Telescope Array (TA) was proposed in 2000 [7] to investigate the origin of super-GZK cosmic rays by employing a large array of fluorescence telescopes with ~ 100 times larger acceptance than AGASA. The HiRes experiment, however, presented an energy spectrum indicating the GZK-cutoff in the 27th ICRC in Hamburg and the result was later published in 2003 [8]. It was a monocular spectrum obtained by the single telescope. A preliminary version of the stereo spectrum using two telescopes was presented in 2005 at the 29th ICRC in Pune [9]. It exhibits a clear cutoff structure although the E^3 multiplied flux below $10^{19.5}$ eV seems larger than the monocular flux by a factor of ~ 1.5 .

With contradictory results on the existence of GZK cutoff appearing, it became urgent to understand the experimental bias in the energy and the acceptance determination of super-GZK cosmic rays. The construction of full TA is thus de-

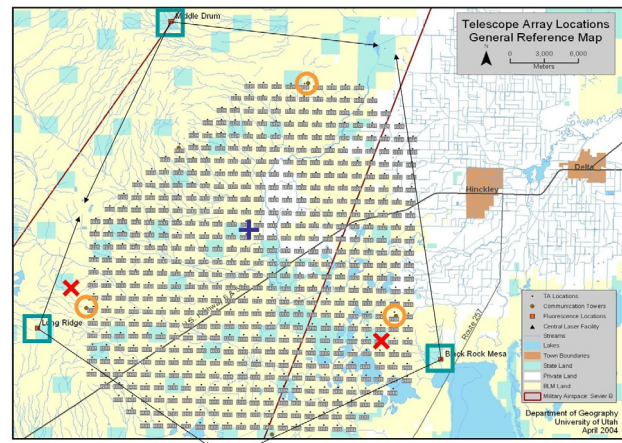


Fig. 1. Detector Arrangement of ph-1 TA. The surface detector locations are indicated by small numbers. The fluorescence telescope stations are marked by square boxes.

ferred, and we initiated constructing a composite detector with AGASA-like ground array and TA fluorescence telescopes [10] instead. We call it as phase-1 TA (ph-1 TA). We expect simultaneous measurement of the same EHECRs by two detectors will sort out the systematics of two methods. It will guide us to a reliable determination of the primary energy and the acceptance of EHECRs.

The phase-1 TA consists of a large plastic scintillator array and 3 stations of air fluorescence telescopes overlooking the array from periphery as shown in Fig.1. The ground array will give an aperture of ~ 1200 km² sr, which is approximately an order of magnitude larger than that of AGASA. The fluorescence telescope will have a stereoscopic aperture of ~ 300 km² sr with 10% duty factor at 10^{20} eV. The telescope will also supply information on the primary particle species by measuring the longitudinal shower profile. It is being built in the West Desert of Utah, 140 miles south of Salt Lake City (lat. 39.3°N, long. 112.9°W, alt. ~ 1400 m).

Ground Array of ph-1 TA

The ground detector consists of 576 plastic scintillators deployed in a grid of 1.2 km spacing. It covers the ground area of ~ 760 km². Approximately 80% of them will be on the Federal land, $\sim 10\%$ on the state trust land and the rest on privately owned land. The detection (trigger) efficiency is $\sim 100\%$ for cosmic rays with energies more than $10^{19.5}$ eV with zenith angle less than 45° .

The counter is composed of two layers of plastic scintillator overlaid on top of each other. The scintillator (CI, CIMS-G2) is 1.2 cm thick, 3 m² large and is read out by 96 wave length shifter fibers installed in a groove on the surface (see Fig.2). The fiber (Kuraray, Y-11(200)M) has a diameter of 1 mm and a length of 5 m. Both ends of the fiber are optically connected to the photomultiplier (Electron Tube 9124B). A passage of cosmic ray muon gives ~ 15 photo-electrons in average. Two layers are used for the coincidence measurement, for the muon calibration trigger and for extending the dynamic range by setting different PMT gains for two counters.

The signal from each PMT is continuously digitized with a 12-bit flash ADC with 50 MHz sampling. When both of the



Fig. 2. Scintillation Detector of TA.



Fig. 3. Deployed Surface Detector.



Fig. 4. Fluorescence Station at Black Rock Mesa.

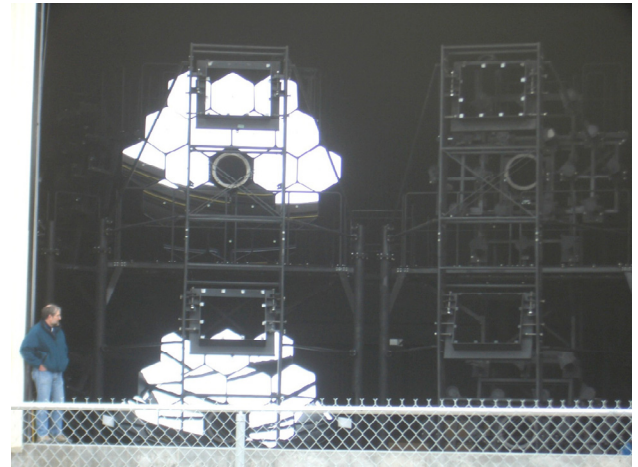


Fig. 5. Fluorescence Telescopes of TA.

PMTs record more than 1/3 of the muon signal, wave forms of $\sim 4 \mu\text{s}$ duration are stored with a time stamp supplied by the GPS. This rate of local buffering is less than 1 kHz. The relative timing between remotely separated counters will be better than $\pm 20 \text{ ns}$ by the GPS, which is sufficient to supply good resolution for the determination of the arrival direction.

When one of the PMT signals exceeds a trigger threshold of 3 muons, the timing is recorded in a local trigger list. The content of the list is transmitted to a branch DAQ board by the wireless LAN at 1 Hz. The list may contain less than 100 events for normal counters. The branch DAQ board is installed on a communication tower built at the periphery of the array. Three main and two sub towers of $\sim 15 \text{ m}$ high will be built for the communication up to $\sim 20 \text{ km}$. An air shower event is identified by the branch DAQ firmware by requiring clustered hits with a good coincidence timing. The air shower event rate will be less than 1 Hz when at least 3 adjacent counters are required in coincidence.

When an air shower trigger is generated in a branch DAQ board, a command is broadcasted to all counters and relevant counters storing the event with good coincidence timing respond by transmitting the wave form data to the branch DAQ board. The data are then transmitted to a central DAQ system via tower to tower wireless communication and stored in a mass storage. We employ a commercially produced wireless transmitter with the maximum speed of 11 Mbps using 2.4 GHz spread spectrum technology. The dead-time-less DAQ operation is aimed with the high transmission speed to-

gether with a large buffering memory at each counter.

One of the counters test-deployed to the field in December 2004 is shown in Fig.3. The total electrical power consumed by the PMT, ADC, GPS and LAN is approximately 7 W and is locally generated by the solar panel of $\sim 120 \text{ W}$ capacity (Kyocera KC-120J, see Fig.3). Behind the panel will be a heat-insulated enclosure containing the backup battery (12V, $\sim 65 \text{ Ah}$ and deep cycle) and all the electronics. A communication antenna is fixed at the top of 3.3 m tall mast. The total weight of the counter is less than 250 kg, such that it can be easily deployed by helicopter without disturbing the wilderness environment.

Fluorescence Telescope

Twelve reflecting telescopes are installed at each station (see Fig.4) and cover the sky of $3^\circ - 34^\circ$ in elevation and 108° in azimuth looking toward the center of the ground array.

The field of view of each telescope (see Fig.5) is 18.0° in azimuth and 15.5° in elevation. A spherical dish of 6.8 m^2 is composed of 18 hexagonal mirrors with a radius of curvature of 6067 mm. The direction of each mirror is individually adjustable and a spot size of less than 20 mm in diameter is realized at the focal plane (2960 mm). The mirror is made by 10.5 mm thick high thermal resistivity glass (Schott Borofloat) and is aluminum coated by vacuum deposition. The surface of the aluminum is protected by producing a $\sim 50 \text{ nm}$ thick anodization layer.

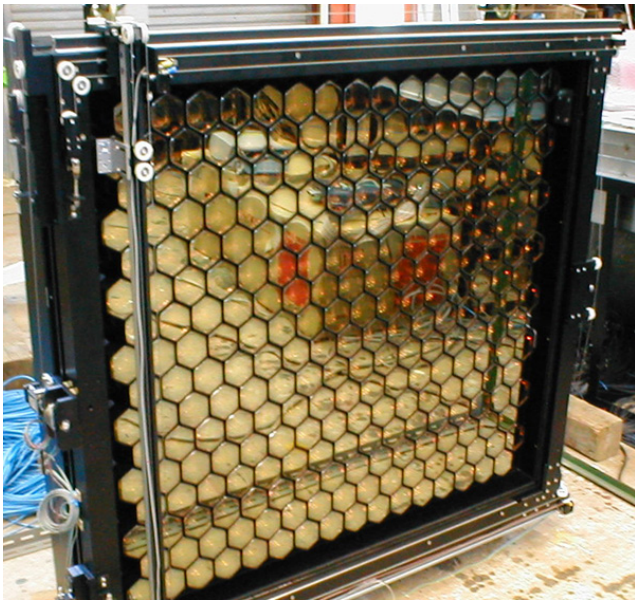


Fig. 6. Prototype of TA Camera.

The air shower image is detected by a mosaic PMT camera on the focal plane (see Fig.6). A set of 16×16 PMTs (Hamamatsu 6234) with a hexagonal window is used for one camera. Each PMT covers $1.1^\circ \times 1.0^\circ$ patch of the sky. A UV transmitting glass filter (Schott BG3, 4 mm thick) is attached in front of each PMT for blocking the night sky background in the visible light range. The whole camera is assembled in a chassis with a window made by a UV transparent plexiglass.

Negative high voltage is applied to the PMT by a bleeder circuit using zener diodes to ensure a stable operation under high night sky background. The high voltage is individually adjustable for all PMTs. With a PMT gain of $\sim 10^5$, a linearity of up to 32 k photoelectrons in 100 ns was achieved.

A signal from the PMT is amplified by a factor of 50 by the pre-amplifier and is sent to a Signal Digitizer and Finder (SDF) with 25 m twisted pair cable. The SDF module receives the signal with a shaping filter and digitizes it with a 12-bit, 40 MHz FADC. Consecutive 4 samplings are added by the following FPGA. A trace of fluorescence signal is searched in pipeline at the FPGA employing a sliding sum algorithm for every $25.6 \mu\text{s}$ of the time window. The dc component from the night sky background is estimated every 1 ms and is subtracted. The SDF is a 9U VME module and 16 channels are mounted in one module.

The result of the “hit” search by the SDF is reported to a Track Finder (TF) in the same VME crate and an air shower track is searched in one camera. A track is found when 5 or more than 5 adjacent PMTs are fired. A looser track definition is applied to a camera-crossing event. The results of all TF modules are concentrated to a Central Trigger Decision (CTD) module and the decision of data acquisition is made. The wave form data stored in the SDF memory are read out to “a camera PC” in parallel and a complete event is subsequently built from the camera PCs by Ethernet. Sample PMT wave forms triggered and collected in Utah by the prototype electronics is shown in Fig.7.

The calibration of the telescope sensitivity is important

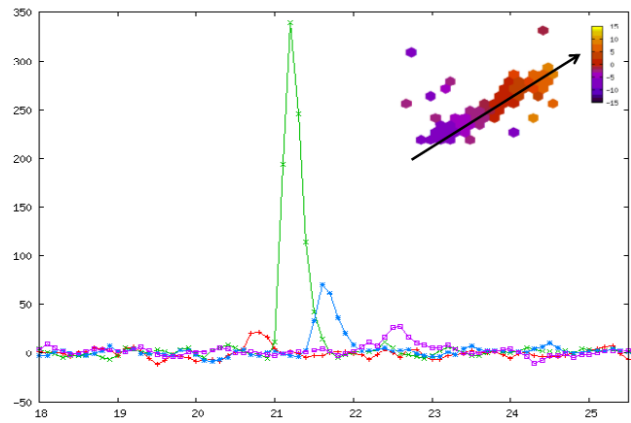


Fig. 7. One of the First Fluorescence Signals of TA. Wave forms of several PMTs in the track are overlaid in order to show the time evolution of the signal.

for the measurement of energy. Characterizing parameters of each component such as the mirror reflectivity, filter transmission, PMT quantum efficiency and the electronics gain will be measured piece by piece at the production. The relative gain of all PMTs will be adjusted in situ by the Xenon flasher installed at the center of the mirror. The light from the flasher is diffused and filtered by BG3. The xenon flasher supplies a light pulse of good uniformity ($<3\%$) to all PMTs in a camera.

There are 3 “standard” PMTs installed in a camera. The efficiency and the gain of the standard PMT are calibrated before installing to a camera and their values are transmitted to other PMTs by the Xenon flasher calibration. A tiny YAP ($\text{YAlO}_3:\text{Ce}$) scintillator with 50 Bq ^{241}Am source is embedded in the BG3 filter of the standard PMT. The YAP generates a short light pulse of ~ 3000 photons around 370 nm and has an excellent temperature stability. The calibration of the standard PMT will be maintained by the YAP pulser.

For the calibration of the standard PMT, we developed a light source using a Rayleigh scattering of nitrogen laser (337 nm) in the nitrogen atmosphere. The power of laser is measured pulse by pulse to an accuracy of 5% and the known cross section of Rayleigh scattering is applied to calculate the intensity of the scattered light.

The UV fluorescence light generated by the air shower is scattered and lost along the path of transmission to the telescope. The responsible processes are Rayleigh scattering by the air molecule and Mie scattering by the aerosol. The Rayleigh scattering can be calculated with an accuracy of $\sim 5\%$ from the known density and temperature distribution of the atmosphere. The amount of Mie scattering differs from place to place and changes with time reflecting the aerosol distribution in the air. It has to be continuously monitored on site.

A lidar system located at each station will be used for the atmospheric monitoring. It consists of a pulsed Nd:YAG laser (the 3rd harmonic, 355 nm) and a telescope attached to an alto-azimuth mount and sharing the same optical axis as shown in Fig.8. The laser can be shot to any direction and the back-scattered light is received by the telescope to analyze the extinction coefficient along the path of the laser. We had



Fig. 8. TA Lidar at Black Rock Mesa.

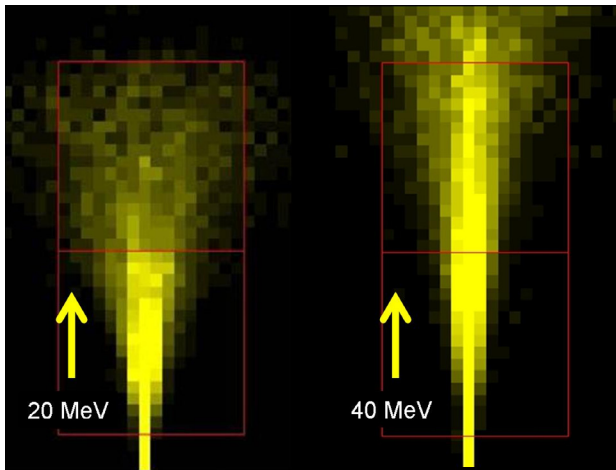


Fig. 9. Electron Linac Beam seen by the Fluorescence telescopes (simulation by GEANT).

shown in Akeno that the change of the 3-dimensional distribution of extinction coefficient can be monitored within 10 km from each station [11].

We are also building a laser shooting facility in the middle of the array. The site is chosen such that a vertical shot of the laser from this station is equidistant to all fluorescence stations. The intensity of the laser shot is monitored to 5% accuracy and the Rayleigh scattering at high altitude can be considered as a “standard candle” observable at all stations. The comparison of the received light will give a reliable information for the difference and the change of atmospheric conditions. For monitoring the cloud in the night sky, we will install an infra-red CCD camera at each station.

In order to confirm the absolute energy scale of the fluorescence detector in situ, we are planning to deploy a small accelerator ~ 100 m away from the fluorescence station and inject an electron beam vertically up into the atmosphere. The simulation of observed fluorescence signal by 20 and 40 MeV electron beams is shown in Fig.9. A beam of 10^9 electrons with a duration of $1 \mu\text{s}$ well simulates a shower energy deposition of $\sim 4 \times 10^{16}$ eV. The calibration is obtained by comparing the observed fluorescence signal with the expected energy deposition calculated by the GEANT simulation. The design of the accelerator is being pursued with a collaboration of KEK accelerator physicists.

Prospects

The phase-1 TA is being built by the collaboration of Japanese and American physicists. The group consists of physicists who have been working in AGASA, HiRes and other HEP experiments in US and Japan. The Japanese fund for ph-1 TA was approved in 2003 by the Grants-in-Aid for Scientific Research (Kakenhi) of Priority Areas. The US group has submitted a matching proposal to NSF in 2005. The US proposal includes a construction of TALE, a Low Energy extension of TA down to 10^{17} eV, to investigate the modulation of CR composition and spectrum expected by the galactic to extra-galactic transition of CR origins. The infrastructure of TA and TALE in Utah is also the responsibility of US group.

As of December 2005, a total of 370 surface detectors were produced, of which 18 were test-deployed in the field in 2004. We plan to build communication towers and deploy the rest of counters into the field when the land use permit by the Bureau of Land Management is granted, which is expected in February, 2006. The first fluorescence station was built and 12 telescope frames were installed, of which two were equipped with mirrors and a test observation was made with prototype camera and electronics in July, 2005. We plan to complete the construction and start taking data in April, 2007.

The Pierre Auger group is constructing a large hybrid experiment in Argentina with 1600 water tank detectors. The construction will be complete by the end of 2006. The group presented the first EHECR spectrum at the 29th ICRC in August 2005 using an exposure already larger than what AGASA had accumulated in 13 years of operation. There was no event exceeding 10^{20} eV. The group considers, however, premature to conclude the existence of GZK-cutoff because the present systematic error of energy determination is estimated to be at least 40%. The Auger group calibrated the ground array energy estimator $\rho(1000)$, the muon density 1000 m away from the shower center, by the measurement of shower energy from the fluorescence telescope. The extrapolation of the calibration from the lower energy, where most of the hybrid events were collected, caused the major part of the systematic error.

The construction of ph-1 TA will be finished a few months after the Pierre Auger is completed in Argentina. The acceptance of Auger ground array is ~ 4.5 times larger than that of ph-1 TA assuming the same zenithal acceptance. The scintillator of TA counts the number of penetrating charged particles and it is dominated by the electrons which outnumber the muons by an order of magnitude. The water tank of Auger on the other hand is more sensitive to the penetrating high energy muons rather than the soft electrons which stop near the surface of the water tank and do not generate as many Cherenkov photons.

The energy measurement of ph-1 TA therefore is less sensitive to the unknown composition of the primary cosmic rays and the details of hadronic interactions at EHE, whereas its sensitivity to the composition determination using the muon content is severely limited particularly for the EHE gamma rays and neutrinos. It is our belief that the characteristic features of ph-1 TA, the sampling of electromagnetic shower energy, the unique calibration of fluorescence generation and the measurement in the Northern Hemisphere, will make an essential contribution to the understanding of the intricate prob-

lem of GZK cutoff.

Bibliography

- [1] K.Greisen, Phys. Rev. Lett. **16**, 748 (1966); T.Zatsepin and V.A.Kuzmin, JETP Lett. **4**, 178 (1966).
- [2] D.J.Bird et al., Astrophys. J., **424**, 491 (1994).
- [3] Y.Uchihori et al., Astropart. Phys. **13**, 151 (2000); G.Sigl et al., Phys. Rev. **D63**, 081302 (2001).
- [4] H.Sato and T.Tati, Prog. Theo. Phys. **47**, 1788 (1972); S.Coleman and S.L.Glashow, Phys.Rev. **D59**, 116008 (1999).
- [5] T.J.Weiler, Astropart.Phys. **3**, 303 (1999).
- [6] V.Kuzmin and I.Tkachev, JETP Lett. **68**, 271 (1998); V.Berezinsky, P.Blasi and A.Vilenkin, Phys.Rev. **D58**, 103515 (1998); K.Hamaguchi, I.Izawa, Y.Nomura and T.Yanagida, Phys.Rev. **D60**, 125009 (1999); V.Berezinsky, Nucl. Phys. Proc. Suppl. **81**, 311 (2001).
- [7] The Telescope Array Project: Design Report, July, 2000.
- [8] T.Abu-Zayyad et al., Phys. Rev. Lett. **92**, 151101 (2004); T.Abu-Zayyad et al., Astropart. Phys. **23**, 157 (2005).
- [9] Proc. of 29th ICRC, Pune (2005) to be published.
- [10] M.Fukushima et al., Proc. of 28th ICRC, Tsukuba, **2**, 1025 (2003); S.Kawakami et al., Proc. of 28th ICRC, Tsukuba, **2**, 1033 (2003); F.Kakimoto et al., Proc. of 28th ICRC, Tsukuba, **2**, 1029 (2003); M.Fukushima, Proc. of APPI2003 workshop, KEK Proceedings 2003-6.
- [11] T.Yamamoto et al., Nucl. Instr. and Methods **A488**, 191 (2002).

Tibet AS γ Project

[Spokesperson : Masato Takita]

ICRR, Univ. of Tokyo, Kashiwa, Chiba 277-8582

In collaboration with the members of:

Hirosaki Univ., Hirosaki; Utsunomiya Univ., Utsunomiya; Saitama Univ., Urawa; Kanagawa Univ., Yokohama; Yokohama National Univ., Yokohama; Shonan Inst. of Technology, Fujisawa; Tokyo Metropolitan Coll. of Aeronautical Eng., Tokyo; NII, Tokyo; Konan Univ., Kobe, Shibaura Inst. of Technology, Tokyo; Waseda Univ., Tokyo; Riken, Saitama; Institutes in China

Since 1990, the Tibet air shower array has been successfully operated at Yangbajing (4 300 m above sea level) in Tibet. It has continuously made a wide field-of-view (approximately 2 steradian) observation of cosmic rays and gamma rays in the northern sky. The research purpose is the understanding of origin, acceleration and propagation mechanisms of cosmic rays by studying (1) celestial gamma-ray point/diffuse sources, (2) chemical composition and energy spectrum of primary cosmic rays in the knee energy region.

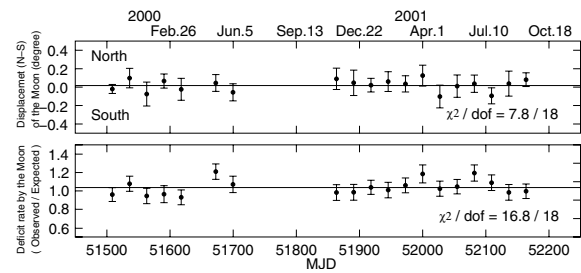


Fig. 1. Tibet-III long-term stability in pointing accuracy and angular resolution.

We also aim at studying the global 3-dimensional structure of the solar and interplanetary magnetic fields by observing the Sun's shadow in cosmic rays (3) as well as at measuring the cosmic-ray anisotropy in the multi-TeV region with high precision(4).

The first air shower array (Tibet-I) was updated in late 1994 by increasing the number of scintillation detectors from 65 to 221, and then this array (called Tibet-II) has been fully operating. The Tibet-II array consists of 185 first-timing (FT) plastic scintillation detectors of 0.5 m² each. With a FT detector, equipped is a plastic scintillator plate in 3 cm thickness each viewed by a 2" ϕ PMT (HPK H1161). They are placed at a grid point with 15 m spacing, as in Tibet-I. Among these, each of the 52 FT detectors also contains a 1.5" ϕ PMT (HPK H3178) for a wide dynamic-range measurement of the particle density. The FT array is also surrounded by 32 density detectors of 0.5 m² each to obtain a good core location for an individual air shower event. The effective area for detecting an contained air shower event is about 8 times as large as Tibet-I. The air shower events have been accumulated at a rate of about 150 Hz to efficiently detect air showers with energies around 10 TeV. In 1996, a high-density array was constructed near the center of the Tibet-II array. This array (HD-array) consists of 110 plastic scintillation detectors, each of which was deployed at a grid point with 7.5 m spacing. The HD array is sensitive to air showers with energies around a few TeV. The trigger rate of the HD array has been set to about 150 Hz. Using this HD array, in 1999, we succeeded in observing multi-TeV γ ray signals from the Crab Nebula at 5.5 σ confidence level. This was the first detection of multi-TeV γ -ray signals by a conventional air shower array. Subsequently, we also detected multi-TeV γ rays successfully at 3.7 σ level from Mrk501 which was in a highly flaring state between March 1997 and August 1997.

In the late fall of 1999, the area of the HD array was enlarged up to 22000 m² (Tibet-III). It is equipped with 533 plastic scintillation counters (497 FT + 36 density PMTs) in total. The trigger rate has been set approximately to 680 Hz.

The performance of the Tibet air shower array has been well examined by observing the moon's shadow in cosmic rays, and the deficit map of cosmic rays around the moon demonstrates the angular resolution to be around 0.9 $^{\circ}$ at a few TeV for the Tibet-III array. The long-term stability in pointing accuracy (less than 0.02 $^{\circ}$) and angular resolution is demonstrated in Fig. 1.

Multi-TeV γ -ray signal was successfully detected at $\sim 5\sigma$ level from the Crab (the standard candle in γ -ray astron-

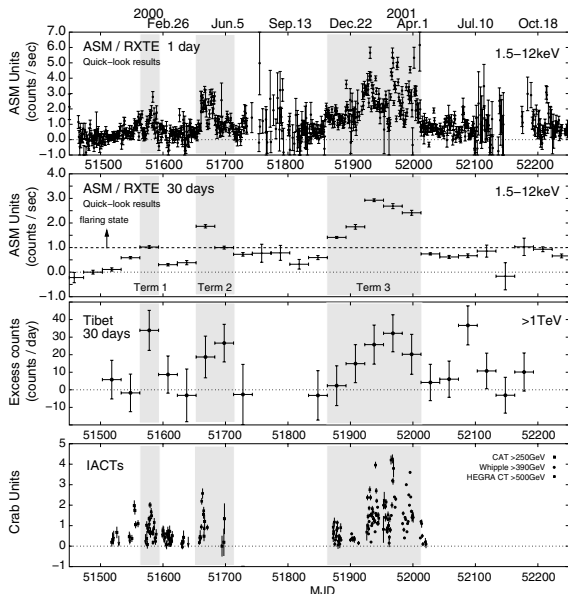


Fig. 2. Correlation between the TeV γ -ray data by Tibet-III and X-ray data by the RXTE satellite during the flaring states in Mrk421 in 2000 and 2001

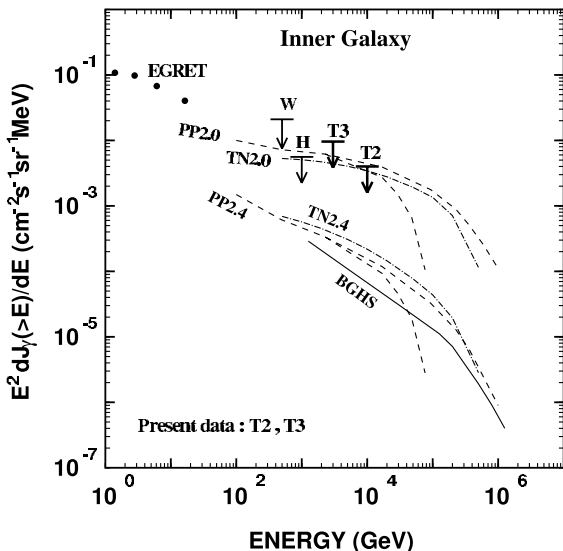


Fig. 3. Upper limits on diffuse gamma rays from the inner galaxy. Present data are labelled by T2 and T3 as 99 % CL upper limits, assuming a gamma-ray spectral index 2.4. W and H indicate Whipple (99.9 % CL) and HEGRA (99 % CL) The numbers 2.0 and 2.4 before the theoretical curves indicate the electron source differential spectral indices.

omy) by the Tibet-III array. We also succeeded in observing multi-TeV gamma-ray flares at 5.1σ level from Markarian 421 which was in a very active phase during the year 2000 and 2001. We observed a clear long-term positive correlation between X-ray data (RXTE satellite) and our TeV γ -ray data from Mrk421 in the active period, as shown in Fig. 2.

We also searched for multi-TeV diffuse γ rays from the galactic plane. As there was no significant signal, flux upper limits were obtained from the inner galaxy ($20^\circ < l < 55^\circ$, $-2^\circ < b < 2^\circ$) and the outer galaxy ($140^\circ < l < 225^\circ$, $-2^\circ < b < 2^\circ$). Accordingly, we set the most stringent upper limits as shown in Fig. 3 and Fig. 4 at multi-TeV energies.

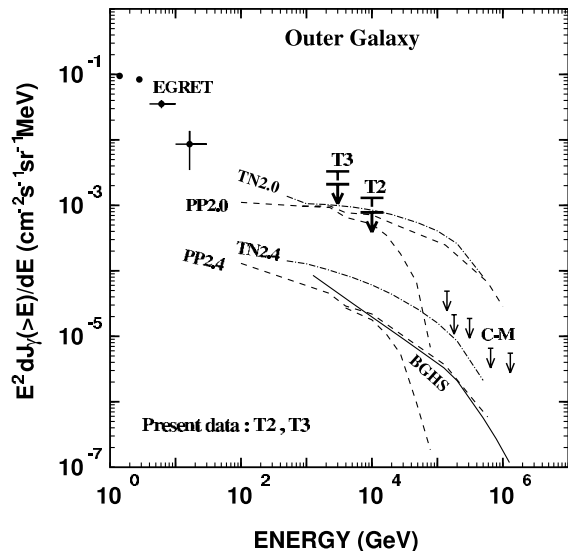


Fig. 4. Upper limits on diffuse gamma rays from the outer galaxy. Present data are labelled by T2 and T3 at 99 % CL (upper bars) and 90 % CL (lower bars), assuming a gamma-ray spectral index 2.4. C-M indicates CASA-MIA (90 % CL) results based on moon airshower data. The numbers 2.0 and 2.4 before the theoretical curves indicate the electron source differential spectral indices.

We search for TeV steady point sources in the northern sky. No statistically significant point source is found except for well established Crab and Mrk421[2]. The flux upper limits at 90% confidence level obtained is typically 0.2 to 0.3 in unit of Crab γ -ray intensity.

We search for steady PeV γ -ray emission from the Monogem ring region with the Tibet air shower array from 1997 to 2004[3]. As shown in Fig. 5 no evidence for statistically significant γ -ray signals is found in a region $111^\circ < R.A. < 114^\circ$, $12.5^\circ < decl. < 15.5^\circ$ in the Monogem ring where the MAKET-ANI experiment recently claimed a positive (approximately 6σ) detection of PeV high-energy cosmic radiation, although our flux sensitivity is approximately 10 times better than MAKET-ANI's. We set the most stringent integral flux upper limit at 99% confidence level of $4.0 \times 10^{-12} \text{cm}^{-2} \text{s}^{-1} \text{sr}^{-1}$ above 1 PeV on diffuse γ rays extended in the $3^\circ \times 3^\circ$ region.

Then, autumn 2002, the Tibet-III array was further extended to 37000m^2 with 733 plastic scintillation counters by adding 200 more FT counters (i.e., 697 FT + 36 density PMTs in total), as is shown in Fig. 6. The trigger rate has been set to 1500 Hz at a few TeV energy threshold. In 2003, 56 FT detectors were further added in the outer region of the array in order to expand the effective high-density area up to 37000m^2 . The 37000m^2 Tibet-III with 789 counters are in continuous operation. at a trigger rate of 1700 Hz. We are now accumulating Tibet-III data to obtain a standard TeV γ -ray flux from the Crab and to search for unknown constant/transient TeV γ -ray sources. Possible proton/ γ -ray separation is under extensive study.

A hybrid experiment of emulsion chambers (EC) and air shower array started in 1996 to obtain the energy spectrum of the primary cosmic-ray proton flux around the knee energy region The total area of EC, each having the size of $40 \text{cm} \times$

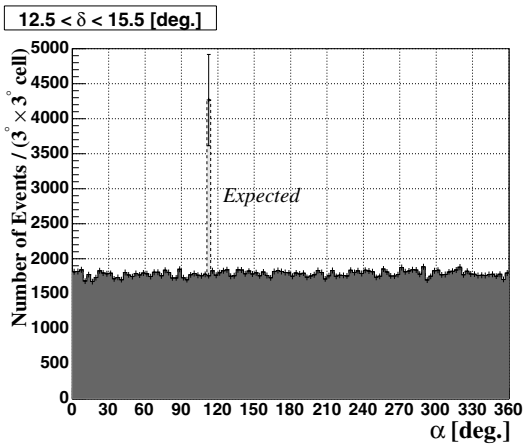


Fig. 5. Number of events above 1 PeV in each of the 120 cells in the declination band $12.5^\circ < \text{decl.} < 15.5^\circ$. The shaded histograms are obtained from Tibet-III, while the dashed histogram denotes the number of events expected from the MAKET-ANI result



Fig. 6. 37000 m^2 Tibet-III array operating at Yangbajing.

50 cm, is 80 m^2 and the total thickness of lead plates is 14 r.l. High-sensitivity X-ray films were interleaved between the 14 r.l. lead plates at every 2 r.l. to detect γ -ray families. Just below the emulsion chambers, the burst detectors (BD) with the same area as EC were set up to locate the air shower cores of the family events to be observed in EC. This detector complex was set up near the center of the Tibet-II array (AS) to get on the information on air showers accompanied with the family events. The first EC exposure was terminated in August of 1997 and X-ray films inserted in EC were developed for analysis. A high-energy family event of about 500 TeV was observed in this exposure and its primary energy is estimated to be about 10^{16} eV from the size of the accompanying AS data. This hybrid experiment continued until 1999. Using the BD + AS data, we obtained the energy spectrum of primary protons (820 proton-induced events during 690-day detector live time) with its primary energies 200–1000 TeV by a neural network method. The differential energy spectrum obtained in this energy range can be fit by a power law with the spectral index of -2.97 ± 0.06 , which is steeper than that obtained by direct measurements at lower energies. We also obtained the energy spectrum of helium nuclei. All of the features of BD events are wholly compatible the heavy enriched composition in the knee region. In 2003, we finished the analysis of all the EC data by means of an automatic analysis program

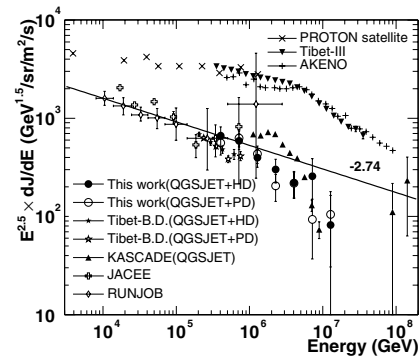


Fig. 7. Primary proton energy spectrum in the knee energy region, assuming the QGSJET model.

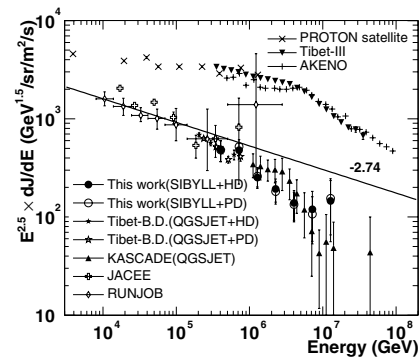


Fig. 8. Primary proton energy spectrum in the knee energy region, assuming the SIBYLL model.

based on track information read out by the image scanners. The primary proton spectrum including the EC + BD + AS data around the knee region[4], being inaccessible by any direct observations, are analyzed with the 3-year data obtained by the hybrid experiment as shown in Fig. 7 and Fig. 8.

We also obtained a preliminary result on the primary cosmic-ray all-particle energy spectrum, as shown in Fig. 7, which is consistent with the one obtained by the Tibet-I experiment. The (all-particle - (proton+He))/all-particle flux ratio is shown in Fig. 9 and Fig 10, indicating that the knee is composed of nuclei heavier than helium. It should be noted that the flux ratio largely cancels out the systematic energy scale uncertainty in the airshower energy determination.

Based on the Tibet-III data from 1999 and 2003, we succeeded in observation of the multi-TeV galactic cosmic-ray anisotropy (approximately 0.05 % level) at solar time frame due to the terrestrial orbital motion around the Sun, i.e. Compton-Getting (C-G) effect. As shown in Fig. 11, we observed a clear C-G anisotropy in the 6.2 and 12 TeV data samples, while the anisotropy observed in the 4 TeV data sample deviates from the expected C-G anisotropy. This suggests an additional anisotropy superposed at the multi-TeV energies, e.g., the solar modulation effect.

As the precision of the Tibet-III is back-checked by the observation of the C-G effect, we proceed to measure the multi-TeV cosmic-ray anisotropy in sidereal time frame with the world best statistics[1]. Their is no significant energy dependence in the 24-hour profile in the anisotropy as shown in

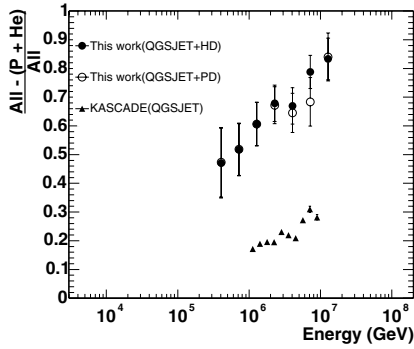


Fig. 9. Primay (all-particle-(proton+helium))/all-particle flux ratio in the knee energy region, assuming the QGSJET model.

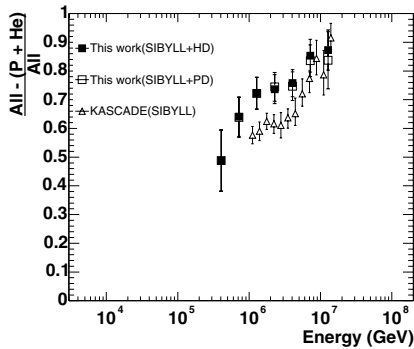


Fig. 10. Primay (all-particle-(proton+helium))/all-particle flux ratio in the knee energy region, assuming the SIBYLL model.

Fig. 12

The 2-dimensional anisotropy in the equatorial coordinates are obtained for the first time in the multi-TeV energy range, thanks to high statistics, as shown in Fig. 13 and Fig. 14. There is a very interesting excess in the Cygnus region, which we can not discriminate currently whether it is caused by γ rays and/or a local cosmic-ray anisotropy.

The Tibet air shower array is very powerful to get new information on the relation between time variation of the large-scale structure of the solar and interplanetary magnetic fields and the solar activities by the sun's shadow in cosmic rays, since high-statistics data taken by the Tibet air shower array can follow up the movement of the sun's shadow at every one-two months. The yearly change in the sun's shadow is demonstrated in Fig. 15. The sun's shadow was observed in the direction significantly away from the optically observed sun's position during the period from 1990 through 1993. Note that this period corresponded to the near-maximum or at the decreasing phase in the solar cycle 22. In 1996 and 1997, however, we found that the sun's shadow was observed in the direction close to the optically observed sun's direction, since the solar cycle was in a quiet phase then. Since 1998, the sun's shadow began to be obscure shown in Fig. 15, as the solar activities were back in an active phase. We expected that the sun's shadow would change its position again, according to the solar activities as the next solar cycle (Cycle 23) goes toward its maximum around the year of 2001 or 2002. As the maximum showed a double-peak structure and the solar activities

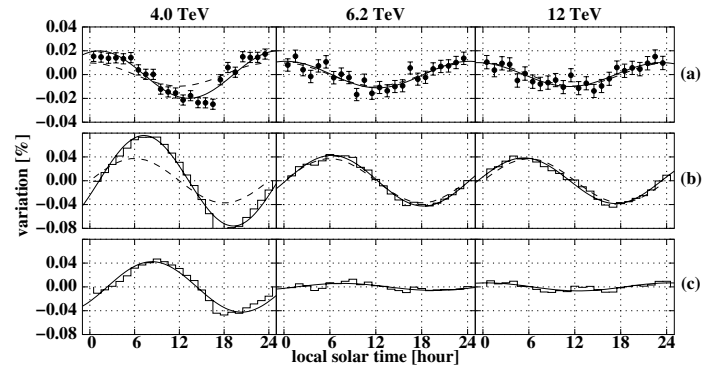


Fig. 11. Multi-TeV cosmic-ray anisotropy at solar time frame obtained by Tibet-III.

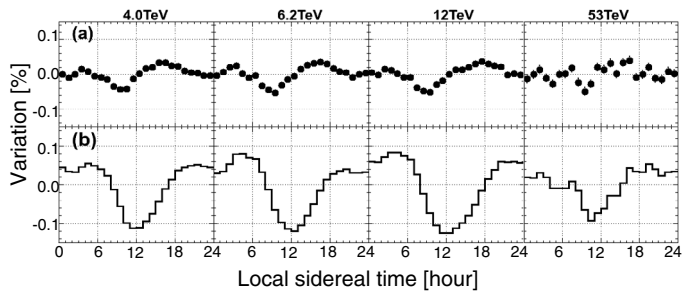


Fig. 12. Energy dependence of multi-TeV cosmic-ray anisotropy at sidereal time frame obtained by Tibet-III.

were still in high states in 2002, we have not observed a clear sun's shadow yet, although the sun starts exhibiting a darker shadow in cosmic rays in 2003. Thus, the results will contribute considerably to the study of solar terrestrial physics.

This group has developed and completed several automatic measuring systems that are powerful for analyzing cosmic ray tracks or air shower spots, that is, automatic microdensitometers, precise coordinate-measuring systems and image scanners controlled by a computer. Enormous data recorded on nuclear emulsion plates or X-ray films are rapidly and precisely measured by the use of these measuring systems.

The emulsion-pouring facilities can meet the demands for making any kind of nuclear emulsion plates which are used for cosmic ray or accelerator experiments. The thermostatic emulsion-processing facilities are operated in order to develop nuclear emulsion plates or X-ray films. Using these facilities, it is also possible to make and develop emulsion pellicles in 600-micron thickness each. In this way, these facilities are open to all the qualified scientists who want to carry out joint research program successfully.

List of Other Inter-University Research Programs

Code No.: 44

Title: Sidereal daily variation of ~ 10 TeV galactic cosmic-ray intensity observed by the Tibet air shower array.

Spokesperson: K. Munakata (Shinshu University)

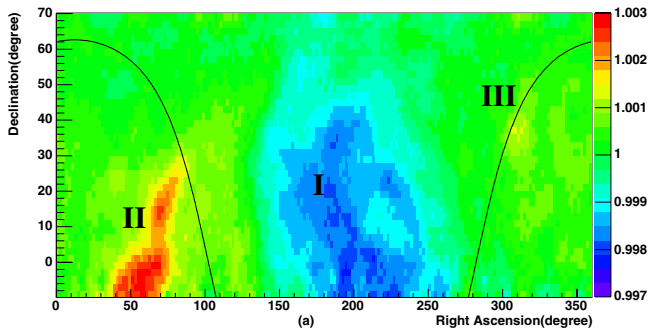


Fig. 13. 2-dimensional intensity map of multi-TeV cosmic-ray anisotropy at sidereal time frame obtained by Tibet-III.

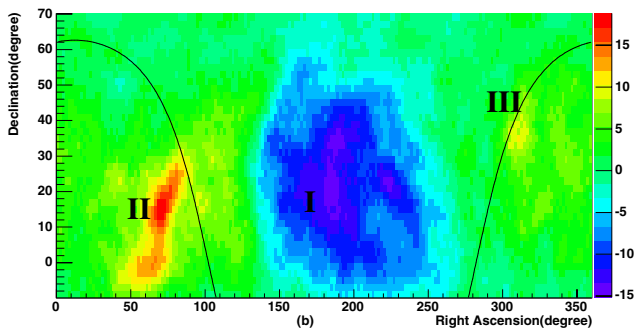


Fig. 14. 2-dimensional significance map of multi-TeV cosmic-ray anisotropy at sidereal time frame obtained by Tibet-III.

Participating Institutions: Shinshu Univ.

Code No.: 74

Title: Observation of High-Energy Electrons and Gamma Rays with a Balloon-borne Instrument

Spokesperson: Shouji Torii (Kanagawa University)

Participating Institutions: Kanagawa Univ., ISAS, Rikkyou Univ.,

ICRR Univ. of Tokyo, and Shibaura Inst. of Technology.

Code No.: 45

Title: Observation of high-energy primary electrons and atmospheric gamma rays by emulsion chambers.

Spokesperson: T. Kobayashi (Aoyama Gakuin University)

Participating Institutions: Utsunomiya Univ., Kanagawa Univ., ICRR Univ. of Tokyo, Univ. of Tokyo.

Bibliography

- [1] M. Amenomori *et al.*, *ApJ*, **626**, L29-L32 (2005).
- [2] M. Amenomori *et al.*, *ApJ*, **633**, 1005-1012 (2005).
- [3] M. Amenomori *et al.*, *ApJ*, **635**, L53-L56 (2005).
- [4] M. Amenomori *et al.*, *Phys. Lett.* **B632**, 58-64 (2006).

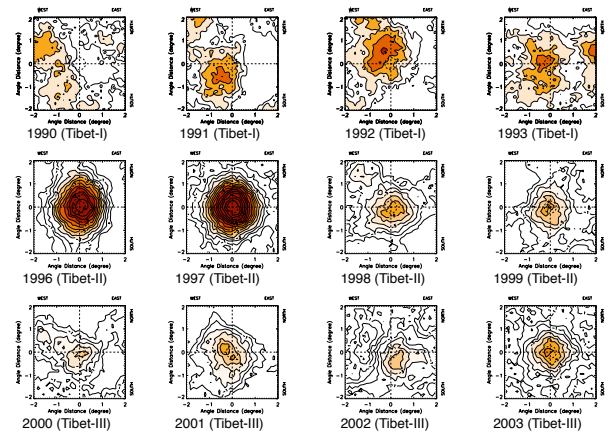


Fig. 15. Yearly variation of the Sun's shadow observed by the Tibet air shower array from 1990 to 2003. Mode energies are 10 TeV.

Ashra Project

[Spokesperson: Makoto Sasaki]

ICRR, Univ. of Tokyo, Kashiwa, Chiba 277-8582

ICRR, Univ. Tokyo; Chiba Univ.; Ibaraki Univ.; NAOJ; KEK; Toho Univ.; Tokyo Inst. Tech.; Univ. Hawaii Manoa; Univ. Hawaii Hilo;

Overview

The All-sky Survey High-Resolution Air shower detector (Ashra) was designed primarily to elucidate the cosmic ray origins even if they are transient objects such as Gamma Ray Bursts (GRB), Soft Gamma Ray Repeaters (SGR), and so on, detecting not only very high energy (VHE) γ s, ν s, and nuclei, but also ultra-violet and blue lights. Ashra records in unprecedented arc-minute detail images of VHE cosmic particle interactions in the atmosphere and star lights using new ultra-wide-angle high resolution optics, an image intensifier (II) and CMOS technology. The first data collection run using prototype versions of the optical and trigger systems was performed in 2004-2005, allowing us to evaluate the performance of the systems and to develop an analysis strategy. Full configuration of the Mauna Loa site will be achieved by 2007. We will summarize the Ashra project and the pilot data using the analysis for optical transient and TeV γ -ray search.

Mission

The All-sky Survey High-Resolution Air shower detector (Ashra) [1] [2] [3] was designed primarily to elucidate the cosmic ray origins involving transient objects which are plausible candidates for the particle accelerators. Ashra records in unprecedented arc-minute detail images of VHE cosmic particle interactions in the atmosphere, so called air-shower, and star lights using new ultra-wide-angle high resolution optics, an image intensifier (II) and CMOS technology. The survey will simultaneously map 80% of the entire sky, in reasonable detail with a few arcmin resolution, determining the positions and absolute energies of very high energy gamma

rays (VHE γ s), very high energy neutrinos (VHEVs), and extremely high energy cosmic rays (EHECRs), as well as the positions and brightnesses of ultra-violet (UV) and blue (B) lights radiated from celestial objects.

From an observational point of view, VHEV events are unambiguously characterized by tau lepton air-showers come from the Earth or a mountain as shown in Fig. 1. The clear identification of the horizontally upward air-shower events induced by VHEVs requires precise pointing accuracy of arc-minutes. VHE γ events are efficiently distinguishable from background hadron air-showers with Cherenkov imaging analysis considering the association angles with respect to the sources and comparing the observed shower shapes with the expected ones. We can expect the higher efficiency of the shower shape analysis for the p/γ separation with the good advantage of higher resolution of images taken by Ashra. For EHECRs we will utilize the air fluorescence lights generated air-showers. With the sufficient angular resolution of Ashra the strength and coherence properties of the cosmic magnetic field along the line of sight towards the sources can be estimated from the arrival directions and energies of the clustered events, that induces determination of the cosmic ray composition [4]. The capability of detecting UV-B lights allows us enjoy optical transient search independently even without any satellite trigger.

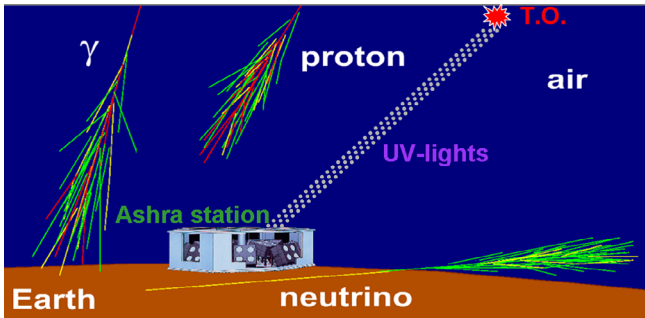


Fig. 1. Topologies of air-showers induced by VHE γ , ν , p , and light rays from transient object (T.O.).

Observationally driven high energy astrophysics calls for detailed multi-messenger based modeling of plausible sources of high energy radiation, both in the Galaxy and beyond, for multiwavelength and multi-particle observations, as well as for detailed population studies. The powerful approach of Ashra monitoring simultaneously multi-particle and light in almost all-sky will thus address fascinating, fundamental questions about the high energy universe, and will provide a unique opportunity to probe into very energetic phenomena such as prompt optical flashes and particle radiations from high energy transients such as Gamma Ray Bursts (GRBs) and Soft Gamma Ray Repeaters (SGRs) and so on.

Cosmic GRBs appear to be the most relativistic phenomenon observed thus far. GRBs are of two classes: long (>2 s) soft spectrum bursts and short (<2 s) hard events. The most significant progress has been made with respect to understanding long GRBs, which are typically observed at high redshift ($z > 1$) and are found in subluminal star-forming host galaxies. Long GRBs are likely to be produced

in core-collapse explosions of massive stars. In contrast, no short GRB other than GRB050709, which was discovered by HETE-2 [5], has been accurately and rapidly identified. However, phenomena responsible for short GRBs, especially for the central engine, have not been unambiguously identified yet. Systematic study of optical flashes accompanying GRB could impose important limits on theories explaining burst mechanisms and their energy engines. The jet opening angle has been inferred for several GRBs, and appears to range from 2° to 30° [6]. Therefore, the true GRB rate may be greater than approximately 100 times that detected by satellite experiments such as BATSE, HETE-2, INTEGRAL, and Swift. The appearance of these off-axis afterglows remains an open question. The discovery of “orphan” GRBs (optical transients with no gamma rays) would provide definitive evidence of the jet model [7].

It is also quite likely that other particles, in addition to γ -rays, are emitted in GRB events. For instance, it has been pointed out that the fireball model of GRBs is closely related to extragalactic cosmic rays [8], extremely high energy cosmic rays [9][10][11], and high energy neutrinos [12]. Neutrino productions with ~ 10 TeV to 10 PeV in a mechanism in the context of the supernova model as precursors to GRBs are also advocated [13] [14]. There are important hypotheses suggesting that bursts of very high energy γ having energies of ~ 1 -10 TeV that are associated with GRBs originate from inverse Compton cooling [15] and synchrotron radiations from protons accelerated to extremely high energy [16] in the jets. Since cosmological GRBs appear to be a relatively homogeneous population of sources with a narrow luminosity function [17][18], GRBs can also be considered in exploring cosmology.

SGRs are explosions in the Milky Way possibly due to starquake of highly magnetized neutron star [19]. The giant flare of SGR 1806-20 was the brightest cosmic transient to date for ~ 0.1 sec with flux ~ 10 erg s^{-1} [20]. Detectable TeV-PeV neutrinos, EeV cosmic rays and possibly TeV gamma-rays in coincidence from giant flares of magnetars such as SGR 1806-20 have been suggested [21] [22].

From the overview on the studies on transient objects, the major function of Ashra, watching the transients in all-sky simultaneously through multi-messengers involving VHE particles and optical lights, could be of great consequence for more profound apprehension of details of progenitors and mechanism of transient objects.

System

Ashra records optical images in 1.2 arc-minute detail of VHE cosmic particle interactions in the atmosphere using new optical system, II, and CMOS technology. Tracks of nitrogen fluorescence and beams of Cherenkov radiation reveal the arrival direction, energy, and identity of cosmic rays (neutrinos, nuclei and gamma rays) over an energy range of seven orders of magnitude, from the TeV scale to the EeV scale and beyond. Ashra sees not only near horizontal air showers caused by neutrinos, but also showers exiting the earth or the nearby mountains due to conversion of traversing tau neutrinos, and includes a view of the Galactic Center region. Moreover, the

detector can be used to seek optical transients, providing early alert to telescopes for more detailed observation, particularly those located nearby.



Fig. 2. Ashra-1 station layout on the Hawaii Island.

Ashra will eventually consist of three complete full-stations to be incrementally installed at Mauna Loa (3,300 m a.s.l.), Camp Kilohana (2,014 m) on the side of Mauna Kea, and Hualalai (2,320 m) on the side of Mauna Kea on the island of Hawaii. Each full-station, separated by 30–40 km, observes the entire moonless night sky with 12 detector units of one main station and 4 detector units of one sub-station via the stereoscopic observation method.

From the viewpoint of funding strategy, the Ashra project is subdivided into two project phases. The first phase (Ashra-1) includes the complete main station (Ashra-main) at Mauna Loa and two incomplete sub-stations in a cost effective manner (Fig. 2). One sub-station (subH: sub-detector for higher field of view) at Ashra-1, which is dedicated to near-zenith viewing (zenith angle $\lesssim 50^\circ$) with four detector units, will be installed at a distance of 100 m between the centers of the main station and the sub-station at the same Mauna Loa site area. The locations and directions of the detector units were determined after maximizing the total field of view from the station with a ray-tracing technique and detailed measurements of levels in and around the Mauna Loa site area as shown in Fig. 3. Another sub-station (subL: sub-detector for lower field of view) at Ashra-1, which is dedicated to near-horizon viewing with eight detector units (elevation angle $< 40^\circ$), will be installed at Camp Kilohana at a distance of 32 km from the Ashra main station. Using both the main and subH stations, we can enjoy stereoscopic observation primarily for air Cherenkov images of VHE γ induced air-showers. Using both the main and subL stations, we can enjoy stereoscopic observation for hybrid air Cherenkov and fluorescence images or for fluorescence images of earth or mountain skimming VHE ν -induced air-showers as well as air fluorescence images of EHECR-induced air-showers. The main, subH, and subL stations are shown in Fig. 2.

In the Ashra light collector optics, as shown in Fig. 4, UV and B ($\lambda = 300\text{--}420$ nm) photons from air showers and directly from celestial objects are collected using modified

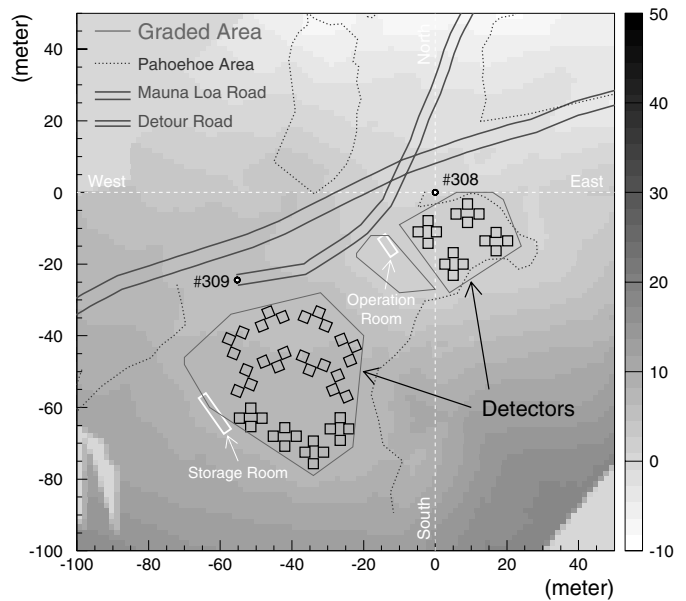


Fig. 3. Detector layout plan at the Ashra Mauna Loa site.

Baker-Nunn optics [23] [24]. The light collector utilizes 2.2-m projected diameter spherical reflector for viewing a 0.42 sr (full FOV 42°) region of the sky. The ray tracing study shows the RMS point spread corresponds to 0.8 arc-minutes for incident parallel lights stably within the full FOV of 42° , not strongly depending on the spectrum functions of the three kinds of lights: Cherenkov, fluorescence, and star lights. Air lights from air-showers and stars are firstly passed through a correcting aspherical lens composed by three acrylic plates directly cut and polished, which can significantly reduce spherical and coma aberrations. The reflector consists of seven segmented glass-mirrors coated with aluminum and aluminum oxide in a cost effective manner, of which RMS point spread and reflectivity have been tested and evaluated to be 0.4 arc-minutes and 90% respectively. Following the optical system of the correcting lens and reflector, a 20-inch diameter photoelectric lens imaging tube is equipped on the focal sphere of the modified Baker-Nunn optical system, which makes demagnified images on the 25 mm diameter output window after the photoelectric conversion, electrostatic lensing, and scintillation on the phosphor-coated fiber optic window. The followed images pass through a photoelectric pipeline which transports images without degrading the required performance of resolution and brightness for trigger processing and recording on 4-megapixel CMOS sensors with trigger controls, as well as recording on 4-megapixel CCD sensors for untriggered images of UV-B star lights periodically with 4-s exposure and 1-s readout. The image pipeline also makes an important role of making time delay utilizing sustained afterglow in the output phosphor screen just before the CMOS sensor with trigger controls.

Covering the sky with 49 megapixels, an approximately thousand-fold improvement over currently employed technology in terms of pixel cost and ultra wide field of view not sacrificing fine pixelization, allows resolution to be measured

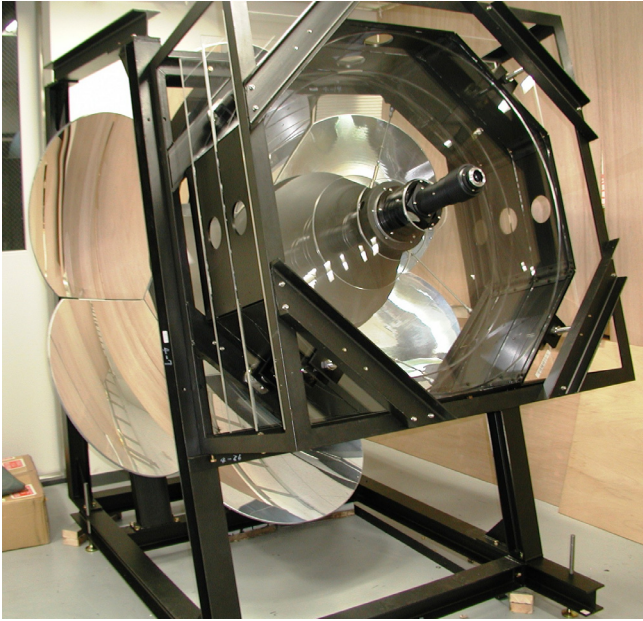


Fig. 4. Ashra optical system and photoelectric lens image tube system.

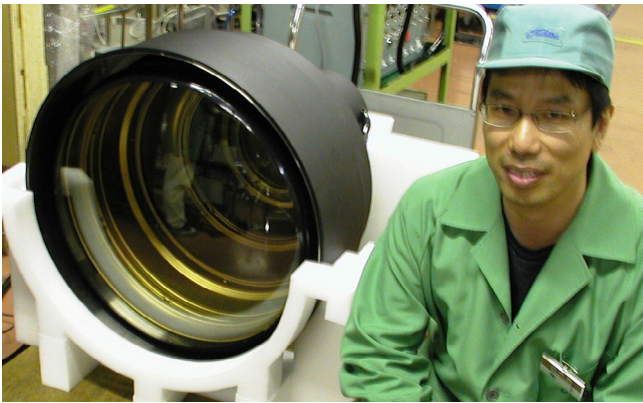


Fig. 5. Ashra 20-inch photoelectric lens image tube.

in a few arc-minutes rather than in degrees (as is the case with photomultipliers). This 1.2-arc-minute pixelization together with the stereoscopic observation technique provides shower reconstruction with better pointing accuracy (for instance a few arc-minutes for EHECRs with the stereo fluorescence technique), improved energy determination, and an extension of the range at which distant high energy showers can be detected (because of the ability to resolve shorter tracks across the sky).

The most unique feature of Ashra, however, is its ability to serve as a simultaneous detector for both long duration (several μ to several tens μ s) fluorescence events and short duration (several ns) air Cherenkov events, which was not possible with earlier instruments. The problem of integrating background light over long times for fluorescence events is solved by an image delay system to the CMOS sensors and a moving electronic shutter driven from a parallel 64×64 hybrid multi-anode photomultiplier trigger. Note that the effective area of

Ashra for such a search is much larger than either in ground array type air-shower detectors or in water Cherenkov-based detectors.

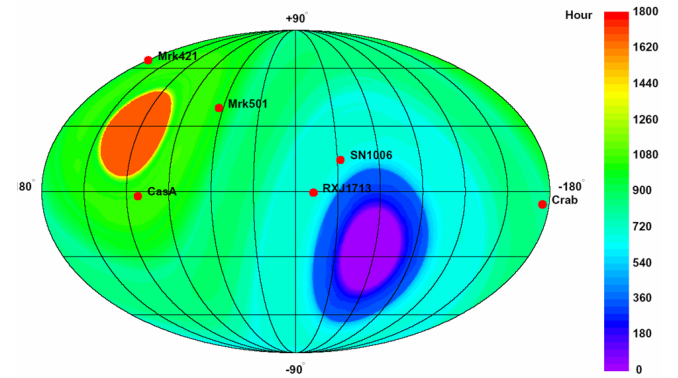


Fig. 6. Expected observation time of Ashra for 2-year operation, taking into account the realistic operational efficiency (55%) estimated from the test observation at the Haleakala site.

The key improvement here is the ability to continuously monitor almost the entire sky for extended (dark) periods, which enables searches for new point (and time varying) sources, such as numerous GRBs, soft SGRs, hidden sources in the galactic center region, and unidentified EGRET sources. The effective observation time is expected to be approximately one thousand hours per year for objects near Polaris and several hundreds hours per year for typical objects in the northern hemisphere, such as Mkn501, as shown in Fig. 6, while taking into account the realistic operational efficiency calculated from the test observation over a ten-month period at the Haleakala observatory (3030 m a.s.l.) on the Maui island next to the Hawaii island where Ashra-1 is under construction at the similar altitude (3300 m a.s.l.). As a result, the sensitivity for steady TeV γ sources with Ashra-1 is estimated to be $\sim 5\%$ Crab requiring the signal-to-noise ratio (SNR) to be more than 5 for 1000 hours observation corresponding 2-year operation reasonably assuming the primary energy threshold of 2 TeV, the only p/γ discrimination cut of the association angle of 0.1° with respect to the tracked source object.

The photoelectric image pipeline consists of a focal sphere photoelectric imaging tube (PLIT) [25] [26], as shown in Fig 7, relay lens systems, a delay II, a half-mirror light splitter, which provides the functions of light splitting and optical delay, a trigger image sensor and a high resolution CMOS image sensor. The use of a multiple stage pipeline and three-way light splitter allows image transportation to the CMOS image sensor with sufficient gain without sacrificing the fine image resolution and self-trigger for short-time phenomena, such as atmospheric Cherenkov and fluorescence signals. In addition, an on-board commercial CCD chip can continuously catch untriggered light images. Since the examined resolution at the focal surface is much better than the required resolution, four FOP-bundle light guides after sub-telescopes, which can be connected into one set of trigger sensor system, contribute significantly to the high cost-performance of this system. Following the light splitter, a proximity focused II is equipped in

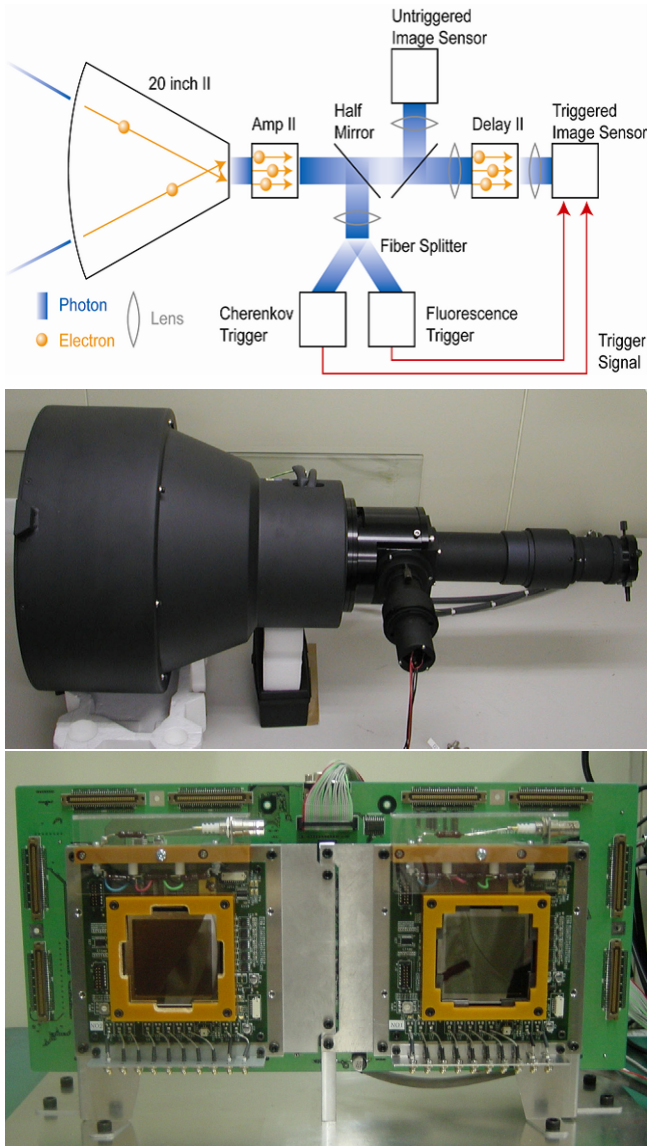


Fig. 7. Ashra photoelectric image pipeline (PIP) system. Block diagram (top), prototype (center), and 32×32 -pixel Cherenkov and fluorescence independent trigger sensor prototype (bottom).

order to produce a delay for the trigger decision time using the scintillation light on phosphor P-46, the 10%-decay-time of which is 160 ns.

The Ashra trigger device [27] is composed by two trigger sensors dedicated to triggering Cherenkov and fluorescence signals transmitted through 64×64 optical fiber bundle with 4 m length and following level-1 (L1) and level-2 (L2) trigger decision circuits which issue exposure and readout control signals to the fine CMOS image sensors mounted on the light collectors. The trigger image sensor consists of photocathode, electrostatic lens, and 64×64 Si pixel array sensor (SiPix). The 30 kV operating voltage of the electrostatic lens yields ~ 7500 electron-hole pairs for one photoelectron bombered into the SiPix, of which 64×64 independent output currents can be utilized to make L1 and L2 trigger decisions significantly for Cherenkov and fluorescence lights from air-showers induced by $VHE\gamma$, ν , and EHECR. Each SiPix pixel

is responsible for $0.67^\circ \times 0.67^\circ$ FOV, in which the night sky background flux corresponds to ~ 0.3 photoelectrons / 100 ns in the first cathode on the input window of PLIT. Since time duration of $TeV\gamma$ Cherenkov signal is short (\sim several ns), sufficient SNR can be obtained using simple pixel thresholds and adjacent patterns for L1 and L2 trigger discriminations respectively. On the other hand, air fluorescence tracks from VHEV and EHECR air-showers take rather longer transient times (several μs to several 10 μs) in the LC FOV largely accumulating first-cathode photoelectrons from the night sky background (~ 20 to 200 photoelectrons in the trigger pixel). Therefore, we incorporate L2 trigger of the track reconstruction and the moving exposure on readout one fine CMOS image sensor synchronously with the L1 and L2 trigger controls based on the FPGA techniques combined with digital signal processors (DSPs).

In order to keep a good SNR for a fluorescence track of AS, the 2-dimensional shutter is opened one by one along the AS development in the FOV of the CMOS image sensor following the L1 trigger control. For fine CMOS image sensor response to the L2 trigger, very fast readout scheme (~ 1 kHz) is required in order to keep dead time fraction low. Thus, parallelization of readout line and random access of cell of pixels allowing windowing of region of interest and required. We have developed a custom CMOS image sensor satisfying these various special properties as shown in Fig. 8.

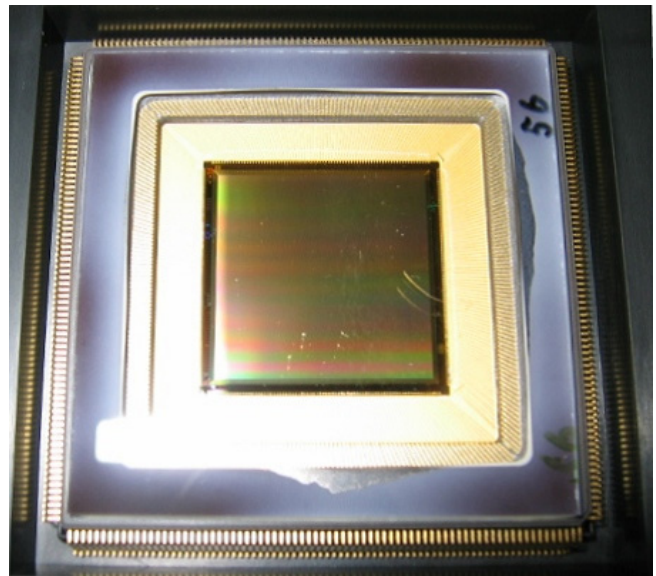


Fig. 8. Developed 2048×2048 Ashra fine CMOS image sensor with the cell exposure and readout control.

Test Observation

All Ashra systems existed in the prototype stage, and the first versions were assembled on Haleakala in Fall 2004. Land acquisition on Mauna Loa via the University of Hawaii has already completed. Installation of the first station on Mauna Loa was planned to begin in 2005 and to be completed in 2006. From October 2004 to August 2005, the moonless night time was 1,526 hours. In this time, we were able to make obser-

vations for 844 hours. This inefficiency is due primarily to bad weather, such as high humidity or rain. The total operational efficiency is estimated to be 55% of the possible moonless night time and 11% of entire time between the starting time and ending time of the test observation era. The observational exposure time distribution on the celestial sphere coordinates are shown in Fig. 9, which can be useful to estimate the possible observation time with the actual Ashra station at the Mauna Loa site.

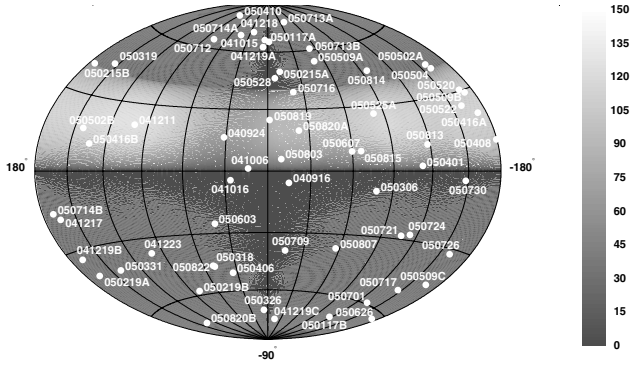


Fig. 9. Integrated exposure time distribution on celestial sphere with the Ashra 2/3-scale prototype detector.

The fine resolution (arc-minutes) in the ultra wide field of view (0.5 sr) has already been demonstrated using a 2/3-scale model. Fig. 10 shows an example of a 50-degree FOV image in which the constellations Taurus and Orion can be clearly identified with the 2/3-scale prototype. The inset, a two-degree square window, shows a close-up view of the Pleiades.

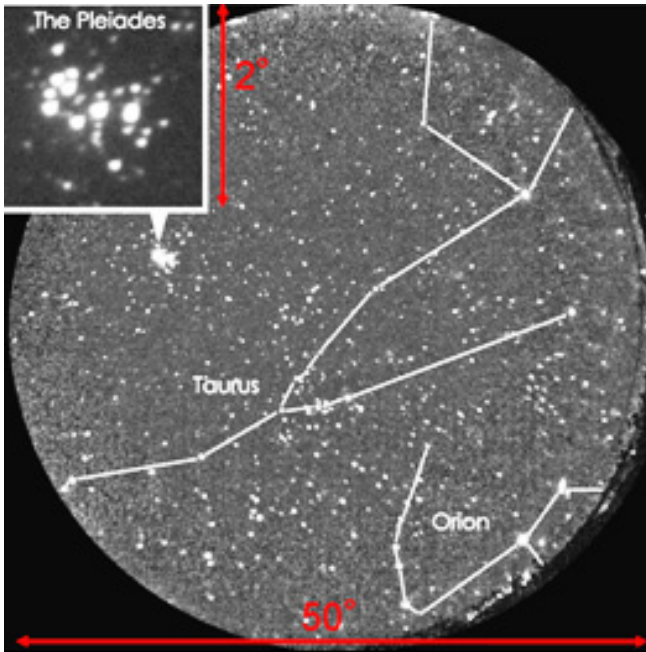


Fig. 10. Example of a 50-degree FOV image in which the constellations Taurus and Orion can be clearly identified. The inset, a two-degree square window, shows a close-up view of the Pleiades.

Using the prototype Ashra optical system, we successfully performed a cross-observation of the field covering the HETE-2 WXM error box of GRB041211 continuously between the time 1h7m before GRB041211 and that 1h41m after GRB041211 taking 2,000 images covering the WXM error box every 5 s with a 4-s exposure time. We detected no new objects in the WXM error box, indicating that the 3-sigma limiting magnitudes are stringently derived [28] [29] [30]. The limiting magnitude is shown in Fig. 11 [31] [32] and can be compared with the GRB990123 light curve detected by ROTSE [35].

We also successfully performed two more world-earliest cross-observations with Swift: GRB050502b [33] and GRB050504 [34].

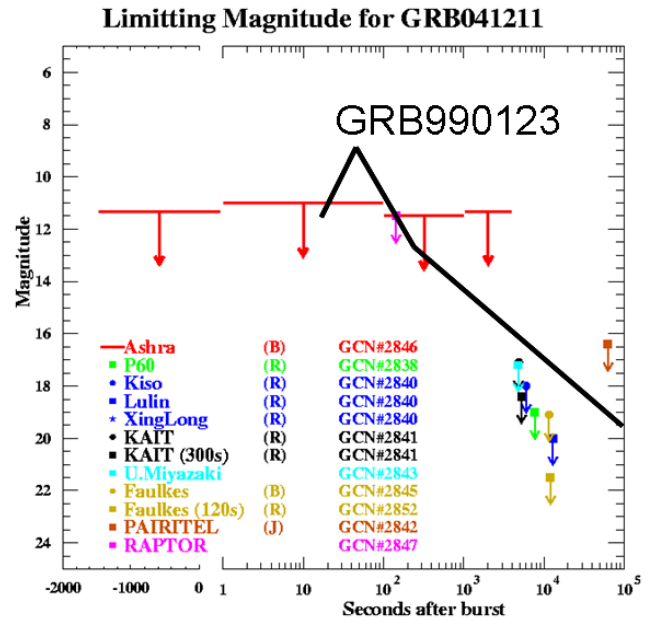


Fig. 11. 3-sigma limiting magnitudes of the present study and comparison with other observations for GRB041211 as a function of time after GRB. The measured optical light curve from GRB990123 [35] [36] is also shown as a thick straight line. Note that the horizontal axis axis unavoidably stans for time (s) in logarithmic scale after the burst (positive) and in linear scale before the burst (negative).

A demonstration alt-az mounted air Cherenkov detector on Haleakala was set up and has also been collecting data with the image pipeline and the self-trigger system. After a detailed analysis, we have confirmed the peak of TeV γ -rays from the Crab nebula to be greater than 5σ . We collected data for TeV γ -rays from Mkr421 and Mkr501 for the observation time of several tens of hours under good weather conditions. The self-triggered Cherenkov image is shown in Fig. 12. In addition, we recently became able to make cross-observations of TeV γ -rays associated with GRB within 10 seconds after appropriate alert from a satellite.

Status of Construction at the Mauna Loa site

Since July 2005, the State of Hawaii has formally approved our application for the use of the proposed site for

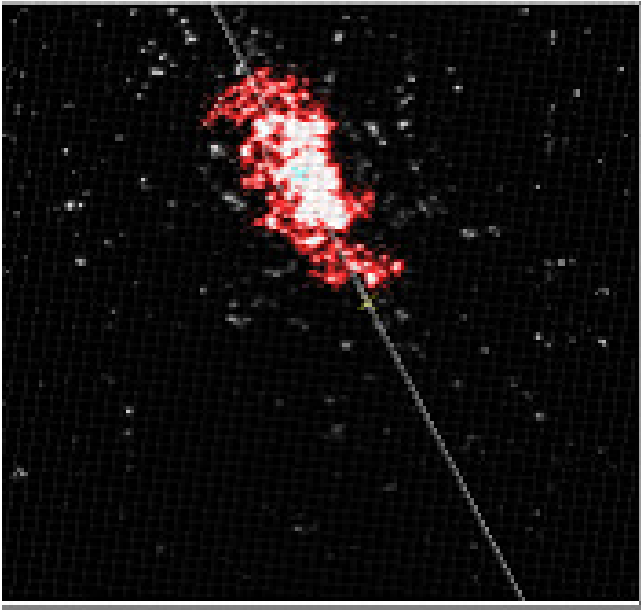


Fig. 12. Self-triggered Cherenkov image of air-shower detected by the Ashra photoelectric image pipeline, which includes a trigger sensor system. The image was taken during tracking Mkr501.

the Ashra main station on Mauna Loa, for viewing almost the entire sky, and for the Ashra station (subH), for viewing higher elevation angles. The detector layout plan is shown in Fig. 3. After approval, we immediately occupied the site and began development. After finishing the grading work for the area of 2,419 m² at the end of July 2005, installation of electrical power lines and transformers was performed until the beginning of September. The materials were received at the Mauna Loa site, and the construction of the detector was started in October. Finally, the construction of the Ashra main station, for viewing higher FOV at zenith angles of less than 42° started in October 2005. Currently, (mid December 2005) a few shelters having motorized rolling doors, acrylic plate windows to maintain air-tightness, and heat-insulating walls and floors have been constructed and positioned on eight construction piers of concrete blocks at the Mauna Loa site, as shown in Fig. 14. In some shelters, the optical elements of the Ashra light collectors have been already installed and are being checked and adjusted for optical performance with respect to star light image data collection by the Ashra optical systems.

In December 2005, we evaluated the night sky background flux at the Mauna Loa site using the actual Ashra LC optical system already installed and aligned in a shelter. The result as shown in Fig. 15 is fairly consistent with the measurements in La Palma and Namibia made by the HESS group [37]. It has provided us a good opportunity to check our good understanding of the light collection efficiency of the Ashra LC system. From the star light observations, we confirmed our understanding of the light correction efficiency of the Ashra LC to be accurate within 5% level.



Fig. 13. The Ashra Mauna Loa site just before detector installation.



Fig. 14. Photograph of an Ashra light collector installed in a shelter. A motorized aluminum rolling door is equipped on the roof. Under the rolling door, an acrylic plate is placed over a 1,800-mm-square window.

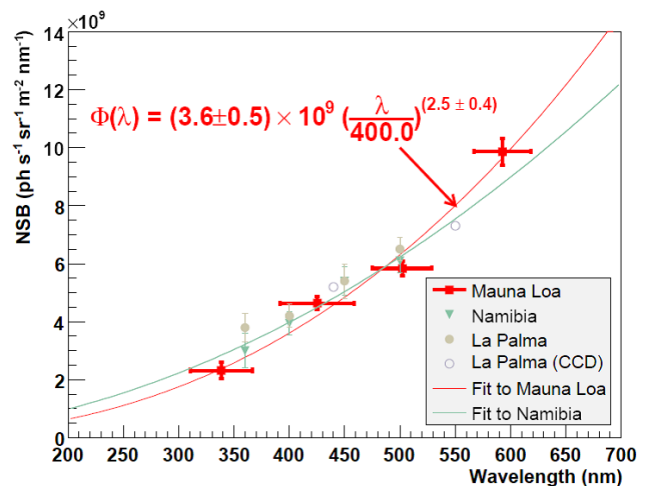


Fig. 15. Measurements of night sky background flux at the Ashra Mauna Loa site. Measurements at La Palma and Namibia made by the HESS group [37] are also shown.

Conclusion

In conclusion, the prototype detectors have met all of our specifications for the ultra-wide-angle high resolution optics

and image pipeline. Thus, we are proceeding confidently with the first phase of construction of the full-scale detector station system at Mauna Loa. Currently, (mid December 2005), the construction of Ashra-1 at the Mauna Loa site is progressing steadily.

Acknowledgment

This study was supported in part by the Coordination Fund for Promoting Science and Technology (157-20004100) and by a Grant-in-Aid for Scientific Research (16740130) from the Ministry of Education, Science, Sports and Culture of Japan.

Bibliography

- [1] <http://www.icrr.u-tokyo.ac.jp/~ashra>
- [2] M. Sasaki, *Progress of Theoretical Physics Supplement*, vol. 151, pp. 192–200, 2003.
- [3] Sasaki, M., et al., 2005. Proc. 29th Int. Cosmic Ray Conf. Pune 8, 17-200.
- [4] D. Harari, S. Mollerach and E. Roulet, *astro-ph/0205484*.
- [5] J. S. Villasenor, *et al.*, *Nature*, 437 855-858 (2005) .
- [6] D. A. Frail, *et al.*, *ApJ*, **562**, L55 (2001).
- [7] J. E. Rhoads, *ApJ*, **487**, L1 (1997).
- [8] A. Shemi, T. Piran, *Astrophys. J.*, **365** (1990) L55.
- [9] E. Waxman, *Astrophys. J. Lett.*, **452** (1995) 1.
- [10] M. Vietri, *Astrophys. J.*, **453** (1995) 883.
- [11] M. Milgrom, V. Usov, *Astrophys. J. Lett.*, **449** (1995) L37.
- [12] E. Waxman, J. N. Bahcall, *Phys. Rev. Lett.*, **78** (1997) 2292.
- [13] J. Granot and D. Guetta, *Phys. Rev. Lett.* **90** (2003) 191102.
- [14] D. Guetta and J. Granot, *Phys. Rev. Lett.* **90** (2003) 201103.
- [15] A. M. Beloborodov, *Astrophys. J.* 618 (2004) L13-L16.
- [16] T. Totani, *Astrophys. J.* 501 (1997) L81-L84.
- [17] E. Cohen, T. Piran, *Astrophys. J.* **444** (1995) L25.
- [18] J. M. Horack, A. G. Emslie, *Astrophys. J.* **428** (1994) 620.
- [19] B. Zhang, Z. G. Dai, P. Meszaros, E. Waxman, A. K. Harding, *ApJ*, **595**, 346 (2003).
- [20] T. Terasawa, *et al.*, *Nature*, 434, 1110 (2005).
- [21] K. Ioka, S. Razzaque, S. Kobayashi, P. Meszaros, *ApJ*. 633 (2005) 1013-1017.
- [22] D. Fargion and M. Grossi, *Nuovo Cim.* **28C** (2005) 809-812.
- [23] M. Sasaki *et al.*, *Nucl. Instrum. Methods*, vol. A492, pp. 49–56, Oct. 2002.
- [24] J. Baker, U.S. Patent 3022708, Feb. 27, 1962.
- [25] M. Sasaki *et al.*, *Nucl. Instrum. Methods*, vol. A501, pp. 359–366, Apr. 2003.
- [26] Y. Asaoka, Y. Aita, T. Aoki, M. Sasaki, *IEEE Trans. Nucl. Sci.*, IEEE, 52, 1773-1778, 2005
- [27] Y. Arai *et al.*, *Proc. 28th Intl. Cosmic Ray Conf. (Tsukuba)*, pp. 961–964, 2003.
- [28] Dezalay, J-P, et al., 2004. GCN Circ. 2839.
- [29] Wozniak, P., et al., 2004. GCN Circ. 2847.
- [30] Sasaki, M., et al., 2004. GCN Circ. 2846.
- [31] M. Sasaki *et al.*, 29th ICRC, June (2005) 1, 101.
- [32] Sasaki, M., et al., 2005. Proc. 29th Int. Cosmic Ray Conf. Pune 5, 319-322.
- [33] Sasaki, M., et al., 2005. GCN Circ. 3499.
- [34] Sasaki, M., Manago, N., Noda, K., Asaoka, Y., 2005. GCN Circ. 3421.
- [35] C. Akerlof *et al.*, *Nature* 398, 400-402 (1999).
- [36] Sari, R., Piran, T., 1999. *ApJ* 517, L109.
- [37] Preuß, et al., *Nucl. Instrum. Methods*, **A481** (2002) 229.

ASTROPHYSICS and GRAVITY DIVISION

Overview

Astrophysics and Gravity Division consists of Gravitational Wave Group, The Sloan Digital Sky Survey Group and Theory Group. The Gravitational Wave Group conducts TAMA project jointly with researchers of gravitational wave experiment and theory in Japan. The Group also conducts a CLIO project that aims to practically test the cryogenic laser interferometer system underground in Kamioka as one of R&Ds for LCGT project to detect gravitational wave events. The Sloan Digital Sky Survey Group continues accumulating data of images and spectroscopic observation of galaxies and publishing papers in collaboration with worldwide researchers. Theory Group conducts both theoretical study of the Universe and astroparticle physics.

TAMA Project

[Spokesperson : Kazuaki Kuroda]

ICRR, Univ. of Tokyo, Kashiwa, Chiba 277-8582

In collaboration with the members of: TAMA collaboration NAOJ, Tokyo; KEK, Tsukuba; UEC, Tokyo; Osaka City Univ., Osaka; Kyoto Univ., Kyoto; Osaka Univ., Osaka; Niigata Univ., Niigata

Overview

A gravitational wave is a physical entity in space-time predicted by Einstein's theory of general relativity. Its existence was proven by the observation of PSR1913+16 by Taylor and Hulse [1], who won the Nobel prize in 1993. However, nobody has succeeded to directly detect gravitational waves. The theory of gravitation can be tested by the detection of gravitational waves. A gravitational wave detector is the last eye of mankind to inspect the universe. In order to directly observe gravitational waves, we have been developing a sensitive interferometric gravitational wave detector, called TAMA, which is a 300 m baseline laser interferometer at the Mitaka campus of the National Astronomical Observatory of Japan (NAOJ) and several observations have been conducted, so far. TAMA was started in April, 1995, as a five-year project and extended by two years after 1999. TAMA is organized by researchers belonging to universities and national laboratories. We regard the TAMA interferometer as a step toward the final scale interferometer in the sense of technology and construction budget. We have so far achieved nine data-taking runs that span from two to eight weeks (Table 1). In the former half runs, its sensitivity improvement was the first priority. Nonetheless, both the stability and reliability had to be improved to check the sensitivity, itself. In the latter half runs, the operation became easier after installing an automatic control system.

Table 1. TAMA data-taking runs including long-term observations

Run	Term	Year	Live Time (Hour)
DT1	6-Aug → 7-Aug	1999	7
DT2	17-Sept → 20-Sept	1999	31
DT3	20-Apr → 23-Apr	2000	13
DT4	21-Aug → 4-Sept	2000	161
DT5	2-Mar → 8-Mar	2001	111
DT6	15-Aug → 20-Sept	2001	1038
DT7	31-Aug → 2-Sept	2002	25
DT8	14-Feb → 14-Apr	2003	1158
DT9	28-Nov → 10-Jan	2004	558

Status of TAMA Project

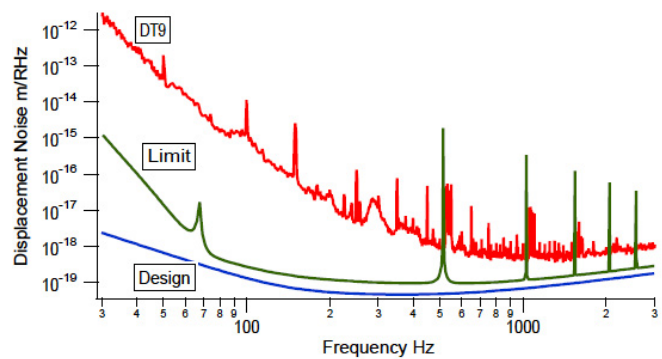


Fig. 1. Achieved sensitivity of TAMA at the time of data-taking run 9 (shown as DT9). The design sensitivity (Design) has several flaws arising from non-established theory to estimate thermal noise. The limit sensitivity (Limit) is a practically attainable one. The sensitivity (DT9) was physically limited by the photon shot noise at frequencies of more than 800 Hz. Since seismic noise at frequencies lower than 30 Hz disturbed the stable operation of the interferometer, a tighter feedback gain of the mirror alignment control loop was adopted, which resulted in an actuator force noise in a frequency range from 30 Hz to 300 Hz. We have not identified the noise source governing the range from 300 Hz to 800 Hz.

The achieved sensitivity of TAMA is shown as that of DT9 in Fig. 1. Since the design sensitivity had several flaws arising from non-established theory to estimate thermal noise of mirrors, we revised it as shown by "LIMIT". We recognize that there is still large gap between the achieved sensitivity and the practically attainable one. However, we could demonstrate that the basic techniques for the interferometer operation was acquired by the fulfillment of the objective noise curve at frequencies more than 800 Hz, where the optical system properly worked and the control system was appropriate. The noise spectrum at frequencies lower than 30 Hz was disturbed by non-stationary ground motion and the spectrum in a frequency range from 30 Hz to 300 Hz was determined by the actuator noise to stabilize the mirror alignment mainly due

to relatively larger seismic noise at Mitaka campus. We have not yet identified the noise source governing the spectrum in a frequency range from 300 Hz to 800 Hz. In regard with the output signal including the former observation runs, the output was contaminated by extensive rate of non-stationary fake events. However, its rate has been gradually reduced during the course of repeating observation runs. This is shown later in the subsection of the analysis of burst waves.

Analysis of inspiraling chirp waves

The main target of interferometric detectors is the event from coalescence of binary neutron stars. Orbiting binary star system is approximated by two point masses orbiting each other with losing kinematic energy and momentum by gravitational radiation. Until the coalescence, the radiated gravitational wave is a kind of sinusoidal wave with their frequencies going up and also with their amplitude increasing, which is called ‘chirp wave’. If we have an exact wave form of this chirp wave, we can apply filtering technique to extract signal from noisy data since the gravitational waves at the detector are so faint that they are usually covered with noise. The detector output, $s(t)$, is represented by

$$s(t) = Ah(t - t_c) + n(t)$$

where $h(t)$ is the template of known gravitational wave form, t_c is the coalescence time, A is the amplitude and $n(t)$ is the noise. The matched filtering is performed by calculation of ρ in a parameter space of masses, coalescence time, amplitude, and signal phase (α) as follows:

$$\rho(t_c, m_1, m_2, A, \alpha) = 2 \int \frac{\tilde{s}(f)\tilde{h}^*(f)}{S_n(f)} df,$$

where $\tilde{s}(f)$ and $\tilde{h}(f)$ are the Fourier transforms of $s(t)$ and $h(t)$, respectively, and $S_n(f)$ is one sided noise power spectrum density. The signal phase α reflects the polarization and the angular configuration between the source and the interferometer direction. The asterisk denotes the complex conjugation. If $s(t)$ contains gravitational wave signal, ρ takes a large value. However, the output of the practical interferometer is contaminated by non-Gaussian noise, the origin of which has not been well identified, yet. Owing to this noise, matched filtering produces extensive fake events. To reduce fake events, we adopted a measure of the deviation of events from real signal, which is a χ^2 time-frequency test, since non-stationary noise does not have the time-frequency behavior of inspiral chirp.[2] The frequency band (dc to Nyquist) is divided into n subintervals, chosen so that, for a chirp superposed on Gaussian noise with the observed power spectrum, the expected contribution to ρ is equal for each subinterval. χ^2 is calculated by summing the square of the deviation of each value of ρ from the expected value. This quantity must satisfy the χ^2 statistic with $2n - 2$ degrees of freedom as long as the data consist of Gaussian noise plus chirp signals only. Figure 2 shows the distribution of events obtained by the data of DT4[3], where χ^2 is renormalized as $\chi^2/(2n - 2)$ and signal-to-noise ratio, ζ , is calculated by $\rho/\sqrt{2}$. In this Fig. 2, the number of events are plotted for $\chi^2 < 2.5$, $\chi^2 < 1.5$, and $\chi^2 < 1.0$ as a function of ζ^2 , and an analytic fitting is

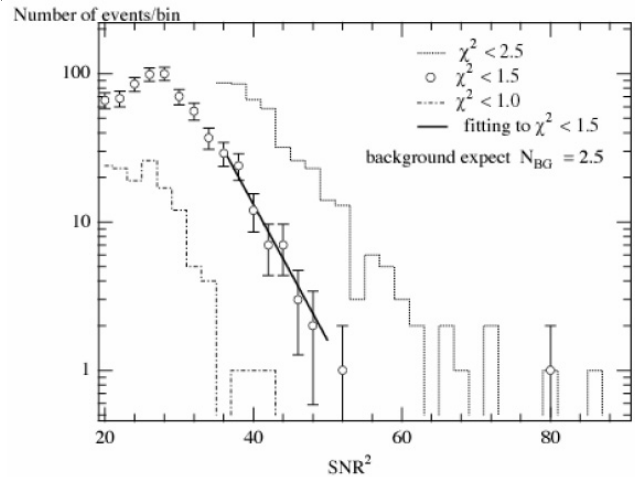


Fig. 2. Distribution of events obtained by the data of DT4[3]. The number of events are plotted for $\chi^2 < 2.5$, $\chi^2 < 1.5$, and $\chi^2 < 1.0$ as a function of ζ^2 , and an analytic fitting is also shown to $\chi^2 < 1.5$. The fitting was determined between $\zeta^2=35$ and 50. This fitting gives the number of events larger than $\zeta=7.2$ and $\chi^2 < 1.5$ as 2.5. The $\chi^2 < 2.5$, $\chi^2 < 1.5$, and $\chi^2 < 1.0$ corresponds to $10^{-3}\%$, 3.8%, and 46% false dismissal rates in Gaussian noise, respectively.

also shown to $\chi^2 < 1.5$. The fitting was determined between $\zeta^2=35$ and 50. This fitting gives the number of events larger than $\zeta=7.2$ and $\chi^2 < 1.5$ as 2.5. The $\chi^2 < 2.5$, $\chi^2 < 1.5$, and $\chi^2 < 1.0$ corresponds to $10^{-3}\%$, 3.8%, and 46% false dismissal rates in Gaussian noise, respectively. By this analysis, we have recognized that non-stationary Gaussian noise produced fake events with high ζ but these fakes were statistically eliminated by introducing χ^2 threshold evaluating signal-noise behavior, which resulted in setting an appropriate threshold of ζ for reliable detection of gravitational wave events. This is the reason why we set $\zeta=10$ in the design sensitivity of LCGT.

After DT4, the sensitivity of TAMA was improved every observation run along with its stability as shown in Fig. 3. The analyzed data of DT6[4] was reanalyzed with those of DT8 and DT9 by applying a revised cut of fake events, which is $\rho/\sqrt{\chi^2} (\equiv \zeta)$. Table 2 summarizes the result [5]. Since the sensitivity was better in DT9 than in DT8, DT9’s detection probability would have been much larger. However, since the first half of DT9 was contaminated by abnormal seismic noise due to building constructions at the campus, fake events exceeding the threshold degraded the detection probability of DT9.

Analysis of burst waves

The second target of gravitational wave (GW) detectors is a burst GW from stellar-core collapse (core-collapse supernova explosion). Since it is difficult to predict its waveform analytically due to the complex time evolution of the mass densities in the explosion process, the process and GW radiation have been investigated by numerical simulations. Among these simulations, Dimmelmeier *et al.* have presented rather systematic surveys on GWs from stellar-core collapses[6]. We adopted 26 waveforms from Dimmelmeier *et al.* to analyze TAMA data. According to the waveforms, the averaged am-

Table 2. Upper limit to the Galactic inspiral events. The unit of mass range is the solar mass and the threshold is set as the false alarm rate is once a year. The upper limit is given in a unit of event/yr for the Galaxy events with C.L.=90%

	mass range	detection probability	threshold of ζ	upper limit
DT6	1-3	$0.18^{+0.05}_{-0.05}$	21.8	130^{50}_{-30}
DT8	1-3	$0.60^{+0.07}_{-0.08}$	13.7	30^5_{-3}
DT9	1-3	$0.69^{+0.05}_{-0.07}$	17.7	60^{+7}_{-4}

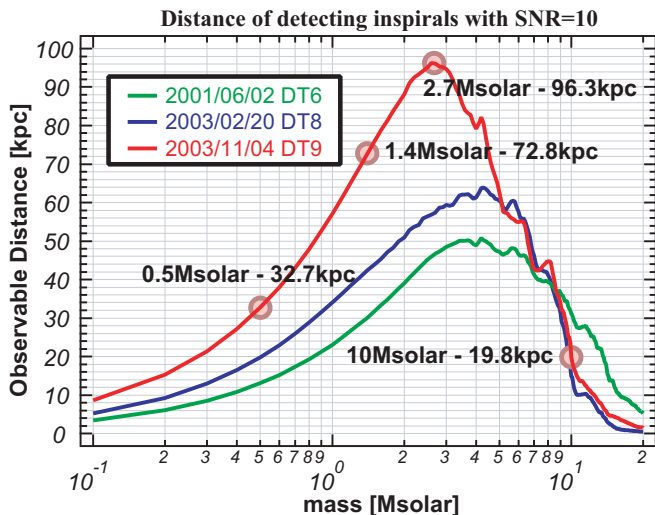


Fig. 3. Detectable range in DT6, DT8, and DT9 for each mass of a neutron star binary system by a signal-to-noise (SN) ratio of 10. The coalescence of the nominal binary system ($1.4 M_{\odot}$ of each mass) can be detected up to 33 kpc for DT6, 42 kpc for DT8 and 73 kpc for DT9.

plitude of GWs radiated by supernovae at the Galactic center (8.5 kpc distance from the detector) is $\langle h_{\text{peak}} \rangle = 1.5 \times 10^{-20}$ in a peak strain amplitude, or $\langle h_{\text{rss}} \rangle = 4 \times 10^{-22}$ [$\text{Hz}^{-1/2}$] in root-sum-square (RSS) amplitude. Here a RSS amplitude is defined by

$$h_{\text{rss}} = \left[\int_{-\infty}^{\infty} |h(t)|^2 dt \right]^{1/2},$$

where $h(t)$ is the strain amplitude of the GW. As for the adopted waveforms, the central frequencies of the waves, which are calculated from the weighting average of the power spectra, range from 90 Hz to 1.2 kHz, which is around the observation band of TAMA[7]. Also, it is estimated that a total energy radiated as GWs in one event is $\langle E_{\text{tot}} \rangle = 8 \times 10^{-8} M_{\odot} c^2$ in average.

Extraction of signals is performed using an excess-power filter[8]. The evaluation parameter is the total noise power in a given time-frequency region. Event triggers are generated by the following steps: (i) A spectrogram (time-domain change in noise spectrum) is calculated for each $\Delta t=12.8$ msec data segment from the output data of the detector. (ii) In each spectrum, power in a preselected frequency band, $\Delta f=2270$ [Hz] from 230 Hz to 2.5 kHz are averaged so as to obtain a time series of averaged power, P_n . Since each spectrum is normalized by the typical noise spectrum within 30 min before a calculation of the average in the frequency components, P_n represents

the signal-to-noise ratio (ζ): the ratio of the averaged signal power to the typical noise power in the region. (iii) Event triggers are extracted if the averaged power is larger than a given threshold, $P_n \geq P_{\text{th}}$. The parameters of the filter, length of the time chunk (Δt) for each FFT and analysis frequency band (Δf) were selected to be effective for the adopted Dimmelmeier waveforms.

We applied two veto methods to reject fake events caused by detector instabilities. One is a veto method using auxiliary signals for the detector monitor. We had noticed that there is some correlation between the non-Gaussian noise in the output and the laser power intensity. We can set a threshold carefully by estimating a false-dismissal rate. However, it is not sufficient to reject all fake events coming from various origins. Therefore, we added another veto method utilizing the waveform behavior; the time scale of the signal. In the burst-wave analysis, the waveforms by numerical simulations suggest that GWs from stellar-core collapse have a short duration, typically less than 100 msec. We know that some of the detector instabilities last longer than a few seconds from experience. Thus, some of the fakes caused by these slow instabilities are rejected by evaluating the time scale of the event triggers. Table 3 lists the data analysis result obtained from TAMA data applying the above veto methods.

Figure 4 shows the event-trigger rates plotted as a function of h_{rss} amplitude. The detector was gradually improved during the intervals of these data-taking runs. The event trigger rates were reduced from DT6 to DT9 by about a few orders for a given GW amplitude and by about an order for given trigger rate (last column in Table 3).

The above analysis is applied to set upper limit for stellar-core collapse events in our Galaxy using Monte-Carlo simulations with a source distribution model of our Galaxy and with adopted waveforms. Considering detection efficiency of TAMA, we obtained an upper limit for the Galactic-event rate to be 5.0×10^3 events/sec, which is considerably larger than the theoretical expectation of about 10^{-9} events/sec. This large discrepancy will be improved in future both by higher sensitivity and reduction of non-stationary detector noise.

Other data analysis

Apart from the above data analysis, many other analysis results have been reported using TAMA data in several conferences [9, 10, 11]. Since DT8 was performed in keeping pace with a data-taking run of LIGO (second science run, S2), the result was analyzed for burst wave [12] and the result for inspiral wave was published [13].

After DT9, we stopped the observational operation of TAMA and entered a work phase of noise-hunting to attain

Table 3. Summary of data-analysis results. The noise-equivalent GW RSS-amplitudes ($h_{\text{rss,noise}}$), the dead times by the vetoes (T_{rej}), the total effective observation times (T_{obs}), the trigger rates for $h_{\text{rss}} \geq 1 \times 10^{-18} [\text{Hz}^{-1/2}]$, and the GW RSS-amplitudes above which the trigger rates are one event per hour are described.

	$h_{\text{rss,noise}}$ [$\text{Hz}^{-1/2}$]	T_{rej} [hours]	T_{obs} [hours]	Rate [sec^{-1}]	1-hour $^{-1}$ amp. [$\text{Hz}^{-1/2}$]
DT6	4.5×10^{-20}	11.8	937.8	2.1×10^{-3}	2.1×10^{-18}
DT8	3.0×10^{-20}	18.0	1064.2	7.0×10^{-4}	1.4×10^{-18}
DT9	1.1×10^{-20}	0.8	194.6	2.5×10^{-6}	2.5×10^{-19}

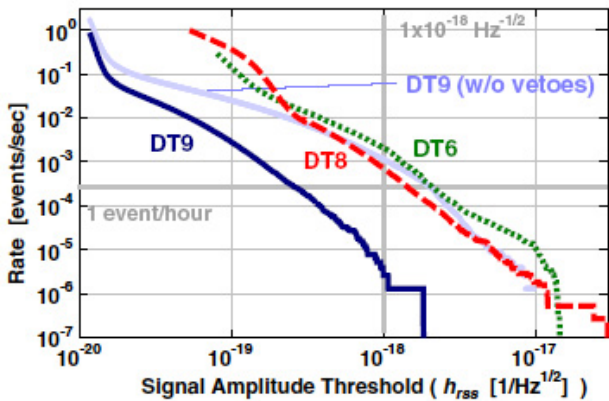


Fig. 4. GW amplitude and corresponding trigger rate: the event rate with larger amplitude than a given h_{rss} is plotted. The thin curve of DT9 represents the rate analyzed without any vetoes.

the final sensitivity.

LCGT Project

[Spokesperson : Kazuaki Kuroda] ICRR, Univ. of Tokyo, Kashiwa, Chiba 277-8582

In collaboration with the members of:

LCGT collaboration; National Astronomical Observatory (Japan), KEK, Physics Department (Univ. of Tokyo), Department of Advanced Material Science (Univ. of Tokyo), Earthquake Research Institute (Univ. of Tokyo), Department of Earth Science and Astronomy (Univ. of Tokyo), Institute for Laser Science (Univ. of Electro-Communications), Department of Physics (Osaka City Univ.), Department of Physics (Osaka Univ.), Physics Department (Kyoto Univ.), Yukawa Institute (Kyoto Univ.), Advanced Research Institute for Sciences and Humanities (Nihon Univ.), Agency of Industrial Science and Technology, National Institute of Information and Communications Technology, Department of Astronomy (Beijing Normal Univ.), Center for Astrophysics (Univ. of Science and Technology, China), Institute for High Energy Physics (Chinese Academy of Science), Inter University Centre for Astronomy & Astrophysics (IUCAA), Physics Department of Physics (University of Western Australia), Laboratory of Laser Interferometry (Sternberg State Astronomical Institute, Moscow Univ.

Overview

After the discovery of the highly relativistic binary neutron star system [14], a new young binary pulsar has been detected [15]. The former discovery had increased the coalescence rate from 10^{-6} to 10^{-5} a year in a galaxy as big as our Galaxy [16] and the latter pushes up by another factor of six. Although it is a good news for the detection of gravitational waves, we still need to wait for long time to detect by the presently existing detectors. This is the reason why we have planed LCGT (Large-scale Cryogenic Gravitational wave Telescope) [17]. There are many other possible gravitational wave sources in the universe other than the coalescence of binary neutron stars. However, the coalescence of binary neutron stars differs completely from other sources in the sense that its wave form is precisely predicted, and its existence has certainly been confirmed.

Current status of LCGT Project

The target sensitivity of LCGT is to observe binary neutron star coalescence events occurring at 257 Mpc with $S/N=10$ in its optimum configuration. This is ten-times more sensitive than that of the LIGO (I), and by two orders more than that of TAMA at their most sensitive frequencies. This will be attained by dual interferometers located underground, using a three-kilometer length baseline, cooling mirrors at cryogenic temperature, and a high-power laser source employing 150 W output. The optical configuration is a power recycled Fabry-Perot-Michelson interferometer with the resonant-sideband-extraction (RSE) scheme (in Fig. 5). The detailed design of the control system is under consideration. Table 4 lists the important parameters of LCGT, which were revised two times from the original design. The ultimate sensitivity of a laser interferometer is determined by seismic noise at low frequencies (10-30 Hz) (which is reduced by improving the vibration isolation system), and it is limited by photon shot noise at higher frequencies (more than 300 Hz), which can be improved only by increasing the light power in the main cavities. The sensitivity of middle frequencies (30-300 Hz) is limited by the photon recoil force noise. This requires that thermal noise is reduced both by decreasing the temperature and by decreasing the internal mechanical loss (*i.e.*, increasing the mechanical Q of vibration modes). The source of thermal noise comes from both mirror internal vibration, mechanical loss of the optical coating and swing noise of the pendulum suspending the mirror. The reduction of thermal noise is attained by cooling down both the mirror, itself, and the suspension system that suspends the mirror. The sen-

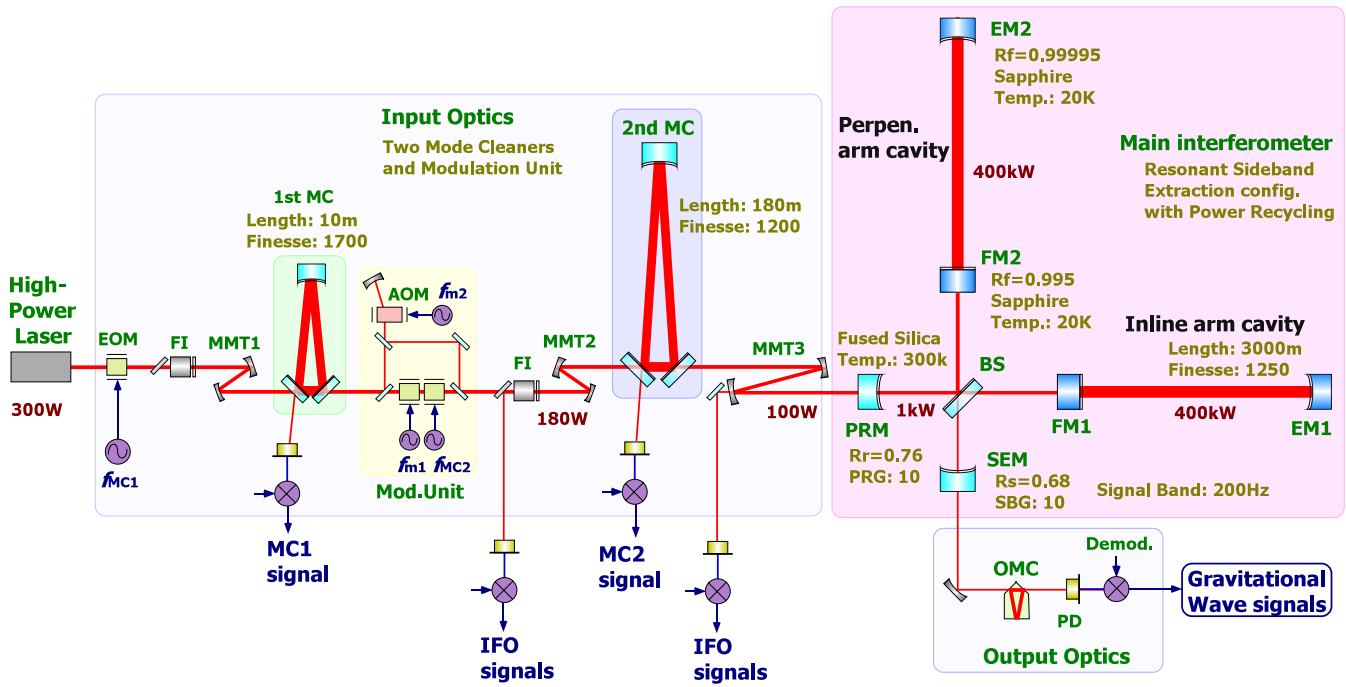


Fig. 5. Optical design of LCGT. The optical configuration is a power recycled Fabry-Perot-Michelson interferometer with the resonant-sideband-extraction (RSE) scheme.

Table 4. LCGT design parameters to detect binary neutron-star coalescence events in 257 Mpc.

Item	Parameter
Baseline Length	3 km
Interferometers	Two set
Optical Power	Power recycled Fabry-Perot-Michelson with RSE Laser: 150 W; Finesse: 1550 Input power at BS: 825 W Cavity power 780 kW
Beam radius at End Main Mirror	3 cm Sapphire 30 kg, 20 K Diameter 25 cm Mechanical Q: 10^8
Suspension pendulum	Frequency: 1 Hz; Q: 1×10^8
Vacuum	$\leq 10^{-7}$ Pa

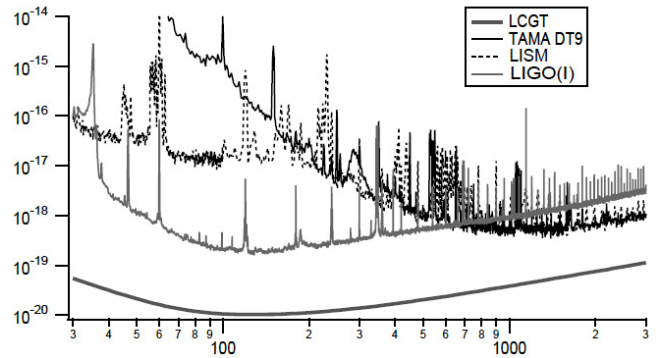


Fig. 6. LCGT sensitivity compared with others. The horizontal axis is frequency [Hz] and the vertical axis represents square root of power spectrum of displacement [$m/\sqrt{\text{Hz}}$]. Thin solid curve represents the noise spectrum of TAMA (DT 9) and dotted curve shows that of LISM placed underground of Kamioka. The lowest smooth curve represents the target sensitivity of LCGT. The second lowest one shows that of recent LIGO(I).

sensitivity attained by LCGT is higher by two orders than that of TAMA and by one order than that of LIGO(I). Figure 6 compares the sensitivity spectrum of LCGT with those of LISM (20m prototype interferometer placed underground of Kamioka mine), TAMA, and LIGO(I). The sensitivity in low frequencies of LCGT is attained by newly designed seismic attenuation system (SAS), which will be proven by the on-going installation of SAS into TAMA. That of higher frequencies is attained by higher laser power, which has been basically shown by TAMA. The mid-frequency region is improved by cryogenic mirror and suspension system, which will be proven

by the on-going project of CLIO. Although the improvement, especially two orders of magnitude at low frequencies, is adventurous, it is not impossible until the construction period of LCGT that needs four years after the beginning.

The main effort on the research and development for LCGT has been placed on cryogenic mirrors for the past years. The implementation of cryogenic mirrors is one of the most straight-forward solutions to improve the sensitivity.

The design of the cryogenic mirror system is shown in Fig. 7. The mirror is suspended by two loops of sapphire fibers connected to an auxiliary mirror that is a part of suspension

point interferometer. This mirror is also suspended from an alignment control platform that is suspended with an insulator rod connected through the center holes of the radiation shields to an isolation table suspended by a low-frequency vibration isolator, which is placed at room temperature. The auxiliary mirror has a heat link to the platform and another heat link connects the platform and a heat anchor point (4 K) inside the vacuum located just above the platform.

Both the cryogenic system and the vibration isolator are put inside a common high-vacuum chamber.

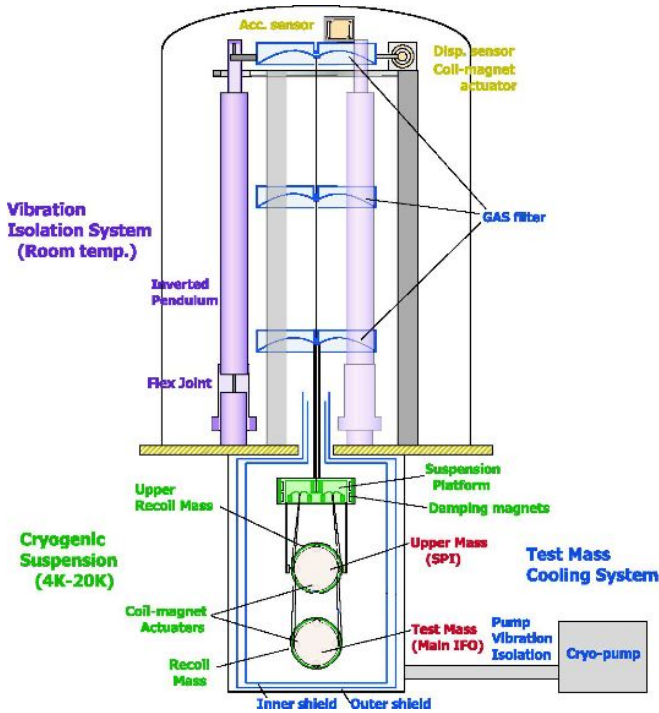


Fig. 7. Schematic design of the cryogenic suspension system. The mirror is suspended by sapphire fibers connected to an auxiliary mirror, which is suspended by metal wires from a platform that has a heat link to a 4 K heat anchor inside the vacuum. The platform is also suspended with an insulator rod connected through the holes of radiation shields to an isolation table suspended by a seismic attenuation system placed at room temperature in the common high vacuum.

To realize this concept, the following research subjects were considered:

1. Removal of heat produced by high-power laser illumination.
2. Holding the high Q s of the mirror internal modes and suspension pendulum.
3. Reducing the contamination of mirror surfaces.
4. Estimating heat production by optical loss in the mirror.
5. Alignment control of mirrors in a cryogenic environment
6. Low mechanical loss of the optical coating.

We had already reported on experimental results of the first two items in the annual report (1997–1998) [18]. In regard to

the third and fourth items, the results were reported in the annual report (2000–2001) and published in papers [19]. As for item 5, we confirmed that a superconducting film could be used for the receptor of the magnetic force in place of permanent bar magnets that are normally used in the existing detectors. The film can be easily sputtered on the mirror surface without harmfully degrading the mechanical Q of the mirror. The basic behavior of this method was reported in a paper [20]. With respect to the last item, we reported on a measurement of the bulk substrate of the mirror at cryogenic temperature in the annual report (2003–2004). We can now correctly estimate the thermal vibration noise of the optical coating while considering the inhomogeneous loss that had been neglected at an early stage of interferometer development. The substrate of the cryogenic mirror is sapphire, which has a large thermo-elastic thermal noise at room temperature. However, since the thermal-expansion ratio of sapphire at cryogenic temperature goes down to nearly 0 and the heat conductivity becomes greater, the thermo-elastic noise drastically reduces at the cryogenic temperature. Thermal noise estimated from the Q of the coating was well below the design sensitivity of LCGT, which means that this coating noise does not limit the sensitivity, whereas, the sensitivity of a room-temperature mirror is limited by this effect. This is the significant merit of the cryogenic mirror system [21]. All of the above R&D confirmed the feasibility of reducing the thermal noise of the interferometer in the middle-frequency region. This research underlines the basis of LCGT. However, for a practical cryogenic detector, many practical R&Ds are needed for the installation of cryogenic mirrors. One of the earliest R&D activities was the Kashiwa cryogenic interferometer system reported in the annual report (2000–2001; 2002–2003; 2003–2004). By this Kashiwa cryogenic interferometer, we learned the necessity of several practical R&D items and began to construct the CLIO interferometer in Kamioka to establish techniques for the cryogenic interferometer. Some of these practical studies were reported in the annual report (2004–2005).

Practical R&Ds: Measurement of the optical qualities of sapphire

The substrate of the main mirrors in the cryogenic interferometer (LCGT) is sapphire, because it has ultra-low mechanical loss and high heat conductivity at cryogenic temperature. Only fluorite is a possible substitute of sapphire, with some difficulties that should be removed if we have to utilize fluorite in place of sapphire. However, sapphire has birefringence, which is not a defect if the laser beam axis is aligned along its c -axis, which is the so-called optical axis. Also, sapphire has a rather high optical scattering loss compared with that of fused silica. A measurement of the birefringence of sapphire was scheduled both for inspecting the crystal quality of sapphire substrates that were purchased from companies producing sapphire, and for estimating the optical quality of each substrate. The measurement principle is shown in Fig. 8. Suppose that there is some imperfection of the crystal that causes an optical phase retardance between two orthogonal polarizations. Through a half-wave plate we introduce linearly polarized light that coincides with one of principle refractive axes. The retardance caused at traveling inside the

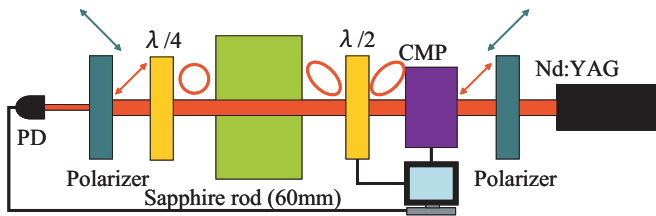


Fig. 8. Optical phase retardance caused by some imperfection is compensated by the Babinet-Soleil compensator (CMP), which is measured by determining two independent angles.

sapphire substrate is compensated by a compensator (CMP), the condition of which is measured by knowing an angle position of a polarizer to extinguish the output light. Without the substrate the angle of this polarizer is orthogonally set with the input polarization angle. The fluctuation of the magnitude of the retardance is represented as the indices of the magnitude of the crystal imperfections. In this measurement, for a typical point of the substrate, the angle of the polarizer and the compensated angle were recorded. Practically, the polarizer angle was determined by knowing the optimum point. Figure 9 shows an example of mapping the measured optical phase shift caused by the substrate, which should be zero if there is no birefringence. The measurement result of the sapphire rod showed no apparent defects inside but a wave-like pattern presenting some kind of an internal structure, and that the magnitude of the imperfection due to this wave-like pattern was negligibly small in the sense of the fluctuated birefringence.

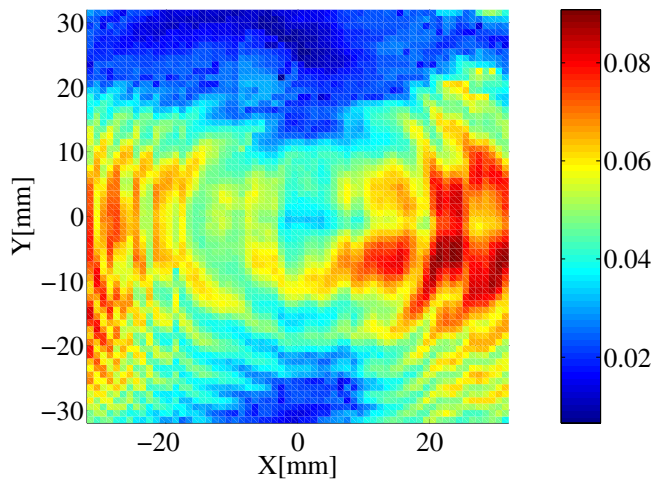


Fig. 9. Measured birefringence fluctuation in terms of the retarded angle. The fluctuation of the magnitude of the retardance represents the magnitude of the crystal imperfections, which is negligibly small for the mirror substrate. The unit of numbers is radians.

In order to measure the optical scattering loss of those sample rods, we brought two sapphire rods to Australia, and made measurements in collaboration with a gravitational wave group in the Physics department, University of Western Australia UWA), where a measuring device of Rayleigh scattering had been developed. We successfully measured the scatter-

ing loss of the samples. And also we measured the birefringence of the sapphire sample that the UWA group prepared to measure its optical scattering. The report of this collaborative measurement was published with a measurement of optical loss by LMA (Laboratoire des Matériaux Avancés - Université Claude Bernard Lyon 1 - IN2P3 / CNRS)[22]. Although we could not recognize any apparent correlation among the birefringence, optical scattering and optical loss, the magnitude of the fluctuation resembles each other. We study further on this point and intend to make our measuring system of the birefringence useful to distinguish the quality of sapphire sample purchased by produces by a required precision for the cryogenic mirror substrates.

Practical R&Ds: Digital Control System

We have tested a digital control system applied to one of TAMA Fabry-Perot cavity in cooperation with the members of NAOJ. The control system of TAMA historically adopts a system of analog circuits. However, since the digital system is superior to the analog system in the sense of flexibility of parameter adjustment, newly designed interferometer tends to adopt the digital system. The recent successful operation of LIGO may be attributed to the digital control system. Although the control design of LCGT has not determined which system is adopted, it is useful to have an experience of the new control system. Therefore, we made a prototype system for the feedback loop of Fabry-Perot cavity length control. Using this prototype, a digital electric filter effectively reduced a time necessary to make the cavity be in lock in the environment of large seismic noise disturbances. This system consists of a digital signal processor (DSP) with AD and DA converters connected to a main computer. We have confirmed the merit of the digital control system. Since the processor speed of DSP limits the frequency bandwidth of the control, at present, low speed systems such as mirror alignment controls will be effectively replaced by the digital system. Higher speed system is the next research items for development.

Apart from the above R&D issues, researchers at the National Astronomical Observatory developed control scheme for the Resonant-side band Extraction method to make wider the bandwidth of the interferometer under high optical power recycling. A high power laser system that produces more than 100 W has been developed by a group in Advanced Material Science, School of New Frontier Science, University of Tokyo. Also, researchers at KEK tested the mechanical strength of bonded pieces made of sapphire, besides quiet refrigerators. We steadily advance towards the realization of LCGT by these R&D activities. The next step in R&D for cryogenic mirrors is to show a reduction of the noise amplitude, itself, which needs a more realistic interferometer other than the prototype with a shorter baseline. For this sake, the CLIO interferometer at Kamioka has been constructed.

Bibliography

- [1] J. H. Taylor and J. M. Weisberg, *Astrophysical J.*, **345** (1989) 434.

- [2] Firstly applied to CALTECH 40 m prototype interferometer appeared in Phys. Rev. Lett. **83**(1999)1498.
- [3] H. Tagoshi *et al.*, Phys. Rev. D **63**(2001)062001-1-5.
- [4] H. Takahashi *et al.*, Phys. Rev. D **70**(2004)042003-1-17.
- [5] H. Tagoshi, GWDATA 10 UTB, Dec. 14-17, 2005.
- [6] H. Dimmelmeier *et al.*, Astrophys. **393** (2002) 523.
- [7] M. Ando *et al.*, Phys. Rev. D **71** (2005) 082002.
- [8] W. G. Anderson *et al.*, Phys. Rev. D **63** (2001) 042003.
- [9] K. Soida *et al.*, Class. Quantum Grav. **20**(2003)S645-S654.
- [10] T. Akutsu *et al.*, in *Proceedings of the 6th Edoardo Amaldi Conference on Gravitational Waves*, Okinawa, 2005.
- [11] Y. Tsunesada *et al.*, Phys. Rev. D **71** (2005) 103005.
- [12] B. Abbott *et al.*, Phys. Rev. D **72** (2005) 122004.
- [13] B. Abbott *et al.*, gr-qc/0512078 (2005)
- [14] M. Burgay, *et al.*, Nature, **426** (2003) 531.
- [15] D.R. Lorimer, *et al.*, Astrophysical J. **640**(2006) 428.
- [16] C. Kim, V. Kalogera and D. R. Lorimer, Astrophysical J. **584** (2003) 985.
- [17] K. Kuroda, *et al.*, Int. J. Mod. Phys. **D 8** (1999) 557; K. Kuroda, *et al.*, Class. Quantum Grav. **19** (2002) 1237; T. Uchiyama, *et al.*, Class. Quantum Grav. **21** (2004) S1161.
- [18] T. Uchiyama, *et al.*, Phys. Lett. **A 242** (1998) 211; T. Uchiyama, *et al.*, Phys. Lett. **A 273** (2000) 310.
- [19] S. Miyoki, *et al.*, Cryogenics **40** (2000) 61; S. Miyoki, *et al.*, Cryogenics **41** (2001) 415; T. Tomaru, *et al.*, Phys. Lett. **A 283** (2001) 80.
- [20] N. Sato, *et al.*, Cryogenics **43** (2003) 425.
- [21] K. Yamamoto, *et al.*, Class. Quantum Grav. **21** (2004) S1075.
- [22] Z. Yan, *et al.*, Applied Optics **40**(2006) 1.

Construction of CLIO at Kamioka

[Spokesperson : Masatake Ohashi]

ICRR, Univ. of Tokyo, Kashiwa, Chiba 277-8582

In collaboration with members of: KEK, Tsukuba; Kyoto-U, Kyoto; ERI of UT, Tokyo

CLIO is a project to construct a 100 m-baseline underground cryogenic interferometer at Kamioka. The CLIO forms a bridge connecting the CLIK(7 m prototype cryogenic interferometer at Kashiwa campus) and the planed LCGT(3 km cryogenic interferometer at Kamioka).

The objective of CLIO is to present the validity of cryogenic interferometers in an intermediate baseline scale (100 m). We focus attention on the decrease of thermal noise by lowering the temperature by this practical interferometer system. For this reason, the interferometer optical system is designed to be as simple as possible in order to make sophisticated control techniques unnecessary during operation. This involves a locked Fabry-Perot configuration with ring mode cleaners (Fig. 1). The main mirrors are cooled at 20 K by refrigerators. The lowest noise level of CLIO is designed to be $10^{-19}\text{m}/\sqrt{\text{Hz}}$ around 100 Hz, which would be $10^{-18}\text{m}/\sqrt{\text{Hz}}$, which results from thermoelastic noise of sapphire mirrors if cryogenics is not applied [1].

Once the objective is attained, the CLIO interferometer is used to observe gravitational wave events in parallel with the TAMA interferometer until completion of the construction of LCGT. The merits of the underground site are lower seismic noise and temperature stability. The former characteristic makes interferometer locking easily controlled, and the latter assures long-term stable operation (LISM) [2]. The site of CLIO, near the Super-Kamiokande neutrino detector, is shown in Fig. 2. The tunnel was dug in 2002, and a strain meter for geophysics was installed in 2003 [3]. The construction of CLIO began in late 2003, and installation of the mode cleaner vacuum system was reported in the annual report (2003–2004). Four sets of cryostats had been installed till 2005, and cooling test was finished for all cryostats (Fig. 3) and one-arm vacuum system with cryostats of both ends had been constructed (annual report 2004–2005). We finally finished the installation of four sapphire mirrors and started the operation of CLIO.

Bibliography

- [1] M. Ohashi, *et al.*, Class. Quantum Grav. **20** (2003) S599.
- [2] S. Sato, *et al.*, Phys. Rev. **D 69** (2004) 102005.

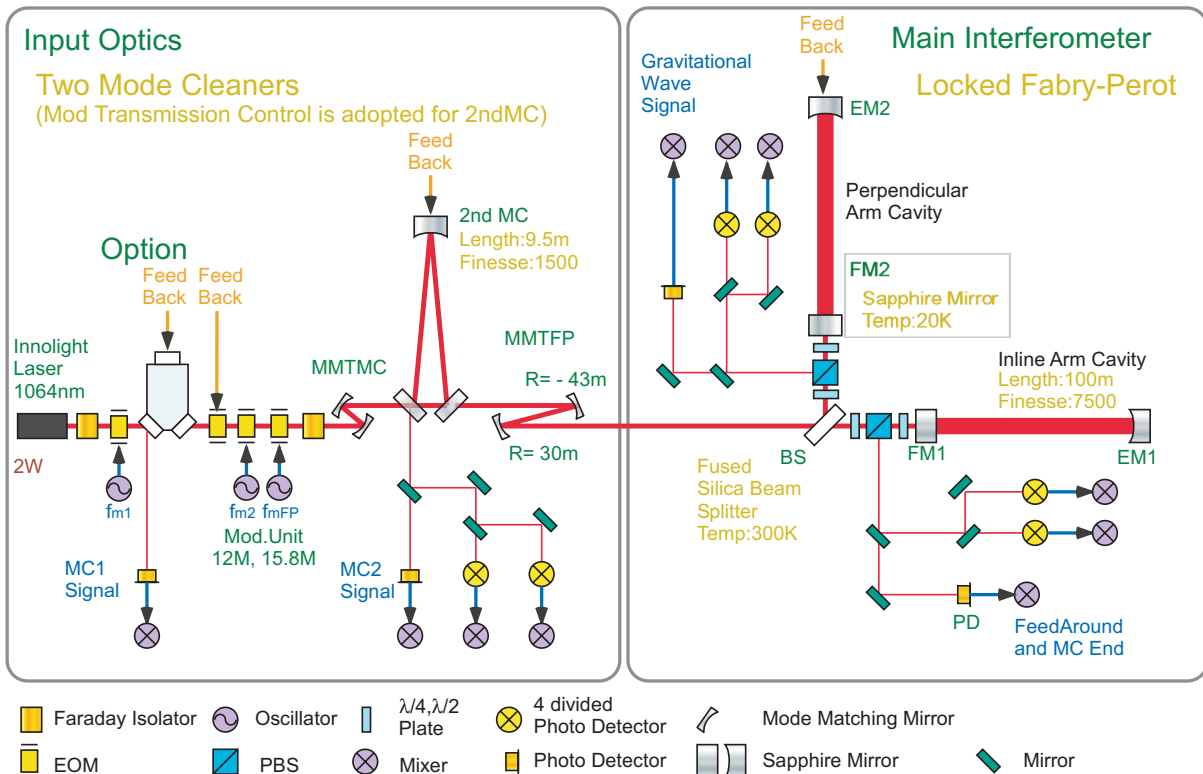


Fig. 1. Optical design of the CLIO interferometer. This is a locked Fabry-Perot configuration with a ring mode cleaner.

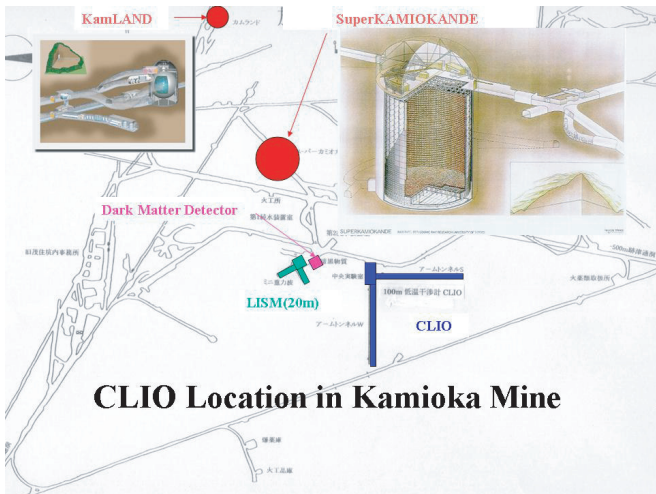


Fig. 2. Location of the CLIO interferometer.

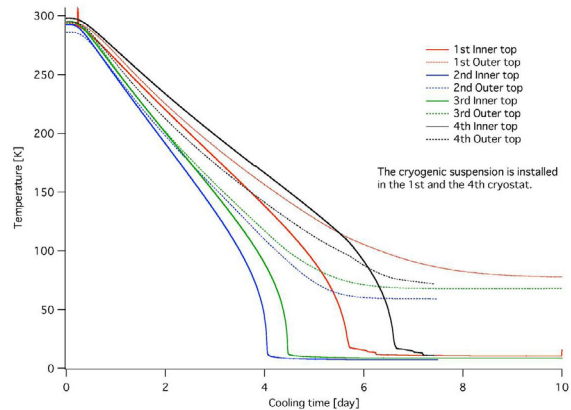


Fig. 3. Four cryostats were installed till 2005 and cooling test has been successfully finished.

[3] S. Takemoto, *et al.*, Journal of Geodynamics **41** (2006), 23.

Sloan Digital Sky Survey

[Spokesperson : Michael Strauss]

Princeton Univ., Princeton, New Jersey 08544 USA

In collaboration with the members of:

University of Tokyo, 7-3-1 Hongo, Bunkyo-ku, Tokyo 113-0033, Japan; Nagoya University, Chikusa, Nagoya 464-8602, Japan; National Astronomical Observatory of Japan, 2-21-1 Osawa, Mitaka, Tokyo 181-8588, Japan; Tohoku Univer-

sity, Aramaki, Aoba, Sendai 980-8578, Japan; Japan Women's University, 2-8-1, Mejirodai, Bunkyo-ku, Tokyo, 112-8681, Japan; The University of Chicago, 5640, South Ellis Ave., Chicago, IL 60637, USA; Fermi National Accelerator Laboratory, P.O. Box 500, Batavia, IL 60510, USA; Institute for Advanced Study, Einstein Drive, Princeton, NJ 08540, USA; Johns Hopkins University, Baltimore, MD 21218, USA; Los Alamos National Laboratory, Los Alamos, NM 87545, USA; Max-Planck-Institute for Astronomy, Königstuhl 17, D-69117 Heidelberg, Germany; Max-Planck-Institute for Astrophysics, Karl Schwarzschildstrasse 1, D-85748 Garching, Germany; New Mexico State University, P.O. Box 30001, Dept 4500, Las Cruces, NM 88003, USA; University of Pittsburgh, 3941

O'Hara St., Pittsburgh, PA 15260, USA; Princeton University, Princeton, NJ 08544, USA; United States Naval Observatory, P.O. Box 1149, Flagstaff, AZ 86002-1149; University of Washington, Box 351580, Seattle, WA 98195, USA

The survey was completed on 30 June 2005 after five years of operation. The goal initially set was to cover 10,000 square degrees of sky, but at the time the production survey began, the Five Year Baseline was developed to provide a more realistic metric against which the progress was evaluated. This decreased the target area to 8,550 square degrees (7,600 square degrees in the northern sky and 750 square degrees in the southern sky). The imaging carried out over 5 years has sustained the planned pace. At the end of the survey 97% of the baseline area were observed for the northern-sky baseline and 99% of southern-sky baseline were completed. Spectroscopic surveys, however, are somewhat behind the schedule. Only 73% of the baseline area were observed for the north (100% for the south). This is due to unusually poor weather conditions in the spring of 2003 and in the winter of 2004. The time consuming spectroscopic runs were severely affected. (The overall fraction of time available for observing in January 2004, for instance, was only 16%, compared with the baseline value of 60%.) Otherwise, all the operations have been working smoothly (98% is the mean uptime fraction), producing the data as expected. Software has undergone extensive fine tunings and all the data were re-reduced for a number of times, which are now made public as *The Data Release of the Sloan Digital Sky Survey I to IV* (DR1-DR4), the last one comprising 6670 square degrees of imaging and 4783 square degrees of spectroscopic surveys done to 30 June 2004. This database contains 180 million objects including 805,000 objects with spectroscopic information. These numbers include 566,000 galaxies and 64,000 quasars obtained with the uniform selection criteria. The final data release is planned in July 2006 as DR5

The prime scientific goals of the SDSS are focused on extragalactic themes, such as the large-scale structure of galaxies over a very large volume of the Universe, and detailed characterisations of the galaxy properties and those of quasars. As the survey has proceeded, these goals have gradually been met, but also new goals emerge on the horizon. The latter includes the structure of Milky Way Galaxy from the distribution of stars and the dark matter distribution in the Universe using gravitational weak lensing.

The clustering of galaxies observed in the SDSS, when mapped in three dimensional space, looks very similar to that expected in the model of the Universe dominated by cold dark matter (CDM) with density fluctuations starting from nearly scale-invariant adiabatic perturbations, as predicted in the model of inflation. As a quantitative measure this density field is characterised by the statistic called the power spectrum, the squared amplitude of the Fourier modes of fluctuations, which is written,

$$P(k) = |\delta_k|^2 = \int d^3r \xi(r) e^{-ik \cdot r} \quad (1)$$

where $\xi(r)$ is the two-point correlation function of galaxies. The important result is an accurate derivation of this power

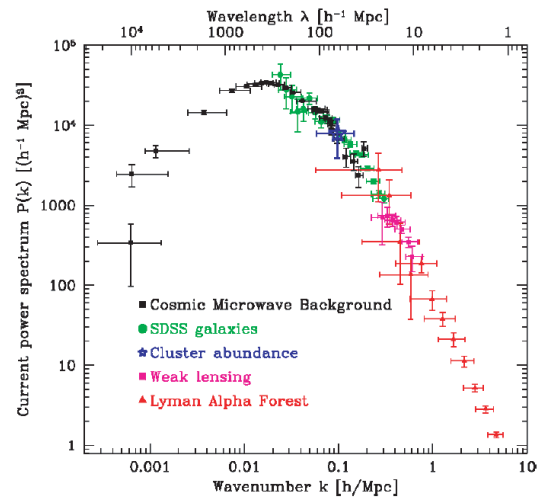


Fig. 1. The power spectrum of galaxy clustering scaled to the present epoch (SDSS galaxies) plotted with four other independent measures, extending four decades on spatial resolution, and demonstrating remarkable consistency. These data provide fundamental constraints on cosmological models. Figure is taken from Tegmark et al. Phys. Rev. D69, 103501 (2004).

spectrum from galaxy clustering over the scale from 10 to 200 Mpc, and the demonstration that it joins smoothly the spectrum derived from the temperature field imprinted on the cosmic microwave background measured by *Wilkinson Microwave Anisotropy Probe* (WMAP) (see Fig. 1). Combined with WMAP that explores the Universe at $z \approx 1000$, this lends the most convincing support to the standard model of structure formation in the Universe based on the Λ CDM model. Moreover, the large-scale structure data of SDSS reduced the parameter degeneracies that exist within the CMB analyses; the combined data of WMAP and SDSS yield the cosmological parameters $\Omega_m = 0.28 \pm 0.04$, $\Omega_\Lambda = 0.72 \pm 0.04$ and $H_0 = 71 \pm 4 \text{ km s}^{-1} \text{ Mpc}^{-1}$. This set is taken an authoritative in the astronomy community.

SDSS has applied another selection of galaxies — the selection of luminous red galaxies (LRG). Approximately 10% of SDSS galaxies belong to this category. The advantage of this selection is to allow us to explore much deep sky. The sight increases from $600h^{-1} \text{ Mpc}$ ($z = 0.2$) to $1200h^{-1} \text{ Mpc}$ ($z = 0.4$), quadrupling the surveyed volume compared with the main galaxy sample. We found that the power spectrum derived from LRG is exactly on the top of $P(k)$ obtained from the main sample allowing for a constant scale factor, called biasing, as expected. An important outcome from the LRG sample is that it allowed us to discover the acoustic peak in the two-point correlation function $\xi(r)$ at $r = 100h^{-1} \text{ Mpc}$ (Fig. 2). This peak is a reminiscence of the sound wave oscillation in the pre-recombination era, which is most dramatically seen in CMB multipoles. This gives not only another strong support for the Λ CDM structure formation model but also enables us to determine the curvature of the Universe to 1% accuracy, $\Omega_\Lambda + \Omega_m = 1.01 \pm 0.01$, a factor 4 improvement over the WMAP+SDSS(main galaxy sample) analysis. The Universe is extremely close to flat. Note that this result rests

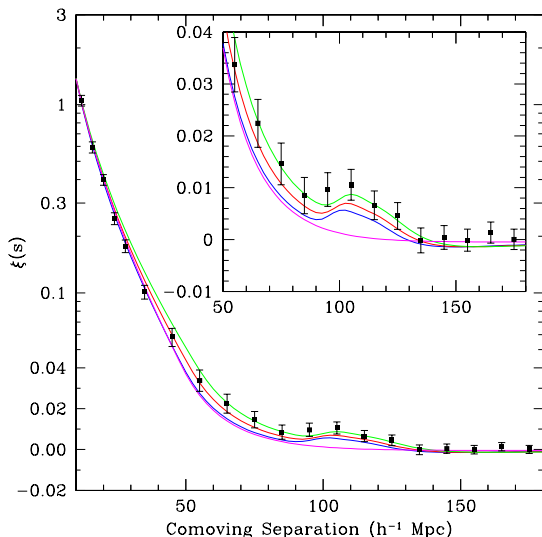


Fig. 2. Two point correlation function of LRG that shows an acoustic peak at $s = 100h^{-1}$ Mpc. The curves are Λ CDM model predictions with various sets of the cosmological parameters. Figure is taken from Eisenstein et al. *Astrophys. J.* **633**, 560 (2005).

on the position of the acoustic peak, measuring the scale of the sound horizon, and thus the determination is geometrical.

Practically the most useful result is a precise determination of the luminosity function of galaxies. This is one of the most fundamental quantities for galaxy science, yet the uncertainty in the derived parameters has often hampered us from extracting a meaningful result from analyses using galaxies. The SDSS with accurate photometry has allowed a precise determination of the parameters in the luminosity function which turned out to show little deviation from the Schechter form. As the survey proceeded and statistics got high, the evolution of galaxies became manifest even at redshift 0.1 – 0.2: without taking account of the evolution one cannot determine the luminosity function in a consistent manner.

Given a few hundred thousands of galaxies with accurate multicolour photometry and spectroscopic information, a number of studies have been conducted to establish statistical properties of galaxies. To mention a few typical results, an estimate was made on the average stellar mass (together with the average age and the heavy element abundance) contained in galaxies with the aid of a population synthesis model and Monte Carlo inferences. Combined with the luminosity function of galaxies, this tells us that baryons in stars are $6 \pm 1\%$ of the total. A related result is a demonstration of the heavy element abundance that shows a clear dependence on the stellar mass: subluminal galaxies have lower metallicity (Fig. 3). A provisional interpretation is the effect due to stellar winds as predicted by Larson some time ago.

Another direction is along the traditional approach starting with visual morphological classification of galaxies into Hubble types. Morphology is the crucial information for galaxy studies in general, yet we know even today no method that replaces the visual inspection to do this. For this is a laborious process, the initial sample contains only 2000 nearby galax-

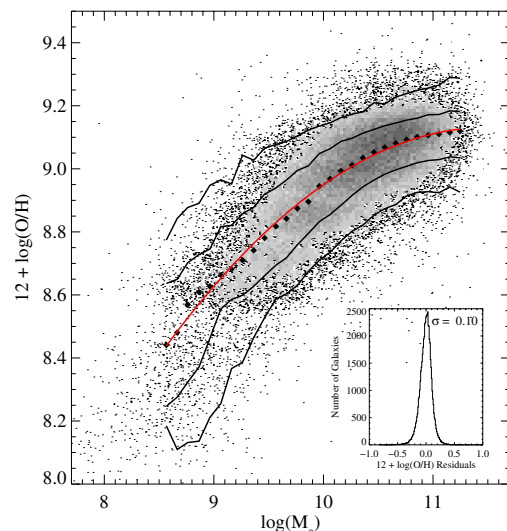


Fig. 3. Oxygen number abundance relative to hydrogen as a function of stellar mass in 50000 galaxies. Figure is taken from Tremonti et al. *Astrophys. J.* **613**, 898 (2004).

ies, notwithstanding this is the largest homogeneous sample of morphologically-classified galaxies ever produced (Paper in preparation). This ‘small’ sample already clarified a number of aspects that were not known or confusing. One example is a discovery of actively ‘star forming elliptical galaxies’ (Fig. 4), which contrasts with the conventional wisdom that elliptical galaxies are those that have long lost star formation activity, consisting only of old stars. We find the fraction of such elliptical galaxies on the order of 0.1%, hardly discernible in samples available before the SDSS. This may be progenitors of E+A galaxies and the relation is being studied. With the morphologically classified samples, a variety of statistical analyses are carried out to study properties of galaxies, such as colour, concentration, effective radius, star formation rate, velocity dispersion, and fundamental plane, which provide the basic data for galaxy science in general. The sample was also used for attempts at automated classification of galaxies, using, e.g., neural network and concentration/texture parameters.

Gravitational lensing is also a subject to which the SDSS is making a significant contribution in a number of ways. The SDSS is one of the first few that observed a weak effect of gravitational lensing of galaxy images by foreground galaxies. The lensing effect appears as distorted images of galaxies due to the gravitational shear field, but it is only on the order of a few percent, compared with the order of unity effect of randomly oriented galaxies that have intrinsically different shapes. Millions of galaxies are needed to extract this small signal from noise of the order of unity. With the SDSS galaxy sample, this distortion was unambiguously detected, showing that the mass concentration around galaxies behaves as $r^{-0.8}$ as a function of distance r , consistently with the famous $r^{-1.8}$ law of the galaxy-galaxy correlation. The uniqueness of the SDSS observation over similar weak lensing projects rests in the fact that the distances to foreground galaxies are

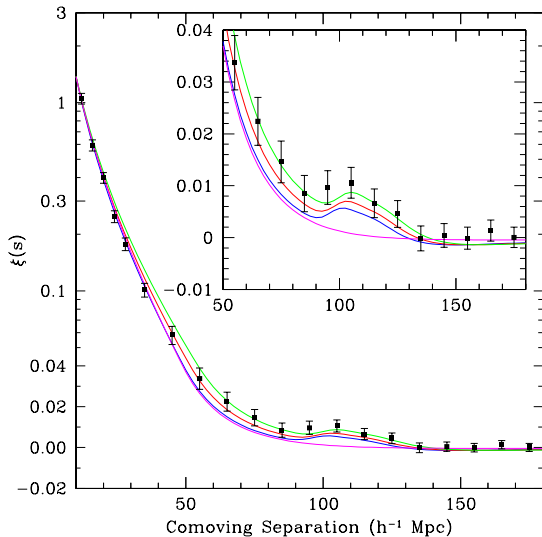


Fig. 4. Images and spectra of the three actively star-forming elliptical galaxies found in the SDSS. The fourth panel represents a *bona fide* elliptical galaxy. The first three show conspicuous emission lines as those observed in late spiral or irregular galaxies, where active star formation takes place. Figure is taken from Fukugita et al. *Astrophys. J. (Letters)* **601**, L127 (2004).

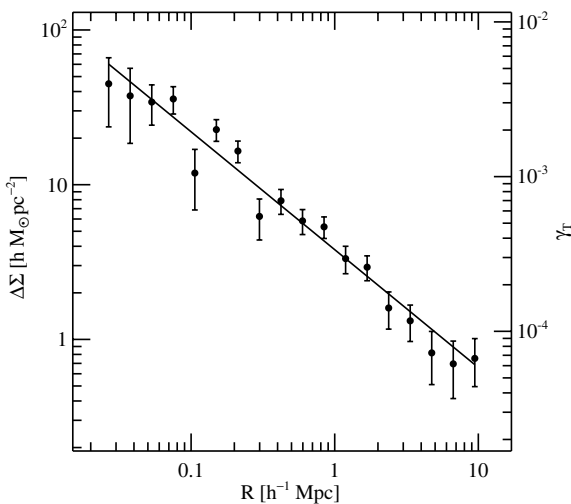


Fig. 5. Surface mass density excess around galaxies $\Delta\Sigma$ (the galaxy-mass correlation function) as a function of the distance from the centres of galaxies, obtained from the shear force of gravitational weak lensing using 120 thousand lensing galaxies together with 9 million background galaxies. Figure is taken from Sheldon et al. (2004).

known, which in turn allows the estimate of the dark mass associated with galaxies. The analysis showed that galaxies are surrounded by the dark mass which amounts to 200 times the light in solar units. This large mass to light ratio had been inferred from a few observations in the past under some assumptions, but this time is derived without resorting to any assumptions. The most recent result of the galaxy-mass correlation $\Delta\Sigma(r)$ (the surface mass density excess around the galaxy) is shown in Fig. 5, which was obtained by stacking 120000 lens galaxies with 9.0 million source galaxies.

The large quasar sample of the SDSS also provides an

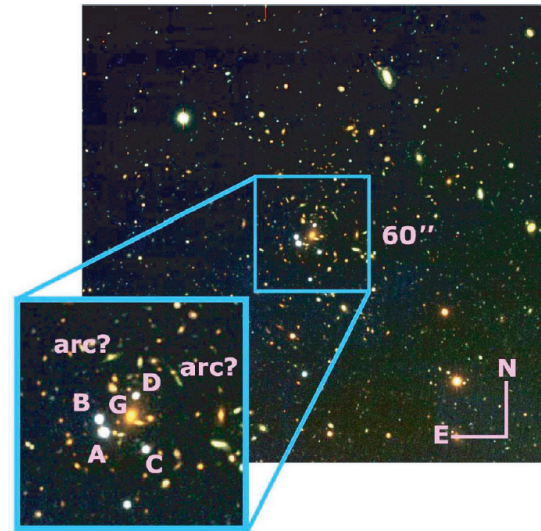


Fig. 6. Subaru telescope follow-up of the quadruple lens discovered with the SDSS. The four images of the quasar are labelled A, B, C and D. A rich cluster of galaxies is evident, centred in the field. The dominant central galaxy of the cluster, which causes splitting of images of the quasar is labelled G. The separation between C and D is 14.43 arcsec, the largest among lenses ever found. Figure is after Inada et al. *Nature* **426**, 810 (2003).

excellent platform to search for classical strong gravitational lenses of quasar images, i.e., splitting of images. 15 lenses are found from 26000 quasar images. Among the novel cases that deserve special scientific discussion, we quote a lens of four images with their maximum separation being 14.4 arcsec, 2.5 times larger than has ever been found (Fig. 6). This is the case where split lensed images are further enhanced by a cluster of galaxies. A statistical analysis to infer cosmological and mean galaxy parameters from the lens sample is underway.

As it became apparent already at Imaging First Light, the SDSS project has made unrivalled contributions to our understanding of high redshift quasars from its commissioning phase. By now the project has found 19 quasars with redshift higher than 5.7 (*i*-dropout quasars) from 4600 square degrees — Among them 9 are with $z \geq 6$: there are no $z > 6$ quasars reported from other projects. The highest redshift is 6.42, which means that the light was emitted only 0.84 Gyr after the Big Bang. These high z quasars, together with a sample for lower z , show the abundance of luminous quasars declining exponentially with redshift from $z \approx 3$ towards early epochs. This is a significant constraint on the model of quasar formation at high redshifts.

Also important aspect with high redshift quasars is that they allowed us to observe a change of the ionisation state of the intergalactic medium (IGM) in a high redshift universe. We know that a free electron and a proton recombine to form a neutral hydrogen atom at $z \approx 1500 - 1000$. We also know that IGM was again highly reionised before $z \approx 3$. When and how the reionisation took place is a matter of significant interest from the point of view of galaxy formation. The SDSS quasar spectra show the flux shortwards the Lyman α line rapidly vanishing at $z \geq 6$ (called the Gunn-Peterson trough), indicating the change of state of the IGM at this redshift. This may contrast with the reionisation epoch of $z \approx 17$ inferred from

WMAP, but the uncertainty is large with its one-year data: $z_{\text{reion}} \approx 6$ is allowed at a 1.5 standard deviation. A problem newly created is the question whether the star formation activity, as inferred from faint galaxy observations, is sufficient to ionise the entire IGM at $z \approx 6$.

Besides high redshift quasars, a large number of quasars are collected and their properties are being studied. We have released three catalogues of quasars, the third one containing 44200 quasars in 4200 square degrees. The long-awaited quasar luminosity function (the work requires proper understanding of the selection function) is now available.

After data taking started, it has been recognised that the excellent quality of multicolour photometry and enormous volume of the data produced by SDSS are also useful to make progress for understanding the Galactic structure and the low mass end of stars. The most interesting finding for the former perhaps is the discovery of tidal debris which were left behind when dwarf galaxies travel through the Galactic halo. The first evidence was a conspicuous enhancement in the number density of stars in a small area when it was studied as a function of radius. It was soon identified as the tidal leftover of the Sagittarius dwarf galaxy orbiting around the Galaxy. Another tidal track was then discovered for disruption of a globular cluster, Palomar 5. The tidal tail contains a comparable mass as does the cluster. The third case is the Monoceros stream. These pieces of evidence indicate a view that the Galaxy is still being built up in the halo. The perturbations on the tidal tracks tell us that the Galactic halo is appreciably non-spherical and lumpy.

Another notable contribution from the SDSS to stellar science is the collection of many low temperature stars in the extension of the M dwarf, named the L and T dwarfs. T dwarfs are dominated by methane and water features in their spectrum as with Jupiter. Despite their discontinuous behaviour in colour space L and T dwarfs are on a single sequence in temperature. The sample allows detailed studies of low temperature stellar atmosphere. The mass contained in these low mass stars is no more than a few percent of the total star mass: therefore they cannot be a dominant component of the Galaxy mass.

To date more than 1000 scientific papers have been written for regular journals and conference proceedings (about 150 include Japanese team members). The number of papers using the SDSS data by authors outside the SDSS is also rapidly increasing. Nevertheless, we feel that the state of analyses is still quite premature, far from exploitation of the data we produced.

Theory Group

Investigation of Possible Dark Matter Direct Detection in Electron Accelerators

[Spokesperson : M. Senami]

ICRR, Univ. of Tokyo, Kashiwa, Chiba 277-8582

In collaboration with the members of ICRR and KEK.

We investigate a possibility of neutralino dark matter

(DM) direct detection in the future electron accelerators. That is counting of high p_T electron recoil events by neutralinos in halo. If selectron and neutralino masses would be precisely measured in future collider experiments, the beam energy could be tuned so that the scatterings are dominated by on-pole selectron exchange. When selectron and neutralino mass difference is smaller than $O(10)$ GeV, the elastic cross section exceeds over micro barn. Discovery of the high p_T electron events would be a firm prove of the neutralino DM component in halo. In the experiment, the electron beam energy must be tuned within $O(10)$ MeV and the electron beam with high currents of $O(100)$ A is required for the detectors of the total length of a few hundred meters so that the sufficient event rate is obtained. The dependence of the event rate on the DM velocity distribution in halo is also discussed. This method might be applicable to other DM candidates.

Bibliography

- [1] J. Hisano, M. Nagai, M. M. Nojiri and M. Senami, Phys. Rev. D **73**, 031701 (2006).

Heavy wino-like neutralino dark matter annihilation into antiparticles

[Spokesperson : M. Senami]

ICRR, Univ. of Tokyo, Kashiwa, Chiba 277-8582

In collaboration with the members of ICRR and KEK.

The lightest neutralino is a viable dark matter (DM) candidate. In this paper we study indirect detection of the wino-like neutralino DM using positrons and antiprotons from the annihilation in the galactic halo. When the mass is around 2 TeV, which is favored from the thermal relic abundance, the non-perturbation effect significantly enhances the annihilation cross sections into positrons and antiprotons. We find that the positron and antiproton fluxes with energies larger than 100 GeV may become larger than the expected backgrounds. Since the positron flux is less sensitive to the astrophysical parameters, the detection may be promising in the upcoming experiments such as PAMELA and AMS-02. We also find the wino-like neutralino DM with mass around 2 TeV is compatible with the HEAT anomaly.

Bibliography

- [1] J. Hisano, S. Matsumoto, O. Saito and M. Senami, Phys. Rev. D **73**, 055004 (2006).

The relic abundance of the LKP dark matter in Universal Extra Dimension model

[Spokesperson : M. Senami]

ICRR, Univ. of Tokyo, Kashiwa, Chiba 277-8582

In collaboration with the members of ICRR, KEK, Bonn Univ. and Saitama Univ..

We investigate the relic abundance of the lightest Kaluza-Klein particle (LKP) dark matter in universal extra dimension (UED) models. We pointed out that the LKP efficiently annihilates through the coannihilation process including the first

KK Higgs bosons when the Higgs mass is slightly heavy as 200 - 230 GeV, which gives the large Higgs self-coupling. We also include the second KK s -channel resonance to calculate the relic abundance of the LKP dark matter.

Bibliography

- [1] M. Kakizaki, S. Matsumoto, Y. Sato and M. Senami, *Phys. Rev. D* **71**, 123522 (2005).
- [2] M. Kakizaki, S. Matsumoto, Y. Sato and M. Senami, *Nucl. Phys. B* **735**, 84 (2006).
- [3] S. Matsumoto and M. Senami, *Phys. Lett. B* **633**, 671 (2006).

Abundance of cosmological relics in low-temperature scenarios

[Spokesperson : M. Kakizaki]

ICRR, Univ. of Tokyo, Kashiwa, Chiba 277-8582

In collaboration with the members of Bonn Univ..

We investigate the relic density of non-relativistic long-lived or stable particles χ in cosmological scenarios in which the temperature is too low for χ to achieve full chemical equilibrium. The case with a heavier particle decaying into χ is also investigated. We derive approximate solutions for the χ number density which accurately reproduce numerical results when full thermal equilibrium is not achieved. If full equilibrium is reached, our ansatz no longer reproduces the correct temperature dependence of the χ number density. However, it does give the correct final relic density, to an accuracy of about 3% or better, for all cross sections and initial temperatures.

Bibliography

- [1] M. Drees, H. Iminniyaz and M. Kakizaki, *hep-ph/0603165*.

Constraint on Right-Handed Squark Mixings from $B_s - \bar{B}_s$ Mass Difference

[Spokesperson : M. Endo]

ICRR, Univ. of Tokyo, Kashiwa, Chiba 277-8582

In collaboration with the member of IAS.

We point out that the right-handed squark mixings can sizably enhance SUSY contributions to ΔM_s by taking into account renormalization group effects via the CKM matrix. The recent result of ΔM_s from the $D\bar{D}$ experiment at the Tevatron thus implies a strong constraint on the right-handed mixings.

Bibliography

- [1] M. Endo and S. Mishima, *arXiv:hep-ph/0603251*.

Moduli Dynamics in Heavy Gravitino Scenario

[Spokesperson : M. Endo]

ICRR, Univ. of Tokyo, Kashiwa, Chiba 277-8582

In collaboration with the members of ICRR, Tohoku Univ., Kyushu Univ. and DESY.

We study phenomenological aspects of a new class of the supersymmetry-breaking mediations, which is called the mixed modulus-anomaly/KKLT model, where both the modulus and gravitino have relatively heavy with mass of order 10-100 TeV. The general form of soft supersymmetry breaking masses is derived, and the pattern of the superparticle mass spectrum in the minimal supersymmetric standard model is discussed. It is shown that the moduli mediation and the anomaly mediation make comparable contributions to the soft masses. At the weak scale, the gaugino masses are rather degenerate compared to the minimal supergravity, which bring characteristic features on the superparticle masses. In particular, the lightest neutralino, which often constitutes the lightest superparticle and thus a dark matter candidate, is a considerable admixture of gauginos and higgsinos. We also find a small mass hierarchy among the moduli, gravitino, and superpartners of the standard-model fields. Next we investigate the cosmological moduli problem by studying a modulus decay in detail and find that the branching ratio of the gravitino production is generically of $O(0.01 - 1)$, which causes another cosmological disaster. Consequently, the cosmological moduli problem cannot be solved simply by making the modulus mass heavier than 100 TeV. We also illustrate our results by explicitly calculating the branching ratio into the gravitinos in the mixed modulus-anomaly/KKLT- and racetrack-type models.

Bibliography

- [1] M. Endo, M. Yamaguchi and K. Yoshioka, *Phys. Rev. D* **72**, 015004 (2005) [*arXiv:hep-ph/0504036*].
- [2] M. Endo, K. Hamaguchi and F. Takahashi, *arXiv:hep-ph/0602061*.

Gravitino Overproduction in Inflaton Decay

[Spokesperson : F. Takahashi]

ICRR, Univ. of Tokyo, Kashiwa, Chiba 277-8582

In collaboration with the members of ICRR and University of Tokyo.

We show that most of the inflation models are plagued with the gravitino overproduction problem, and are thereby excluded or on the verge of being excluded.

Bibliography

- [1] M. Kawasaki, F. Takahashi and T. T. Yanagida, *arXiv:hep-ph/0603265*.

Q-ball Instability due to U(1) Breaking

[Spokesperson : F. Takahashi]

ICRR, Univ. of Tokyo, Kashiwa, Chiba 277-8582

In collaboration with the members of ICRR.

We study a Q-ball which arises in the Affleck-Dine mechanism for baryogenesis and consider its possible instability due

to U(1) breaking term (A-term) indispensable for successful baryogenesis.

Bibliography

- [1] M. Kawasaki, K. Konya and F. Takahashi, Phys. Lett. B **619**, 233 (2005).

The oscillation effects on thermalization of the neutrinos in the universe with low reheating temperature

[Spokesperson : F. Takahashi]

ICRR, Univ. of Tokyo, Kashiwa, Chiba 277-8582

In collaboration with the members of ICRR.

We study how the oscillations of the neutrinos affect their thermalization process during the reheating period with temperature $O(1)$ MeV in the early universe. We find that including the oscillations makes different predictions, especially for ${}^4\text{He}$ abundance.

Bibliography

- [1] K. Ichikawa, M. Kawasaki and F. Takahashi, Phys. Rev. D **72**, 043522 (2005).

Unification of Dark Energy and Dark Matter

[Spokesperson : F. Takahashi]

ICRR, Univ. of Tokyo, Kashiwa, Chiba 277-8582

In collaboration with the members of University of Tokyo.

We propose a scenario in which dark energy and dark matter are described in a unified manner. The ultralight pseudo-Nambu-Goldstone (pNG) boson, A, naturally explains the observed magnitude of dark energy, while the bosonic supersymmetry partner of the pNG boson, B, can be a dominant component of dark matter. The decay of B into a pair of electron and positron may explain the 511 keV gamma ray from the Galactic Center.

Bibliography

- [1] F. Takahashi and T. T. Yanagida, Phys. Lett. B **635**, 57 (2006).

511 keV Gamma Ray from Moduli Decay in the Galactic Bulge

[Spokesperson : M. Kawasaki]

ICRR, Univ. of Tokyo, Kashiwa, Chiba 277-8582

In collaboration with the members of University of Tokyo

We show that the $e^+ + e^-$ decay of a light scalar boson of mass $1 - 10$ MeV may account for the fluxes of 511 keV gamma ray observed by SPI/INTEGRAL. We argue that candidates of such a light scalar boson is one of the string moduli or a scalar partner of the axion in a supersymmetric theory.

Bibliography

- [1] M. Kawasaki and T. Yanagida, Phys. Lett. **B624** (2005) 162-165.

Evolution of Dark Energy and its implications to the Determination of Neutrino Masses and the Curvature of the Universe

[Spokesperson : T. Takahashi]

ICRR, Univ. of Tokyo, Kashiwa, Chiba 277-8582

In collaboration with the members of ICRR

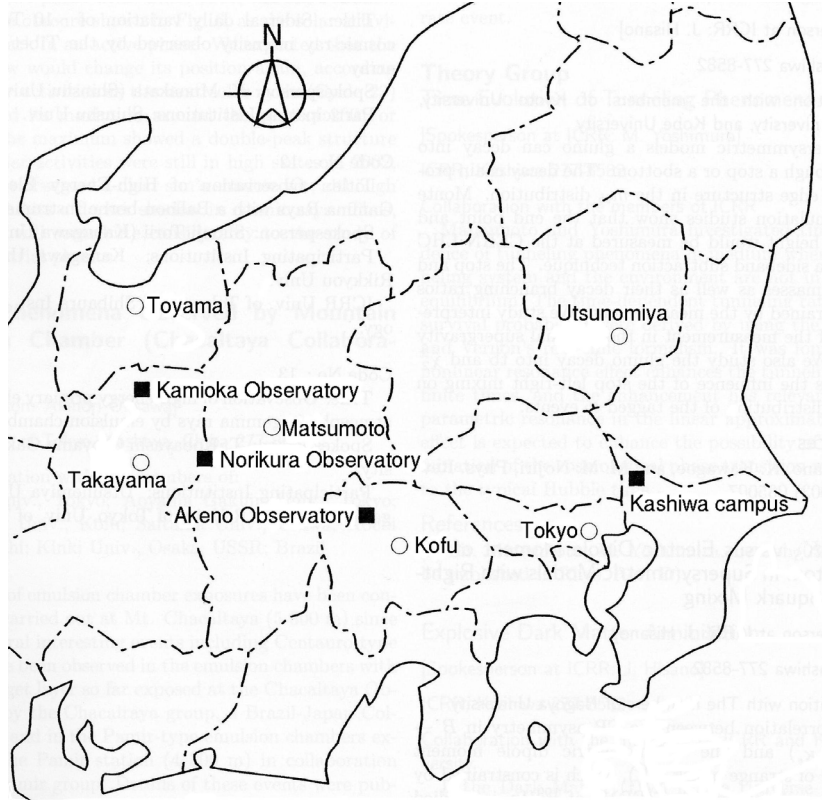
We discussed the possibilities of the simultaneous determination of the neutrino masses and the evolution of dark energy from future cosmological observations such as cosmic microwave background (CMB), large scale structure (LSS) and the cross correlation between them. Recently it has been discussed that there is a degeneracy between the neutrino masses and the equation of state for dark energy. It is also known that there are some degeneracies among the parameters describing the dark energy evolutions. We discussed the implications of these on the cross correlation of CMB with LSS in some details. We have also discussed the constraints on the time-varying equation of state for dark energy and the curvature of the universe using observations of type Ia supernovae from Riess et al. and the most recent Supernova Legacy Survey (SNLS), the baryon acoustic oscillation peak detected in the SDSS luminous red galaxy survey and cosmic microwave background. Due to the degeneracy among the parameters which describe the time dependence of the equation of state and the curvature of the universe, the constraints on them can be weakened when we try to constrain them simultaneously, in particular when we use a single observational data. However, we showed that we can obtain relatively severe constraints when we use all data sets from observations above even if we consider the time-varying equation of state with a particular parametrization and do not assume a flat universe. We also found that the combined data set favors a flat universe even if we consider the time variation of dark energy equation of state with a particular parametrization.

Bibliography

- [1] K. Ichikawa and T. Takahashi, arXiv:astro-ph/0510849.
[2] K. Ichikawa and T. Takahashi, arXiv:astro-ph/0511821.

OBSERVATORIES and A RESEARCH CENTER

Location of the Institute and the Observatories in Japan



Norikura Observatory

Location: Nyukawa-mura, Ohno-gun, Gifu Prefecture 506-2100
 N 36°06', E 137°33', 2770 m a.s.l.
 Telephone (Fax): +263-33-7456
 Telephone (satellite): 090-7721-5674
 Telephone (car): 090-7408-6224

Akeno Observatory

Location: Akeno-mura, Kitakoma-gun, Yamanashi Prefecture 407-0201
 N 35°47', E 138°30', 900 m a.s.l.
 Telephone / Fax: +551-25-2301 / +551-25-2303

Kamioka Observatory

Location: 456 Higashi-mozumi, Kamioka-cho, Hida-shi, Gifu Prefecture 506-1205
 N 36°25'26", E 137°19'11", 357.5 m a.s.l.
 Telephone / Fax: +578-5-2116 / +578-5-2121

Research Center for Cosmic Neutrinos

Location: 5-1-5 Kashiwanoha, Kashiwa, Chiba Prefecture 277-8582
 Telephone / Fax: +4-7136-3138 / +4-7136-3115

NORIKURA OBSERVATORY

[Director of Norikura Observatory : Masato Takita]

ICRR, Univ. of Tokyo, Kashiwa, Chiba 277-8582

In collaboration with the members of:

Norikura Observatory (36.10°N and 137.55°E) was founded in 1953 and attached to ICRR in 1976. It is located at 2770 m above sea level, and is the highest altitude manned laboratory in Japan. Experimental facilities of the laboratory are made available to all the qualified scientists in the field of cosmic ray research and associated subjects. The AC electric power is generated by the dynamo and supplied throughout the observatory. In 1996, two dynamos of 70 KVA each were replaced with the new ones. The observatory can be accessed easily by the car in summer (June–October) but an aid of snow-mobile is necessary in winter time. The 50th anniversary of the Norikura Observatory was celebrated in 2003.

The feasibility of the automatic operation of the Norikura Observatory during winter period has been tested since winter 2004 in order to study the possibilities to reduce maintenance and labor costs without seriously doing damage to the quality of various researches. For the purpose, A long-distance (~40km) wireless LAN system (11M bps) was set up in 2003. Two new easy-to-handle and easy-to-maintain dynamos of 115 KVA each were installed in 2004 as well. The automatic operation of the Norikura Observatory was successful in the first winter, during which the battery backed-up solar panels and/or wind power generators keep supplying the electricity to the wireless LAN and on-going cosmic-ray experiments.

Present academic interests of the laboratory is focused on the modulation of high energy cosmic rays in the interplanetary space associated with the solar activity and the generation of energetic particles by the solar flares [1],[2].

For the modulation study, two small experiments have been operated continuously for a long time. One is a neutron monitor operated to study the correlation of solar activity and the cosmic ray flux. The other is a high counting meson telescope consisting of 36 m² scintillation counters to study the time variation of cosmic rays with energies of 10–100 TeV.

The Sun is the nearest site to the Earth capable of accelerating particles up to high energies. When the Sun becomes active, flares are frequently observed on its surface. The flare accelerates the proton and ion to high energy and they are detected on the Earth soon after the flare. Among the particles generated by the flare, high energy neutrons provide the most direct information about the acceleration mechanism as they come straight from the flare position to the Earth without being affected by the magnetic field.

The detection of solar flare particles has been very active in the Norikura observatory for the last 10 years. The muon telescope of the observatory successfully detected flare particles in association with a large flare occurred on the 29th of September, 1989. The data suggested that protons could be accelerated at least up to 50 GeV in a large solar flare considering the geomagnetic cut-off rigidity of the proton is esti-

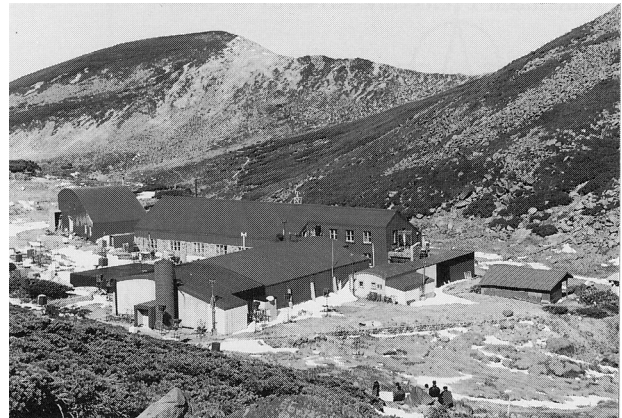


Fig. 1. Norikura Observatory.

mated to be 11.5 GeV at Mt. Norikura. The high altitude of the observatory is essential for detecting the flare particles without significant attenuation.

In 1990, Nagoya group constructed a solar neutron telescope consisting of scintillators and lead plates, which measures the kinetic energies of incoming neutrons up to several hundred MeV. This telescope observed high energy neutrons associated with a large flare occurred on the 4th of June, 1991. The same event was simultaneously detected by the neutron monitor and the high counting meson telescope of the Norikura observatory. This is the most clear observation of solar neutrons at the ground level in almost ten years since the first observation at Jungfrauoch in 1982.

A new type of large solar neutron telescope (64 m² sensitive area) was constructed by Nagoya group in 1996. It consists of scintillators, proportional counters and wood absorbers piled up alternately. This takes a pivotal role among a worldwide network of ground based solar neutron telescopes of the same type in Yangbajing in Tibet, Aragatz in Armenia, Gornegrat in Switzerland, Chacaltaya in Bolivia and Mauna Kea in Hawaii. The Sun is being watched for 24 hours using this network.

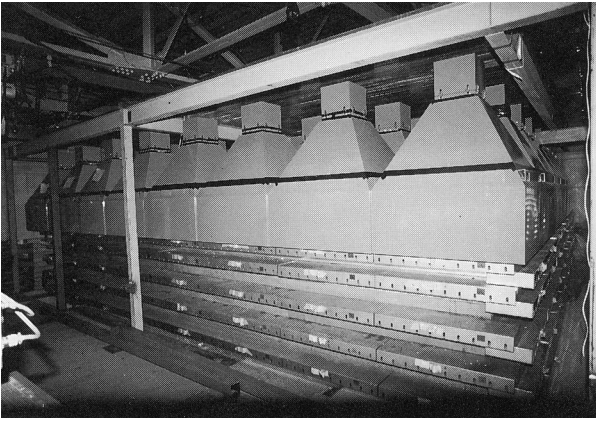


Fig. 2. New Solar-Neutron Telescope of Nagoya Group.

The Sun is reaching the maximum activity in 2001 and the active phase will continue for next few years. All the telescopes in the Norikura observatory, neutron, meson and muon telescopes, will be operated continuously through this solar cycle (Cycle 23) in order to obtain comprehensive information on the solar flare phenomena. Important hints for understanding the mechanism of cosmic ray acceleration will be obtained by this measurement.

Furthermore, the relation between the electric fields induced by thunderclouds was studied recently [3]. The electric fields with thunderclouds change the intensity of secondary cosmic rays observed on the ground. This effect has been investigated using several detectors located at the Norikura Observatory where excesses of 1 % and more of the average counting rate may be observed when the Observatory is covered with thunderclouds. An electric field mill was installed to determine the possible correlation between the intensity variations and the strength and direction of the field near the detector system. The excess was normally observed when a negative electric field (accelerating negatively charged particles downward) greater than 10 kV/m present in the atmosphere over the observatory.

In addition to the long-term cosmic-ray observations mentioned above, various kinds of short-dated experiments are carried out every year taking an advantage of the high altitude of the observatory. As a few examples, following experiments have been performed; a search for super heavy particles with plastic plates, a precise measurement of atmospheric gamma rays and muons, collection of cosmic dusts contained in the snow and the performance study of the balloon borne cosmic ray experiments. A part of the facility has been open for the environmental study at high altitude such as the aerosol removal mechanism in the atmosphere or for the botanical study of the high altitude environment.

Bibliography

- [1] K. Munakata, T. Kuwabara, S. Yasue, C. Kato, S. Akahane, M. Koyama, Y. Ohashi, A. Okada, T. Aoki, H. Kojima and J. W. Bieber, "A "loss-cone" precursor of an approaching shock observed by a cosmic-ray muon hodoscope on October 28, 2003", *Geophys. Res. Lett.*,

Vol.32, L03S04, doi:10.1029/2004GL021469, 2005.

- [2] K. Munakata, T. Kuwabara, J. W. Bieber, P. Evenson, R. Pyle, S. Yasue, C. Kato, Z. Fujii, M. L. Duldig, J. E. Humble, M. R. Silva, N. B. Trivedi, W. D. Gonzalez and N. J. Schuch, "CME-geometry and cosmic-ray anisotropy observed by a prototype muon detector network", *Adv. Space Res.*, doi:10.1016/j.asr.2003.05.064, 2005, in press.
- [3] Y. Muraki *et al.*, *Phys. Rev. D*, **69**, 123010 (2004).

AKENO OBSERVATORY

Observatory

The Observatory is in Akeno town of Hokuto-city situated 20 km west of Kofu and 130 km west of metropolitan Tokyo. The location is at the longitude of 138.5°E and the latitude of 35.5°N. The altitude is ~ 900 m above sea level.

It was established in 1977 as a research center for air shower studies in the very high energy region. The Observatory has been administered by the ICRR as a facility of joint-university-use. An important part of observatory's scientific outputs originates from the university collaborators.

From 1 km² Array to AGASA

The Akeno Air Shower Experiment started in 1979 with an array covering 1 km² area (1 km² array). The array was enlarged to 20 km² in 1985 and was gradually expanded to Akeno Giant Air Shower Array (AGASA) of approximately 100 km² area by 1990. The observation by AGASA continued for 13 years until the beginning of 2004.

One of the distinctive features of Akeno experiments is that the measurement was made over five decades of energies well covering 10¹⁵ eV - 10²⁰ eV by using both the surface detector (for electromagnetic component) and the shielded detector (for muon component). This feature is well demonstrated in Fig.2; the spectra from Akeno 1 km² for 10^{14.7} eV - 10^{18.7} eV [1, 2] and AGASA for 10^{18.6} eV - 10^{20.3} eV [3] are plotted by open squares and solid circles in red. The wide energy coverage was accomplished by the arrays of scintillation detectors of various inter-detector spacings from 3 m to 1 km and with different triggering conditions.

The analysis had been made with similar algorithm under the same definition of single particle throughout the energy range covered. A difference exists however for the conversion method to the primary energy; the total number of electrons N_e is used for 1 km² array and the local density at 600 m from the shower core $S(600)$ is used for AGASA. A shift of $\sim 10\%$ in energy is seen between AGASA and 1 km² array around 10^{18.5} eV. This is due to the difference of energy conversion methods employed by two experiments.

The parameter N_e^{\max} at the maximum of shower development is well known as one of the best primary energy estimators which does not depend sensitively on the interaction model or primary composition. The observed N_e at Akeno was converted to N_e^{\max} experimentally with the longitudinal shower development curves determined with constant intensity cut method of integral N_e spectra measured at Mt. Chacaltaya and at Akeno[1]. The result around the *knee* is consistent with all-particle spectra extrapolated from the direct measurements and those of recent results from Tibet[4] and KASCADE[5].

However, as seen in Fig.2, there are large discrepancies among experiments in the highest energy region. It should be noted that the systematic deviation among experiments already starts at 10¹⁷ eV. New data coming from TA and Pierre

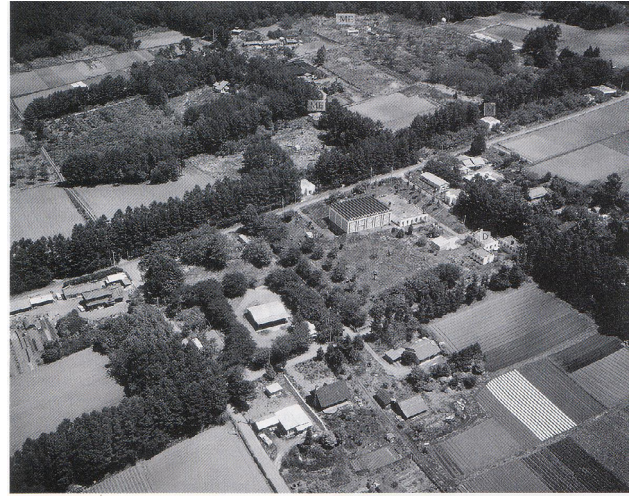


Fig. 1. Aerial View of Akeno Observatory and 1 km² Array Area

Auger will have to be understood in a consistent manner with existing lower energy data.

Research and Development

Facilities of Akeno Observatory have been used for a variety of air shower studies, detector developments and associated researches. Activities of recent 6 years (2000 - 2005) are listed below.

- Study of EHECRs by AGASA by M.Teshima^{a,b}, N.Hayashida^a and AGASA collaboration (2000-2005).
- Research and Development of Telescope Array Detectors by Y.Arai^c, M.Chikawa^d, M.Fukushima^a, K.Hashimoto^e, K.Honda^e, N.Inoue^f, F.Kakimoto^g, S.Ogio^{g,h}, H.Sagawa^a, M.Sasaki^a, Y.Tanakaⁱ, S.Yoshida^j and TA collaboration (2000-2005).
- Observation of UHECRs with Lead-Burger Detector by K.Honda^e et al. (2000-2003).
- Observation of Air Shower Core for $E > 10^{16}$ eV by H.Sakuyama^k and N.Suzuki^k et al. (2000-2004).
- Test Measurement of HE Cosmic Rays using Wide Angle Refractive Optics by H.Shimizu^l, S.Ebisuzaki^l and EUSO collaboration (2001-2005).
- Energy Calibration of AGASA Event with Schmidt Type Air Fluorescence Telescope (CRIS) by S.Yoshida^j et al. (2002).
- Measurement of Galactic Cosmic Ray Flux with Large Muon Telescope by S.Kawakami^h et al. (2000-2005).
- Study of Cosmic Evolution by Quick Observation of GRBs by S.Kawai^g et al. (2003-2005).

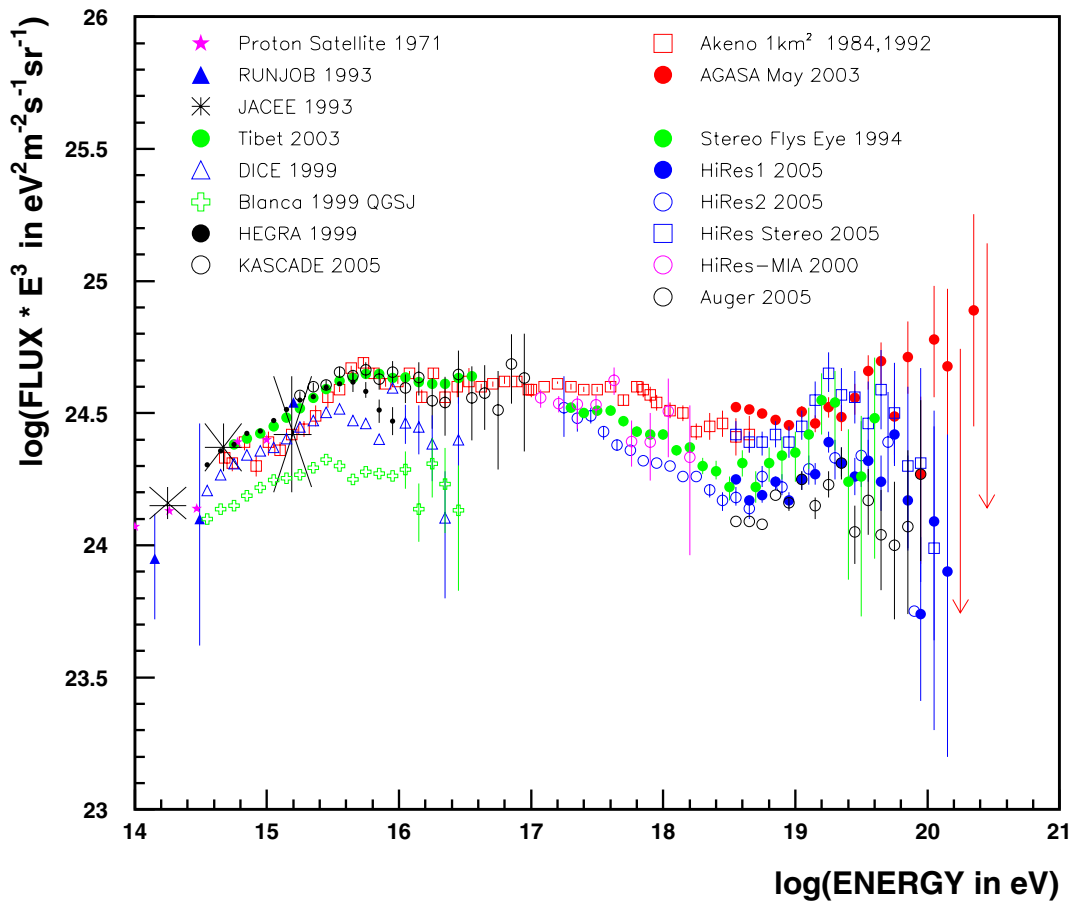


Fig. 2. Energy Spectra of Cosmic Rays between 10^{14} eV and $10^{20.3}$ eV. The data marked as “Auger 2005” and “HiRes Stereo 2005” were presented in the 29th ICRC in 2005, Pune and are preliminary [6].

- On-line Observation of GRBs by Wide Angle Optical Telescope by T.Tamagawa^l et al. (2003-2005).
- Chemical Composition of Primary Cosmic Rays for 10^{17} eV < E < 10^{18} eV by M.Nagano^m et al. (2003).
- Research and Development for High Resolution All Sky Cosmic Ray Telescope by Y.Arai^c, M.Ieiri^c, R.Ogawaⁿ, M.Sasaki^a, Y.Tanaka^l, Y.Watanabe^g et al. (2003-2005).
- Effect of Cloud for Cosmic Ray Observation from Space by M.Nagano^m et al. (2005).

a: Institute for Cosmic Ray Research, University of Tokyo
b: Max Planck Institute for Physics, Muenchen
c: Institute of Particle and Nuclear Studies, KEK, Tsukuba
d: Kinki University, Osaka
e: Yamanashi University, Kofu
f: Saitama University, Saitama
g: Tokyo Institute of Technology, Tokyo
h: Osaka City University, Osaka
i: Nagasaki Institute of Applied Science, Nagasaki
j: Chiba University, Chiba

k: Meisei University, Tokyo
l: Riken Institute of Physical and Chemical Research, Tokyo
m: Fukui University of Technology, Fukui
n: Toho University, Tokyo

This manuscript was prepared by M.Nagano and M.Fukushima.

Bibliography

- [1] M. Nagano et al., J. Phys. G: Nucl. Phys. **10**, 1295 (1984).
- [2] M. Nagano et al., J. Phys. G: Nucl. Phys. **18**, 423 (1992).
- [3] M. Takeda et al., Astropart. Phys. **19**, 447 (2003).
- [4] M. Takita et al., ICRR Annual Report (2005) p.23.
- [5] T. Antoni et al., astro-ph/0505413 v1 (2005) accepted for publication in Astroparticle Physics.
- [6] S. Yoshida, Slides in Rapporteur Talk at the 29th Int. Cosmic Ray Conf. (2005).

KAMIOKA OBSERVATORY

Kamioka observatory is located at 1000m underground (2700 m.w.e.) of the Kamioka Mine, Gifu prefecture, Japan. The observatory was established in 1995 in order to operate Super-Kamiokande. Super-Kamiokande discovered evidence for neutrino oscillations using atmospheric neutrinos in 1998. Solar neutrino oscillation was established in 2001 by comparing results from the SNO experiment in Canada. In 2002, neutrino oscillation was confirmed using artificial neutrinos produced by a proton accelerator at KEK.

There are also 100 m long laser interferometers in Kamioka Mine which are aiming to study gravitational waves and geophysics (details are described in the section of the gravitational wave group). Using the low background environment in Kamioka Mine, dark matter search experiments are also being prepared. One of the experiments is called XMASS which is described in the section of Neutrino and Astroparticle Division.

There are research offices, a computer facility and a dormitory for researchers located outside of Kamioka Mine and easy access to the detectors in the mine.

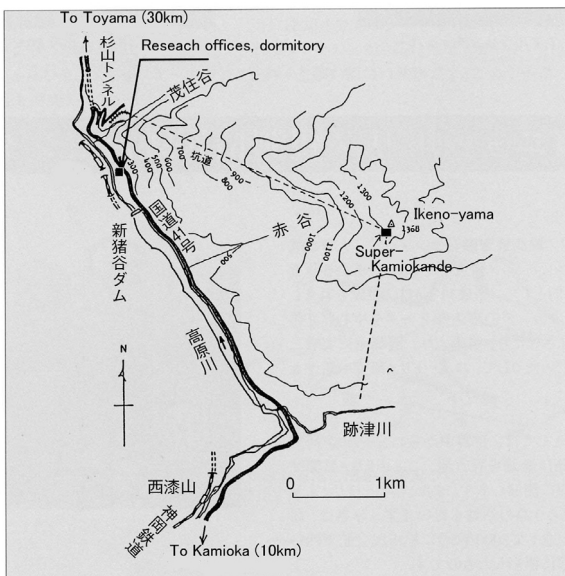


Fig. 1. Map of Kamioka observatory.

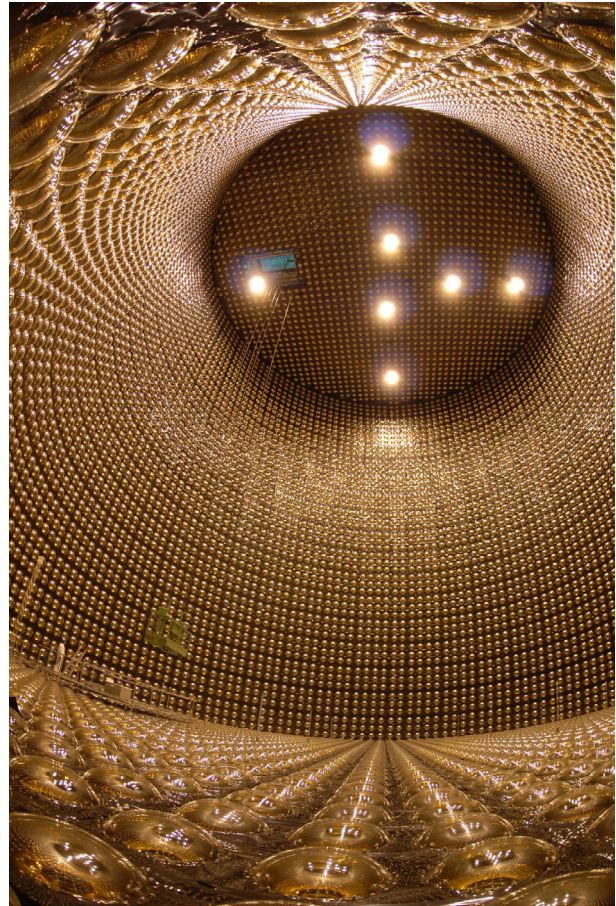


Fig. 2. Super-Kamiokande detector.



Fig. 3. 100 m baseline laser interferometers for gravitational wave and geophysics in Kamioka mine.



Fig. 4. Research offices and computer facility.



Fig. 5. Dormitory for researchers.

RESEARCH CENTER FOR COSMIC NEUTRINOS

Research Center for Cosmic Neutrinos was established in April 1999. The main objective of this center is to study neutrinos based on data from various observations and experiments.

In order to promote the studies of neutrino physics, it is important to provide the opportunity for discussions on theoretical ideas and experimental results on neutrino physics. Therefore, one of the most important, practical jobs of this center is the organization of neutrino related meetings. In the fiscal year 2005, we organized two local neutrino meetings. In one of the local meetings, we discussed Supernova neutrinos, and independently flavor structure of neutrinos. In the other workshop, we discussed neutrinos generated in the Earth (geo-neutrinos) following the first indication for the geo-neutrino observation in KamLAND. In each workshop, about 30 researchers participated.

It is important that the general public knows the achievements in the present science. Because of this reason, we had a public lecture on neutrinos at Kashiwa in May 2005. Two active scientists related to neutrino physics lectured on various aspects of neutrino physics.

In addition, from Nov. 2005, an outreach project “Development of a method of an outreach using science museums” was carried out based on a Grant from Japan Science and Technology Agency (JST). We developed a model of the outreach, where the researchers in universities explain the science (in our case, neutrinos) at a nearby science museum. We developed this exhibition model trying to explain “neutrinos” to the general audience, and carried out a test exhibition at Tamarokuto Science Center in March 2006. About 600 people came to this event during 5 days of our test exhibition. A photo taken during this test exhibition is shown. This test exhibition was successful.

This Center is also in charge of the computer system and the related network system for the inter-university research programs of ICRR together with the members of the computer committee in ICRR. The systems were operated with a very high efficiency without any serious problem in FY 2005. A noticeable upgrade in the computer system in FY 2005 was the addition of about 70% more disks for the data storage.

Since 2004, this Center has been acting as the body for accepting the ICRR inter university programs related to the Underground lab in the Kashiwa campus. The lab. is currently equipped with 4 Ge detectors mainly for the measurements of cosmic radioactive isotopes. The scientific activities that are related to this lab. is described elsewhere.

Finally, the scientific staffs in this center are actively working in the Super-Kamiokande and K2K experiments. These research activities are described in the section of Neutrino and Astroparticle Division. In addition to the Super-Kamiokande and K2K experiments, research activities in this Center include the calculation of the flux of atmospheric neutrinos, designing the intermediate detector for the T2K experiment and studying future neutrino detector (Hyper-Kamiokande) and neutrino oscillation experiment in the second phase of the T2K experiment.



Fig. 1. The test exhibition of neutrinos at Tamarokuto Science Center in March 2006.

APPENDICES

A. ICRR International Workshops

B. ICRR Seminars

C. List of Publications

- (a) **Papers Published in Journals**
- (b) **Conference Papers**
- (c) **ICCR Report**

D. Doctoral Theses

E. Public Relations

- (a) **ICCR News**
- (b) **Public Lectures**
- (c) **Visitors**

F. Inter-University Researches

G. List of Committee Members

- (a) **Board of Councillors**
- (b) **Executive Committee**
- (c) **Advisory Committee**

H. List of Personnel

A. ICRR International Workshops

International Workshop on Energy Budget in the High Energy Universe'

Date: February 22-24, 2006

Place: Institute for Cosmic Ray Research, University of Tokyo, Kashiwa campus of the University of Tokyo, Chiba, Japan
(Jointly hosted by ICRR, Department of Physics, and National Astronomical Observatory of Japan)

Outline

The Workshop is devoted to the discussion of our understanding in the non-thermal, high energy Universe. The existence of materials with very high specific energies, much exceeding the local virial temperature, is best represented by cosmic rays, of which the origin has long been a mystery. Recent astrophysical observations in X-ray, gamma-ray, neutrino and high energy cosmic ray experiments, in conjunction with theoretical studies, have been revealing various new aspects of the High Energy Universe, including promising candidates for the cosmic-ray acceleration sites. However, each approach has its own advantage and limitations in proving the whole view of the issue. We therefore expect that joint efforts by experimentalists and theorists in various related fields will be essential in our deeper understanding of the issue. In this Workshop, we discussed to what extent we understand the fluxes, the spectra and the maximum energies of the cosmic radiation produced in various astrophysical sites.

Participants

106 from Japan, 10 from USA, 4 from Germany, 3 from Italy, 2 from Korea, 1 from Canada

The 6th Edoardo Amaldi Conference on Gravitational Waves

Date: 20–24 June, 2005

Place: Bankoku Shinryoukan, Kise, Nago, Okinawa, Japan.

Outline

Amaldi6 is the latest in the series of Edoardo Amaldi Conferences on Gravitational Waves. Since 1999, these conferences, held every two years, have been regarded as the most important international conferences for the gravitational wave detection community. Amaldi6 is especially significant because the global network of ground-based interferometric detectors has begun generating meaningful scientific results to augment those from the existing resonant antennae. This combination is leading us to the establishment of a completely new perspective on the universe, that of "gravitational wave astronomy. Amaldi6 will consist of a series of sessions on gravitational wave sources, status of current detectors, details of current detectors, space detectors, data analysis, advanced detectors, and R&D for advanced detectors. Because of the abundant scientific data available recently, Amaldi6 will have somewhat more focus on data analysis than did previous Amaldi conferences.

Participants

47 from Japan, 39 from U.S.A., 4 from Brasil, 20 from Germany, 27 from Italy, 21 from Australia, 1 from Rusia, 1 from Spain, 6 from U.K., 4 from France, 4 from Holland.

B. ICRR Seminars

Date	Lecturer	Title
Jul 5, 2005	Kei KURITA (ERI, University of Tokyo)	“ Problems in the Earth Thermodynamics ”
Jul 12, 2005	Hiroaki YAMAMOTO (Caltech, USA)	“ The Present Status of LIGO Project in USA ”
Jul 14, 2005	Masahiro IBE (University of Tokyo)	“ Conformally sequestered SUSY breaking in vector-like gauge theories ”
Jul 14, 2005	Naotoshi OKAMURA (Tokyo Metropolitan University)	“ Solving the parameter degeneracy by the T2K+Korea experiment ”
Jul 27, 2005	Takaaki KITAZAWA (University of Tokyo)	“ Towards Realistic Models on D-branes ”
Jul 28, 2005	Sanshiro ENOMOTO (Tohoku University)	“ Neutrino Geophysics and the Detection of the Neutrino from the Earth by the KAMLAND ”
Aug 30, 2005	Kenji KADOTA (FNAL)	“ CMB and inflation model building -particle theorist’s view ”
Nov 8, 2005	Keiji INOKI (RIKEN)	“ Predictions of pp, pbarp total cross section and ratio at LHC and cosmic-ray energies based on duality ”
Nov 18, 2005	Yasuhiro Shimizu (Tohoku University)	“ Reconstructing Dark Matter density at ILC ”
Nov 22, 2005	Antonio Ereditato (INFN, Napoli)	“ Liquid Argon TPC technology for future particle physics experiments ”
Nov 22, 2005	Kaiki INOUE (Kinki University)	“ The Detail Structure of the Dark Matter explored by the Gravity Lensing ”
Mar 10, 2006	Martti Raidal (NICPB, Tallinn)	“ Aspects of Leptogenesis ”

C. List of Publications — 2005 fiscal year

(a) Papers Published in Journals

1. “ Observation of the Anisotropy of 10-TeV Primary Cosmic Ray Nuclei Flux with the Super-kamiokande-I detector ”, G. Guillian *et al.* [Super-Kamiokande Collaboration], Submitted to Phys. Rev.D.
2. “ Solar Neutrino Measurements in Super-Kamiokande-I ”, J. Hosaka *et al.* (Super-Kamiokande collaboration), Accepted by Phys. Rev. D.
3. “ Search for Coherent Charged Pion Production in Neutrino-Carbon Interactions ”, M.Hasegawa *et al.* (K2K Collaboration), Phys. Rev. Lett.95 (2005) 252301.
4. “ Search for Nucleon Decay via Modes Favored by Supersymmetric Grand Unification Models in Super-Kamiokande-I ”, K. Kobayashi *et al.* (Super-Kamiokande Collaboration), Phys. Rev. D72, (2005) 052007.

5. " A measurement of atmospheric neutrino oscillation parameters by Super-Kamiokande I ", Y. Ashie *et al.* (Super-Kamiokande Collaboration), Phys. Rev. D 71, (2005) 112005.
6. "Resolving neutrino mass hierarchy and CP degeneracy by two identical detectors with different baselines ", M. Ishitsuka, T. Kajita, H. Minakata and H. Nunokawa, Phys. Rev. D 72,(2005) 033003.
7. "Atmospheric neutrinos and neutrino oscillations ", T. Kajita and P. Lipari, Comptes Rendus Physique 6 (2005), 739.
8. " Precise Measurements of the Cosmic Ray Antiproton Spectrum with BESS Including the Effects of Solar Modulation ", J.W.Mitchell *et al.* (BESS Collaboration), Adv. Space Res. 35 (2005) (1)135.
9. " Cosmic Ray 1H and 2H Spectra from BESS 98 ", Z.D.Myers *et al.* (BESS Collaboration), Adv. Space Res. 35 (2005) (1)151.
10. " Search for Cosmic-Ray Antideuterons ", H.Fuke *et al.* (BESS Collaboration), Phys. Rev. Lett. 95 (2005) 081101.
11. " Detection of Gamma-Rays around 1 TeV from RX J0852.0-4622 by CANGAROO-II ", Katagiri, H. et al., Astrophys. J. Lett., 619, L163-L165 (2005)
12. " Are protons still dominant at the knee of the cosmic-ray energy spectrum? ", M. Amenomori *et al.*, Physics Letters B, 632, (2006), 58-64.
13. " Flux upper limits of diffuse TeV gamma rays from the Galactic plane using the effective area of the Tibet-II and -III arrays ", M. Amenomori *et al.*, Advances in Space Research, In Press (2005)
14. " Observation of PeV Gamma Rays from the Monogem Ring with the Tibet Air Shower Array ", M. Amenomori *et al.*, The Astrophysical Journal, 635,(2005), L53-L56.
15. " A Northern Sky Survey for Steady TeV Gamma-Ray Point Sources Using the Tibet Air Shower Array ", M. Amenomori *et al.*, The Astrophysical Journal, 633, (2005), 1005-1012.
16. " Large-Scale Sidereal Anisotropy of Galactic Cosmic-Ray Intensity Observed by the Tibet Air Shower Array ", M. Amenomori *et al.*, The Astrophysical Journal, 626, (2005), L29-L32.
17. " Veto analysis for gravitational wave burst signals in TAMA300 data using ALF filter ", T.M. Akutsu *et al.*, Amaldi 6 2005, Okinawa, Japan, June 20-24, 2005. (to be published in Classical Quantum Gravity Special Issue)
18. " CLIO Project ", S. Miyoki *et al.*, Amaldi 6 2005, Okinawa, Japan, June 20-24, 2005. (to be published in Classical Quantum Gravity Special Issue)
19. " LCGT ", K. Kuroda *et al.*, Amaldi 6 2005, Okinawa, Japan, June 20-24, 2005. (to be published in Classical Quantum Gravity Special Issue)
20. " A 100m laser strainmeter system in the Kamioka mine, Japan, for precise observations of tidal strains ", S. Takemoto *et al.*, Journal of Geodynamics, Vol.41 (2006) 23-29.
21. " New York University Value-Added Galaxy Catalog: A Galaxy Catalog Based on New Public Surveys ", Blanton, M.R. *et al.*, Astron. J. 129, 2562 (2005).
22. " The Sloan Digital Sky Survey Quasar Catalog. III. Third Data Release ", Schneider, D.P. *et al.*, Astron. J. 130, 367 (2005).
23. " Oscillation effects on thermalization of the neutrinos in the universe with low reheating temperature ", Ichikawa, K., Kawasaki, M., and Takahashi, F., Phys. Rev. D, 72, 043522 (2005).
24. " O I Line Emission in the Quasar PG 1116+215 ", Matsuoka, Y. *et al.*, Publ. Astron. Soc. Japan, 57, 563 (2005)
25. " The Luminosity and Color Dependence of the Galaxy Correlation Function ", Zehavi, I. *et al.*, Astrophys. J. 630, 1 (2005).
26. " The Properties and Luminosity Function of Extremely Low Luminosity Galaxies ", Blanton, M.R. *et al.*, Astrophys. J. 631, 208 (2005).
27. " Morphological Classification of Galaxies Using Photometric Parameters: The Concentration Index versus the Coarseness Parameter ", Yamauchi, C. *et al.*, Astron. J. 130, 1545 (2005).
28. " Burst Neutrinos from the Nitrogen Flash ", Serenelli, A.M. and Fukugita, M., Astrophys. J. 632, 33 (2005).

29. "Detection of the Baryon Acoustic Peak in the Large-Scale Correlation Function of SDSS Luminous Red Galaxies", Eisenstein, D.J. *et al.*, *Astrophys. J.* 633, 560 (2005).
30. "The Linear Theory Power Spectrum from the Ly α Forest in the Sloan Digital Sky Survey", McDonald, P. *et al.*, *Astrophys. J.* 635, 761 (2005).
31. "A Snapshot Survey for Gravitational Lenses among $z_i=4.0$ Quasars. II. Constraints on the $4.0 < z_i < 5.4$ Quasar Population", Richards, G.T. *et al.*, *Astron. J.* 131, 49 (2006).
"The White Dwarf Luminosity Function from Sloan Digital Sky Survey Imaging Data", Harris, H.C. *et al.*, *Astron. J.* 131, 571 (2006).
32. "The Fourth Data Release of the Sloan Digital Sky Survey", Adelman-McCarthy, J. K. *et al.*, *Astrophys. J. Suppl. Ser.* 162, 38 (2006).
33. "SDSS J103913.70+533029.7: A Super Star Cluster in the Outskirts of a Galaxy Merger", Knapp, G. R. *et al.*, *Astron. J.* 131, 859 (2006)
34. "Clustering of Lyman Break Galaxies at $z = 4$ and 5 in the Subaru Deep Field: Luminosity Dependence of the Correlation Function Slope", Kashikawa, N. *et al.*, *Astrophys. J.* 637, 631 (2006)
35. "A Survey of $z_i > 5.7$ Quasars in the Sloan Digital Sky Survey. IV. Discovery of Seven Additional Quasars", Fan, X. *et al.*, *Astron. J.* 131, 1203 (2006).
36. "Massive Coronae of Galaxies", Fukugita, M. and Peebles, P.J.E., *Astrophys. J.* 639, 590 (2006).
37. "Constraining Neutrino Masses by CMB Experiments Alone", K. Ichikawa, M. Fukugita, M. Kawasaki, *Phys. Rev. D* **71**, 043001 (2005).
38. "Significant effects of second KK particles on LKP dark matter physics", M. Kakizaki, S. Matsumoto, Y. Sato and M. Senami, *Phys. Rev. D* **71**, 123522 (2005).
39. "A bottom-up approach to moduli dynamics in heavy gravitino scenario : Superpotential, soft terms and sparticle mass spectrum", M. Endo, M. Yamaguchi and K. Yoshioka, *Phys. Rev. D* **72**, 015004 (2005).
40. "Relaxing constraints on inflation models with curvaton", T. Moroi, T. Takahashi and Y. Toyoda, *Phys. Rev. D* **72**, 023502 (2005)
41. "Implications of the curvaton on inflationary cosmology", T. Moroi and T. Takahashi, *Phys. Rev. D* **72**, 023505 (2005)
42. "The oscillation effects on thermalization of the neutrinos in the universe with low reheating temperature", K. Ichikawa, M. Kawasaki and F. Takahashi, *Phys. Rev. D* **72**, 043522 (2005).
43. "511 keV line from Q balls in the Galactic Center", S. Kasuya and F. Takahashi, *Phys. Rev. D* **72**, 085015 (2005).
44. "Late-time entropy production due to the decay of domain walls", M. Kawasaki, F. Takahashi, *Phys. Lett. B* **618**, 1 (2005).
45. "Q-ball instability due to U(1) breaking", M. Kawasaki, K. Konya and F. Takahashi, *Phys. Lett. B* **619**, 233 (2005).
46. "511-keV gamma ray from moduli decay in the galactic bluge", M. Kawasaki and T. Yanagida, *Phys. Lett. B* **624**, 162 (2005).
47. "Hadronic EDM constraints on orbifold GUTs", J. Hisano, M. Kakizaki and M. Nagai, *Phys. Lett. B* **624**, 239 (2005).
48. "Investigation of possible dark matter direct detection in electron accelerators", J. Hisano, M. Nagai, M. M. Nojiri and M. Senami, *Phys. Rev. D* **73**, 031701 (2006).
49. "Heavy Wino-like neutralino dark matter annihilation into antiparticles", J. Hisano, S. Matsumoto, O. Saito and M. Senami, *Phys. Rev. D* **73**, 055004 (2006).
50. "Revisiting the Constraint on the Helium Abundance from CMB", K. Ichikawa and T. Takahashi, *Phys. Rev. D* **73**, 063528 (2006)
51. "511 keV line and diffuse gamma rays from moduli", S. Kasuya, M. Kawasaki, *Phys. Rev. D* (2006) in press
52. "Efficient coannihilation process through strong Higgs self-coupling in LKP dark matter annihilation", S. Matsumoto and M. Senami, *Phys. Lett. B* **633**, 671 (2006).

53. “ Unification of dark energy and dark matter ”, F. Takahashi and T. T. Yanagida, *Phys. Lett. B* **635**,57 (2006).
54. “ Relic abundance of LKP dark matter in UED model including effects of second KK resonances ”, M. Kakizaki, S. Matsumoto, Y. Sato and M. Senami, *Nucl. Phys. B* **735**, 84 (2006).
55. “ Leptogenesis with supersymmetric Higgs triplets in TeV region ”, M. Senami and K. Yamamoto, *Int. J. Mod. Phys. A* **21**, 1291 (2006).

(b) Conference Papers

1. M. Nakahata, “ Supernova neutrinos and recent results from Super-Kamiokande ”, the 59th Yamada conference: “Inflating horizon of particle astrophysics and cosmology”, Koshiba Hall, Faculty of Science, The University of Tokyo, June 20, 2005.
2. M. Nakahata, “ Future solar neutrino experiments ”, 5th Workshop on Neutrino Oscillations and their Origin (NOON2004), Tokyo, Japan, 11-15 Feb 2004, *Nucl. Phys. Proc. Suppl.* 145 (2005) 23.
3. M. Nakahata, “ Future projects of Kamioka observatory ”, The CRC future project symposium, ICRR, Kashiwa, Chiba, Jan. 7, 2005
4. M. Nakahata, “ Search for the dark matter ”, JPS Science Seminar 2005, Aug. 27, 2005, Textbook for the JPS science seminar 2005.
5. T. Kajita, “ Recent results from atmospheric and solar neutrino experiments ”, Proc. of the 7th International Workshop on Neutrino Factories and Superbeams, Frascati, Italy, *Nucl. Phys. B. Proc. Suppl.*, 155 (2006) 155-157.
6. T. Kajita, “ Megaton water Cherenkov detectors ”, Proc. of the 7th International Workshop on Neutrino Factories and Superbeams, Frascati, Italy, *Nucl. Phys. B. Proc. Suppl.*, 155 (2006) 87-91.
7. Y. Takenaga, “ The Super-Kamiokande Experiment ”, Proc. of the 1st 21st Century COE QUESTS RA symposium.
8. Y. Suzuki, “ Accelerator and atmospheric Neutrinos ”, Prepared for XXII International Symposium on Lepton-Photon Interactions at High Energy, Uppsala, Sweden.
9. Y. Suzuki, “ Atmospheric Neutrinos and Long-Baseline Experiments ”, Prepared for IX International Conference on Topics in Astroparticle and Underground Physics, Venice, Italy.
10. S. Nakayama, “ Study of Atmospheric Neutrino Oscillations in SK-I and SK-II ”, Prepared for the 29th International Cosmic Ray Conference (ICRC2005), August 3-11, 2005, Pune, India.
11. J. Kameda, “ Review of NEUT ”, Prepared for 5th RCCN International Workshop on Sub-dominant Oscillation Effects in Atmospheric Neutrino Experiments, Kashiwa, Japan, Dec. 9-11, 2004.
12. J. Kameda, “ Neutrino interaction measurement in 1-kton water Cherenkov detector in K2K experiment ”, Prepared for 5th RCCN International Workshop on Sub-dominant Oscillation Effects in Atmospheric Neutrino Experiments, Kashiwa, Japan, Dec. 9-11, 2004.
13. H. Gallagher, D. Casper, Y. Hayato and P. Sala, “ Event generator comparisons ”, Proc. of the 3rd International Workshop on Neutrino Nucleus Interactions in the Few GeV Region (NuInt04), Gran Sasso, Assergi, Italy, 17-21 Mar 2004, *Nucl. Phys. Proc. Suppl.* 139 (2005) 278.
14. Y. Hayato, “ T2K at J-PARC ”, Proc. of the 21st International Conference on Neutrino Physics and Astrophysics (Neutrino 2004), Paris, France, 14-19 Jun 2004, *Nucl. Phys. Proc. Suppl.* 143 (2005) 269.
15. Y. Hayato, “ J-PARC and the T2K experiment ”, Proc. of High Intensity Frontier 2004: INFN Sezione di Pisa, *Nucl. Phys. Proc. Suppl.* 147 (2005), 9.
16. M.Mori, “ CANGAROO-III: Status Report ”, Towards a Network of Atmospheric Cherenkov Detectors VII, (Palaiseau, France, April 27-29 (2005), Ecole Polytechnique, eds. B. Degrange and G. Fontaine), pp.19-27
17. M.Mori, “ CANGAROO ” Third Workshop on Science with the New Generation of High Energy Gamma-ray Experiments, Cividale del Friuli, Italy, May 30-June 1 (2005) (to be published)
18. K.Nishijima, “ Status of the CANGAROO-III Project ” 29th International Cosmic Ray Conference, Pune, India, August 03-11 (2005) (to be published)

19. T.Tanimori, “ Recent status of the analyses for stereoscopic observations with the CANGAROO-III telescopes ”, *ibid.*
20. Y.Sakamoto, “ Search for Very High Energy Gamma-Rays from Active Galactic Nuclei with CANGAROO-III Telescope ”, *ibid.*
21. S.Kabuki, “ Observation of TeV Gamma-ray from the Active Radio Galaxy Centaurus A with CANGAROO-III ”, *ibid.*
22. T.Yoshikoshi, “ Performance of the Imaging Atmospheric Cherenkov Telescope System of CANGAROO-III ”, *ibid.*
23. M.Ohishi, “ Very high energy gamma-ray observations of the Galactic plane with the CANGAROO-III telescopes ”, *ibid.*
24. R.Kiuchi, “ Optical measurements by cooled CCD cameras for CANGAROO-III ”, *ibid.*
25. T.Nakamori, “ Stereoscopic observations with the CANGAROO-III telescopes at the large zenith angles ”, *ibid.*
26. M.Mori, “ Recent Results from CANGAROO ”, International Workshop on Energy Budget in the High Energy Universe, Kashiwa, Japan, February 22-24, 2006 (to be published)
27. .Kiuchi, “ Optical Measurements for CANGAROO-III ”, *ibid.*
28. Y.Yukawa, “ Consideration of Cassegrain Imaging Atmospheric Cherenkov Telescopes ”, *ibid.*
29. M. Amenomori et al., “ New Flux Upper Limits of Diffuse TeV Gamma Rays from the Galactic Plane Observed with the Tibet Air Shower Array ”, the 29th International Cosmic Ray Conference, (3–10 August 2005, Pune, India), Vol. 4, pp 43 – 46.
30. M. Amenomori et al., “ Search for steady PeV gamma-ray emission from the Monogem ring with the Tibet air shower array ”, the 29th International Cosmic Ray Conference, (3–10 August 2005, Pune, India), Vol. 4, pp 207 – 210.
31. M. Amenomori et al., “ Multi-wavelength searches of the Shell-like SNR G40.5-0.5 ”, the 29th International Cosmic Ray Conference, (3–10 August 2005, Pune, India), Vol. 4, pp 93 – 96.
32. M. Amenomori et al., “ A Northern Sky Survey for TeV gamma-ray sources using the Tibet-III air shower array ”, the 29th International Cosmic Ray Conference, (3–10 August 2005, Pune, India), Vol. 4, pp 211 – 214.
33. M. Amenomori et al., “ Search for TeV transient gamma-ray sources of the northern sky using the Tibet- III air shower array ”, the 29th International Cosmic Ray Conference, (3–10 August 2005, Pune, India), Vol. 4, pp 391 – 394.
34. M. Amenomori et al., “ Absolute Energy Scale Calibration of Multi-TeV Cosmic Rays Using the Moon’s Shadow Observed by the Tibet Air Shower Array ”, the 29th International Cosmic Ray Conference, (3–10 August 2005, Pune, India), Vol. 6, pp 53 – 56.
35. M. Amenomori et al., “ An Upper Limit on Cosmic-ray p/p Flux Ratio Estimated by the Moon’s Shadow with the Tibet-III Air Shower Array ”, the 29th International Cosmic Ray Conference, (3–10 August 2005, Pune, India), Vol. 6, pp 45 – 48.
36. M. Amenomori et al., “ The energy spectrum of the light components (P+He) at the knee obtained by the Tibet air shower core detector ”, the 29th International Cosmic Ray Conference, (3–10 August 2005, Pune, India), Vol. 6, pp 185 – 188.
37. M. Amenomori et al., “ Primary cosmic-ray proton and helium spectra at the knee energy region measured by the Tibet hybrid AS experiment ”, the 29th International Cosmic Ray Conference, (3–10 August 2005, Pune, India), Vol. 6, pp 177 – 180.
38. M. Amenomori et al., “ Sidereal Anisotropy of Galactic Cosmic-Ray Intensity Observed with the Tibet Air Shower Array. ” the 29th International Cosmic Ray Conference, (3–10 August 2005, Pune, India), Vol. 2, pp 77 – 80.
39. M. Amenomori et al., “ Two dimensional observation on TeV Cosmic-ray large scale anisotropy using the Tibet Air Shower Array ”, the 29th International Cosmic Ray Conference, (3–10 August 2005, Pune, India), Vol. 2, pp 49 –52.
40. M. Amenomori et al., “ Sun’s Shadow Variation During the Recent Solar Cycle 23 Observed with the Tibet Air Shower Array ”, the 29th International Cosmic Ray Conference, (3–10 August 2005, Pune, India), Vol. 2, pp 207 – 210.
41. C. Zhang et al., “ Observation on Local Group using the Tibet Air Shower Array and the Possible Relation with with Dark Matter Annihilation ”, the 29th International Cosmic Ray Conference, (3–10 August 2005, Pune, India), Vol. 4, pp 275 – 278.

42. S. Ushida et al., “ Research and development of fast-timing large-area thin detector ”, the 29th International Cosmic Ray Conference, (3–10 August 2005, Pune, India), Vol. 5, pp 331 – 334.
43. J. Huang et al., “ A possible approach to check the interaction models by observing AS cores around 20 TeV at 4300 m a.s.l. ”, the 29th International Cosmic Ray Conference, (3–10 August 2005, Pune, India), Vol. 6, pp 49 – 52.
44. J. Huang et al., “ A method to measure the energy spectra of the primary heavy components at the knee using a new Tibet AS core detector array YAC ”, the 29th International Cosmic Ray Conference, (3–10 August 2005, Pune, India), Vol. 6, pp 173 – 176.
45. Y. Katayose et al., “ Development of YAC (Yangbajing Air shower core array) to be used for next phase of Tibet experiment ”, the 29th International Cosmic Ray Conference, (3–10 August 2005, Pune, India), Vol. 8, pp 157 – 160.
46. M. Amenomori et al., “ Primary cosmic-ray energy spectrum around the knee energy region measured by the Tibet hybrid experiment ”, Physics At The End Of The Galactic Cosmic Ray Spectrum, (25–30 April 2005, Aspen, U.S.A.), in press.
47. A. Okutomi et al., “ Development of a radiation pressure noise interferometer ”, The 6th Elardo Amaldi Conference on Gravitational Waves 2005, Okinawa, Japan, June 20-24, 2005. (to be published in Journal of Physic : Conference Series)
48. K. Yamamoto et al., “ Measurement of vibration of the top of the suspension in a cryogenic interferometer with operating cryocoolers ”, The 6th Elardo Amaldi Conference on Gravitational Waves 2005. (to be published in Journal of Physic : Conference Series)
49. T. Uchiyama et al., “ Cryogenic systems of the Cryogenic Laser Interferometer Observatory ”, The 6th Elardo Amaldi Conference on Gravitational Waves 2005. (to be published in Journal of Physic : Conference Series)
50. T. Suzuki et al., “ Application of sapphire bonding for suspension of cryogenic mirrors ”, The 6th Elardo Amaldi Conference on Gravitational Waves 2005. (to be published in Journal of Physic : Conference Series)
51. M. Senami, “ Dark matter direct detection in electron accelerators ”, 11th International Symposium on Particles, Strings and Cosmology (PASCOS 2005), (30 May - 4 Jun 2005, Gyeongju, Korea), AIP Conf. Proc. **805**, 423-426 (2006).
52. M. Kakizaki, “ Hadronic EDMs in SUSY GUTs ”, 11th International Symposium on Particles, Strings and Cosmology (PASCOS 2005), (30 May - 4 Jun 2005, Gyeongju, Korea), AIP Conf. Proc. **805**, 314-317 (2006).

(c) ICRR Report

1. ICRR-Report-518-2005-1 (Month Day, 2005)
“ Dark Matter Direct Detection in Electron Accelerators ”,
J. Hisano, M. Nagai, M. Nojiri, M. Senami.
2. ICRR-Report-519-2005-2 (June 24, 2005)
“ Hadronic EDM Constraints on Orbifold GUTs ”,
J. Hisano, M. Kakizaki, M. Nojiri.
3. ICRR-Report-520-2005-3 (December 2004, 2005)
“ Observation of TeV Gamma-ray from the Active Radio Galaxy Centaurus A with CANGAROO-III Imaging Atmospheric Cherenkov Telescope”,
S. Kabuki.
4. ICRR-Report-521-2005-4 (september 6, 2005)
“ Relic Abundance of LKP dark Matter in UED model including Effects of Second KK Resonances ”,
M. Kakizki, S. Matsumoto, Y. Sato, M. Senami.
5. ICRR-Report-522-2005-5 (November 9, 2005)
“ Heavy Wino-like Neutralino Dark Matter Annihilation into Antiparticles ”,
J. Hisano, S. Matsumoto, A. Saito, M. Senami.
6. ICRR-Report-523-2005-6 (Month Day, 2005)
“ Efficient Coannihilation Process through Strong Higgs Self-Coupling in LKP Dark Matter Annihilation ”,
S. Matsumoto, M. Senami.

D. Doctoral Theses

No doctoral Theses in 2005.

E. Public Relations

(a) ICRR News

ICRR News is a newspaper published quarterly in Japanese to inform the Institute's activities. This year's editors were K.Okumura and M.Ohashi. It includes :

1. reports on investigations by the staff of the Institute or made at the facilities of the Institute,
2. reports of international conferences on topics relevant to the Institute's research activities,
3. topics discussed at the Institute Committees,
4. list of publications published by the Institute [ICRR-Report, ICRR-Houkoku(in Japanese)],
5. list of seminars held at the Institute,
6. announcements,
7. and other items of relevance.

The main topics in the issues in 2004 fiscal year were :

No.57 (March 31, 2005)

- Report on the 2005 ICRC in Pune, India. M. FUKUSHIMA.
- ICRR symposium. S. TORII.
Session I : TA Project EUSO Project.
Session II : Ashra Project, IceCube Project, LCGT Project.
Session III : Sub-Mev-Mev Gamma-ray Astronomical Observation.
Session IV : Tibet Observatory, Super-CANGAROO Project, CALET Project.
Session V : KAMIOKA Future Project Plans, XMASS.
- ICRR seminars and Reports.

No.58 (March 31, 2005)

- Detail report on the 29th ICRC.
Ultra high energy cosmic ray research, S. YOSHIDA.
Ultra high energy gamma-ray, T. YOSHIKOSHI.
Neutrino, S. NAKAYAMA and K. HIGUCHI.
High energy cosmic ray (less than 10^{17} eV) observation using the air shower observation instruments, M. TAKITA.
- Nuclear generated by the cosmic ray and aerosol, Y. SAKURAI.
- Quest of the Einstein Cosmos using Gravitational Wave, K. Kuroda.
- Informations
- ICRR seminars and Reports.
- Self-Introduction
- Changes in a staff

No.59 (March 31, 2006)

- Research Institutes of a University after the University Incorporation, Y.SUZKI.
- Report on the meeting for announce of results of inter-university researches. J.HISANO, M.Ohashi.
- International Workshop on Energy Budget in the High Energy University. M.MORI.
- Report on the 2005 ICRR open house days.
- Reminiscences of NORIKURA observatory. Y.MURAKI.
- ICRR Seminars and Reports

(b) Public Lectures

- “ JPS Science Seminar 2005 ”, August. 26-27 2005, Tokyo.
 - Presenters -
 - “ Search for the dark matter ”, M. Nakahata, (ICRR, University of Tokyo).

- “ Neutrino Exhibition ”, March 1-5, 2006, Tama Rokuto Science Center.
 - Assentient -
 - Neutrino Center of ICRR, Neutrino Center of TOHOKU University, Ice Cube Group of CHIBA University, Japan Science and Technology Agency (JST), TAMA Rokuto Science Center.

- “ The Dream of Einstein (The Cosmos revealed by Gravitational Waves) ”,
 - June 21 2005, Naha, Okinawa,
 - N. Kanda (Osaka City University).

- “ The Survey of the Einstein Cosmos by Gravitational Waves ”,
 - July 14 2005, Science Council of Japan, Tokyo, Japan,
 - Anchorman -
 - M. Ohashi (ICRR, University of University)
 - Presenters -
 - Opening Talk by Y. Ezawa “ Physics aimed by Gravitational Wave Study ”,
 - T. Nakamura (Kyoto university),
 - ” The High Technology used in the Gravitational Wave Detectors ”,
 - N. MIO (University of Tokyo),
 - “ The Present Status of the USA Gravitational Wave Detectors of LIGO and its Future Plan ”,
 - H. Yamamoto, (Caltech, USA),
 - “ Gravitational Wave Detectors in Japan and their Future Plan ”, K. Kuroda (ICRR, University of University),
 - Closing Talk by Y. Suzuki (ICRR, University of Tokyo).

- “ The Cosmos and the Earth explored by Gravity ”,
 - February 19, Notional Museum of Emerging Science and Innovation, Tokyo, Japan
 - Anchorman -
 - A. Ozeki (ASAHI Newspaper Inc.)
 - Presenters -
 - “ Make what is invisible to be visible (Neutrino and Gravitational wave)”,
 - Y. Suzuki (The President of ICRR, Universitu of Tokyo),
 - “The Earth vibration proved by Gravity ”,
 - S. Okubo (The President of ERI, University of Tokyo),
 - “The Survey of Life in the Second Earth ”,
 - M. Miyama (National Astronomical Observatory),
 - “ See the Cosmos by Gravitational Waves ”,
 - M. Ohashi (ICRR, University of Tokyo).

(c) Visitors

KAMIOKA Observatory (Total: 191 groups, 3933 people)

- Mr. Furuta (Governor of Gifu Prefecture) April 19, 2005.
- Mr. Maehara (Member of the House of Representatives), June 11, 2005.
- Mr. Nakayama (Minister of Ministry of Education, Culture, Sports, Science and Technology) September. 27, 2005.
- Mr. Seta (President of Japan Advanced Institute of Science and Technology) October 9, 2005.
- Press conference in the mine (15 publishers) November 4, 2005.
- Mr. Tsujimura (Kyodo news) December 22, 2005.
- Mr. Ikezawa (Novelist) and Mr. Hugo (Photographer) January 26, 2006.
- Mr. Abe (Member of Council for Science and Technology) February 3, 2006.
- Mr. Nishio (Executive Vice-President of Univ. of Tokyo) February 3,2006.
- Mr. Hamada (Executive Vice-President of Univ. of Tokyo) February 23, 2006.
- Mr. Funasaka (Mayor of Hida city) February 25, 2006.
- Mr. Anil (Science Journalist) March 27, 2006.
- Yume-no-Tamago-Juku (Summer school high for the school students)
- MEXT Super Science High School(SSH) project: total 6 schools

F. Inter-University Researches

Researcher Numbers

	Application Numbers	Adoption Numbers	Researchers Numbers
Facility Usage			
Kamioka Observatory	32	32	605
Norikura Observatory	8	8	69
Akeno Observatory	9	9	114
Research Center for Cosmic neutrinos	1	1	7
Emulsion and Air Shower Facilities in Kashiwa	25	25	310
Low-level Radio-isotope Measurement Facilities in Kashiwa	6	6	32
Gravitational Wave Facilities in Kashiwa	5	5	94
Other	5	5	56
Collaborative Researches			
High Energy Cosmic Ray Researches in the Underground and Deep Sea	26	26	536
High Energy Cosmic Ray Researches in Flyers and at High Altitude and Ground	26	26	376
High Energy Gamma Ray Source Researches	11	11	100
Chemical Composition and Isotope Measurement	10	10	44
Development of observational methods and instruments	13	13	196
Theoretical Researches or Rudimental Researches	5	5	35
Others			
Conferences	6	6	58
Special Activity on Abroad	0	0	0

Research Titles

1. Study of the solar neutrino flux
2. Energy spectrum measurement of solar neutrinos in Super-Kamiokande
3. Precise measurement of solar neutrino Day/Night variation
4. Research for Supernova burst monitor
5. Study of Supernova Relic Neutrinos at Super-Kamiokande
6. Study of the atmospheric neutrino flux and neutrino oscillations
7. Particle identification method for atmospheric electron-neutrinos and muon-neutrinos.
8. Study on 3-flavor Oscillation Effect in Atmospheric Neutrinos
9. Study of simulation for atmospheric neutrinos
10. Study of upward-going muons
11. Precise calculation of the atmospheric neutrino flux
12. Search for Nucleon Decay

13. search for proton decay into $e^+\pi^0$
14. Search for proton decay into νK^+
15. Energy calibration for Super-Kamiokande
16. Development of high-sensitivity radon detectors
17. Sidereal daily variation of 10TeV galactic cosmic-ray intensity observed by the Super-Kamiokande
18. Long baseline neutrino oscillation experiment
19. R&D of long baseline neutrino experiment with Super-Kamiokande and 50-GeV high intensity proton accelerator
20. Study of neutrino-nucleus interactions for accurate neutrino oscillation experiments
21. Neutrino interaction simulation study using accelerator data
22. Workshops on Neutrinos
23. Development of detectors for astroparticles by using liquid Xenon
24. Research and development of dark matter detectors
25. Direct dark matter search with liquid xenon detector
26. direction-sensitive dark matter search with a gaseous tracking device
27. Study of ambient gamma and neutron flux in Kamioka underground laboratory
28. A precise measurement of refractive index of liquid xenon
29. R&D for a 1 Mton water Cherenkov detector, Hyper-Kamiokande
30. Geodynamic studies by means of laser strainmeters in Kamioka
31. Study for the Earth's normal modes with the superconducting gravimeter observations
32. The Construction and Test Observation of TA
33. Absolute calibration of air shower energy by small electron LINAC
34. Development of the data acquisition system for TA fluorescence telescopes
35. Integrated test for TA's surface detectors
36. Studies on UHE Air Shower Simulation and Optimization of Data Analysis Method for TA Project
37. A new Atmospheric Monitoring system R&D
38. Experimental Study of High Energy Cosmic Rays in the Tibetan Highland
39. Search for steady sources of TeV gamma-rays in the northern hemisphere with the Tibet air-shower array.
40. Search for steady or flare type TeV gamma-ray sources using the Tibet air shower array.
41. Study of the primary cosmic ray composition at the knee region
42. Primary cosmic - ray spectrum in the knee region
43. Time Variation of Global Solar Magnetic Field through the Sun's Shadow made by the Galactic Cosmic Rays
44. Sidereal daily variation of 10TeV galactic cosmic-ray intensity observed by the Tibet air shower array
45. Observations of high-energy cosmic-ray electrons with emulsion chambers
46. Observation of celestial very-high-energy gamma-rays in Australia
47. CANGAROO-III Observation of Southern Sky
48. Monitoring system of the optical performance of the CANGAROO-III telescopes.

49. Search for extragalactic very high energy gamma-ray sources
50. Systematic study of the pulsar wind nebula with the CANGAROO Stereo observation
51. A search for high energy gamma-ray emission from Galactic disk
52. Development of analysis software for CANGAROO-III
53. Data analysis of the VHE gamma rays observed by 10m imaging Cherenkov telescopes
54. Observation of Galactic Objects by Stereoscopic Air Cherenkov telescopes
55. AGASA Project
56. Observation of air shower core of 10^{16} eV
57. Observation of Cosmic rays with the multidirectional muon telescope
58. Effect of clouds to the cosmic ray observation from space.
59. The high energy cosmic ray observation using the very wide field refracting optics
60. Study of the formation and the evolution of the Universe with prompt observations of gamma-ray bursts
61. Simultaneous observation of Gamma-Ray Burst optical flash by using ultra wide-field telescope
62. Observation of solar neutrons using a new detection method
63. Observations of small air showers and cosmic-ray intensities, by multi-directional muon telescope at Mt.Norikura
64. Muon intensity measurement at Mt. Norikura for the space weather study
65. Observation of night sky light and its reflection and scattering by clouds at a high mountain
66. A Study of the Radiation Damage to Polyimide film
67. Observation on the fluctuation of energetic radiation during thunderstorm activities
68. Continuous observation of microbarographs at high mountains
69. Ecophysiological studies of alpine plants - Photosynthetic response of *Pinus pumila* at different habitats -
70. Chacaltaya hybrid experiment of emulsion chamber and EAS-array
71. Bolivian Air Shower Joint Experiment (BASJE)
72. Development of All-sky Survey High Resolution Air-shower detector Ashra
73. Observation of UHE cosmic rays and TeV gamma rays with Ashra detector
74. Observation of High Energy Electrons and Gamma-Rays by Long Duration Ballooning
75. Absolute Calibration of the IceCube Digital Optical Modules (DOMs)
76. Evaluation of the super heavy particle detector under the high background environment
77. New experiment plan about the cosmic ray interaction in the energy ranges over 10^{16} eV
78. Workshop on "High Energy Gamma-ray Astrophysics"
79. Evolution of the Universe and Particle Physics
80. Search for continuous gravitational-wave signals induced by a binary pulsar system with TAMA data
81. Optical Squeezing for sensitivity improvement of gravitational wave interferometers
82. Quest for the smallest displacement noise in the low frequency range using CLIO.
83. R&D for Large-scale Cryogenic Gravitational wave Telescope (VII)
84. Development of a sapphire mirror suspension for large cryogenic GW detectors

85. Study of Newtonian-force-detection by LCGT interferometer
86. Gravitational Wave Research in Kamioka Mine (IV)
87. Continuous Environment Measurement of the Kashiwa Underground Laboratory
88. Deposition Rate/Flux of Natural Radioactive Nuclides ^7Be and ^{210}Pb
89. Detection of variability in cosmic rays with cosmogenic nuclide Be-7 and/or Na-22
90. Study of variability in cosmic rays at old time with C-14 and low-level radioisotopes in old tree rings
91. Researches into the origin and evolution of cosmic dusts
92. Chemical study for Antarctic micrometeorites
93. Measurements of ^{26}Al radioactivities for minor amount of Antarctic meteorite
94. Ultra-High Energy Particle Astronomy
95. Development of the IceCube Detector Simulation
96. Symposium for CRC's Future Projects
97. Enhancement of the trigger sensitivity for ASHRA

G. List of Committee Members

(a) Board of Councillors

SUZUKI, Yoichiro	ICRR, University of Tokyo
KURODA, Kazuaki	ICRR, University of Tokyo
KAJITA, Takaaki	ICRR, University of Tokyo
FUKUSHIMA, Masaki	ICRR, University of Tokyo
IWASAWA, Yasuhiro	University of Tokyo
KIRINO, Yutaka	University of Tokyo
KOBAYASHI, Makoto	KEK
KUGO, Taichi	Kyoto University
KAIFU, Norio	National Astronomical Observatory
SATO, Humitaka	Konan University
TOKI, Hiroshi	Osaka University
SUZUKI, Atsuto	Tohoku University
OHTA, Itaru	Utsunomiya University
INOUE, Hajime	Institute of Space and Astronautical Science
ITO, Nobuo	Osaka City University

(b) Advisory Committee

SUZUKI, Yoichiro	ICRR, University of Tokyo
TORII, Shoji	Kanagawa University
MURAKI, Yasushi	Nagoya University
TANIMORI, Toru	Kyoto University
KAWAKAMI, Saburo	Osaka City University
YANAGIDA, Manabu	University of Tokyo
NAGAE, Tomohumi	KEK
NISHIKAWA Koichiro	Kyoto University
NAKAMURA, Takashi	Kyoto University
MINOWA, Makoto	University of Tokyo
KURODA, Kazuaki	ICRR, University of Tokyo
FUKUGITA, Masataka	ICRR, University of Tokyo
FUKUSHIMA, Masaki	ICRR, University of Tokyo
MORI, Masaki	ICRR, University of Tokyo
NAKAHATA, Masayuki	ICRR, University of Tokyo
TAKITA, Masato	ICRR, University of Tokyo

(c) User's Committee

KAJINO, Fumiyoshi	Konan University
NISHIJIMA, Kyoshi	Tokai University
TORII, Shoji	Kanagawa University
TANIMORI, Toru	Kyoto University
MATSUBARA, Yutaka	Nagoya University
KANDA, Nobuyuki	ICRR, University of Tokyo
SAKURAI, Takahisa	Yamagata University
ITO, Yoshitaka	Nagoya University
OHASHI, Masataka	ICRR, University of Tokyo
YOSHIKOSHI, Takanori	ICRR, University of Tokyo
SHIOZAWA, Makoto	ICRR, University of Tokyo
KANEYUKI, Kenji	ICRR, University of Tokyo
TAKITA, Masato	ICRR, University of Tokyo
HISANO, Junji	ICRR, University of Tokyo

H. List of Personnel

Director SUZUKI Yoichiro

Vice-Director KURODA Kazuaki

Kamioka Observatory(Neutrino and Astroparticle Division)

Scientific Staff SUZUKI Yoichiro, NAKAHATA Masayuki, MORIYAMA Shigetaka,
TAKEUCHI Yasuo, SHIOZAWA Masato, HAYATO Yoshinari
MIURA Makoto, OBAYASHI Yoshihisa, KOSHIO Yusuke,
KAMEDA Jun, TAKEDA Atsushi, ABE Ko,
SEKIYA Hiroyuki,

Chief Secretary AKIMOTO Masatoshi,

Technical Staff MIZUHATA Minoru, FURUTA Takashi, KUMAMARU Seiichi,
NAKAZIMA Tetsue,

Research Fellows OGAWA Hiroshi,

Secretary OKURA Youko, MAEDA Yukari, OKADA Eri,

Research Center for Cosmic Neutrinos(Neutrino and Astroparticle Division)

Scientific Staff KAJITA Takaaki, KANEYUKI Kenji, OKUMURA Kimihiro,

Technical Staff SHINOHARA Masanobu,

Research Fellows SAJI Choji, NAKAYAMA Shoei, HIGUCHI Itaru,

HONDA Morihiko,

Secretary FUKUDA Yoko, KITSUGI Atsuko,

High Energy Cosmic Ray Division

Scientific Staff FUKUSHIMA Masaki, MORI Masaki,
ENOMOTO Ryoji, YOSHIKOSHI Takanori, TAKITA Masato,
SASAKI Makoto, SAGAWA Hiroyuki, TAKEDA Masahiro,
HAYASHIDA Naoaki, HATANNO Yoshikazu, Ohishi Michiko,
OHNISHI Munehiro, ASAOKA Yoichi, SAKURAI Nobuyuki

Technical Staff TOYODA Setsuko, AOKI Toshifumi, KOBAYASHI Takahide@

Research Fellows OZAWA Shunsuke, UDO Shigeharu, TOKUNOU Hisao,

SHIBATA Tatsunobu, KOBAYASHI Noriko, Fabrice Cohen,

YAMAKAWA Toshie, SHIOMI Atsushi, KONDO Yoshimi,

KAWATA Kazumasa, HUANG Jing, TANAKA Akiko,

SAWANNO Sumiko, HATSUMI Ryoichi, KANAZAWA Shuji,

SOMENO Hidemasa, FUKUDA Hisahe, MASUDA Masataka,

YAN Zhitao, WANG Xiao,

Secretary KOBAYASHI Noriko, TANAKA Akiko, SAWANO Sumiko,

KOKUBUN Yayoi,

AKENO Observatory(High Energy Cosmic Ray Division)

Scientific Staff SAGAWA Hiroyuki*,

Technical Staff TORII Reiko, OHOKA Hideyuki, KAWAGUCHI Masami,

Norikura(High Energy Cosmic Ray Division)

Technical Staff YAMAMOTO Kuniyuki, AGEMATSU Yoshiaki, USHIMARU Tsukasa,

ISHITSUKA Hideki, SHIMODAIRA Hideaki,

Astrophysics and Gravity Division

Scientific Staff FUKUGITA Masataka, KURODA Kazuaki, KAWASAKI Masahiro,
OHASHI Masatake, YASUDA Naoki, HISANO Junji,
MIYOKI Shinji, UCHIYAMA Takashi,

Research Fellows YAMAMOTO Kazuhiro, OKADA Atsushi, ICHIKAWA Kazuhide,

TSUZUKI Yumihiko, SENAMI Masato, TAKAHASHI Tomo,

Secretary SAKAI Akiko,

Graduate	TAKETA Akimichi(M2), IKEDA Daisuke(M1),	KIDO Eiji(M1),	HIYAMA Kazunori(M1),
Students	KIUCHI Ryuta(D1), YUKAWA Ryohei(M2), MANAGO, Naohiro(D3), NODA Koji(M2), MINAMINO Akihiro (D2), IIDA Takashi(M1), ISHIHARA Chizue(M1), KONDO, Kazuhiro(D3), TOKUNARI Masao(D2), NAKAGAWA Noriyasu(M2), KONISHI Kohki(M1), KONYA Kenichiro(D1), KANZAKI Toru(M2), NAKAYAMA Kazunori(M1)	YUASA Midori(D2), SAITO Takayuki(M2), AITA Yuichi(D1), TAKENAGA Yumiko(D1), MITSUKA Gaku (M2), KASAHARA Kunihiko(D3), AKUTSU, Tomomi (D1), KIRIHARA Hiroyuki(M1), NAGAI Minoru(D1), TAKAHASHI Hiroyuki(M2), SAITO Osamu(D1), NAGANAWA Tatsuya(M1),	KAWASAKI Sho(M2), SAKO Takashi(M1), OKUMURA Akira(D1), UESHIMA Kota(M1), NISHINO Haruki (M2), OKUTOMI Akira(D3), KAMAGASAKO Shogo(M2), AGATSUMA Kazuhiro(M1), TAKAYAMA Tsutomu(M2), SEKIGUCHI Toyokazy(M1),
Administration Division Staff	NAKATSUKA Kazuo, IIDA Nobuyuki TASHIRO Megumi, MATSUMOTO Kenichi MARUMORI Yasuko	KARINO Shinji, HAMANO Teruko, AKIYAMA Makiko, KITA Aiko,	YAMAMOTO Tetsuya, YAMAGUCHI Yoshiyuki, SAITO Akiko, WATANABE Yohko,